A dynamic global vegetation model for studies of the coupled atmosphere-biosphere system

G. Krinner, Nicolas Viovy, Nathalie N. de Noblet-Ducoudré, Jérôme Ogée, Jan Polcher, Pierre Friedlingstein, Philippe Ciais, Stephen Sitch, I Colin Prentice

A dynamic global vegetation model for studies of the coupled atmosphere-biosphere system

G. Krinner,[1] Nicolas Viovy,[2] Nathalie de Noblet-Ducoudré,[2] Jérôme Ogée,[2,3] Jan Polcher,[4] Pierre Friedlingstein,[2] Philippe Ciais,[2] Stephen Sitch,[5,6] and I. Colin Prentice[7]

Received 1 December 2003; revised 11 October 2004; accepted 24 November 2004; published 26 February 2005.

[1] This work presents a new dynamic global vegetation model designed as an extension of an existing surface-vegetation-atmosphere transfer scheme which is included in a coupled ocean-atmosphere general circulation model. The new dynamic global vegetation model simulates the principal processes of the continental biosphere influencing the global carbon cycle (photosynthesis, autotrophic and heterotrophic respiration of plants and in soils, fire, etc.) as well as latent, sensible, and kinetic energy exchanges at the surface of soils and plants. As a dynamic vegetation model, it explicitly represents competitive processes such as light competition, sapling establishment, etc. It can thus be used in simulations for the study of feedbacks between transient climate and vegetation cover changes, but it can also be used with a prescribed vegetation distribution. The whole seasonal phenological cycle is prognostically calculated without any prescribed dates or use of satellite data. The model is coupled to the IPSL-CM4 coupled atmosphere-ocean-vegetation model. Carbon and surface energy fluxes from the coupled hydrology-vegetation model compare well with observations at FluxNet sites. Simulated vegetation distribution and leaf density in a global simulation are evaluated against observations, and carbon stocks and fluxes are compared to available estimates, with satisfying results.

Citation: Krinner, G., N. Viovy, N. de Noblet-Ducoudré, J. Ogée, J. Polcher, P. Friedlingstein, P. Ciais, S. Sitch, and I. C. Prentice (2005), A dynamic global vegetation model for studies of the coupled atmosphere-biosphere system, *Global Biogeochem. Cycles*, *19*, GB1015, doi:10.1029/2003GB002199.

1. Introduction

[2] Recognition of the importance of land surface processes in the global climate system has been growing in recent years. Among these processes, those implicating the terrestrial biosphere are crucial simply because most of the land is covered by vegetation.

[3] The impact of the terrestrial biosphere on the global climate system is twofold: First, vegetation cover directly influences land-atmosphere heat, momentum, and moisture fluxes. Second, biospheric processes exert a strong control on the atmospheric composition, in particular on greenhouse gas concentrations on interannual and longer timescales [e.g., *Intergovernmental Panel on Climate Change* (*IPCC*), 2001]. Understanding biospheric processes on global and regional scales is therefore necessary for correctly analyzing the global climate system as a whole. Modeling the climate system or its individual components can help us test and improve our knowledge of the complex interactions at work. Depending on the type of scientific question to be addressed, different approaches to vegetation modeling have been taken.

[4] The first major axis of research concerns the impact of vegetation on land-atmosphere exchanges and therefore on climate. Surface-vegetation-atmosphere transfer schemes (SVATs [e.g., *Henderson-Sellers et al.*, 1996]) are used in general circulation models (GCMs) to simulate exchanges of sensible, latent, and kinetic energy at the surface. Using SVATs, a large number of studies have been carried out to quantify the impact of changes in prescribed distributions or physiological characteristics of vegetation on the simulated climate and climate changes [e.g., *Bonan et al.*, 1992; *Foley et al.*, 1994; *Kutzbach et al.*, 1996; *Douville et al.*, 2000; *Betts*, 2000].

[5] Several studies have been undertaken with GCMs asynchronously coupled to equilibrium vegetation models to examine the stability of the coupled atmosphere-

[1]Laboratoire de Glaciologie et Géophysique de l'Environnement/CNRS, Université Joseph Fourier Grenoble, St. Martin d'Hères, France.
[2]Laboratoire des Sciences du Climat et de l'Environnement, CEA/CNRS, Saclay, France.
[3]Now at Ecologie Fonctionelle et Physique de l'Environnement (Ephyse), INRA, Villenave d'Ornon, France.
[4]Laboratoire de Météorologie Dynamique/CNRS, Paris, France.
[5]Potsdamer Institut für Klimafolgenforschung (PIK), Potsdam, Germany.
[6]Now at Met Office (JCHMR), Wallingford, UK.
[7]Department of Earth Sciences, University of Bristol, Bristol, UK.

0886-6236/05/2003GB002199$12.00

vegetation system [e.g., *Henderson-Sellers and McGuffie*, 1995] and feedbacks between climate and vegetation change [e.g., *de Noblet-Ducoudré et al.*, 1996, 2000]. However, the need for a viable prediction of the transitory impact of the human activity on the global climate system implies that unified atmosphere-biosphere models have to be developed that can predict transient vegetation, carbon flux, and climate changes as well as their interactions for the next century at least. This motivates the development of dynamic global vegetation models (DGVMs) [e.g., *Foley et al.*, 1996; *Beerling et al.*, 1997; *Kirilenko and Solomon*, 1998; *Arora*, 2002] which are able to simulate the transient structural changes of vegetation cover in response to climatic changes by explicitly modeling competition and disturbance. The coupling of a DGVM with a GCM SVAT and, consequently, with a GCM itself, is one step toward integrated Earth system models. This kind of coupling has first been undertaken by *Foley et al.* [1998].

[6] The second major research axis of concern here is the role of terrestrial vegetation in the global carbon cycle. Carbon sequestration and release by terrestrial vegetation played an important role in past climate changes, and feedback loops involving climate, greenhouse gas concentrations, and vegetation in the next century have been identified [*Douville et al.*, 2000; *Cox et al.*, 2000; *Friedlingstein et al.*, 2001]. On the other hand, at least during the last decades, the biosphere seems to have been acting as a sink for a part of the human emissions of greenhouse gases, with the identification of the sink regions being a field of intensive research [e.g., *Fan et al.*, 1998; *Bousquet et al.*, 2000]. Understanding interannual variability and secular changes of global carbon fluxes and stocks is a primary research goal in this respect.

[7] These two research axes are of course intimately related. For example, in general, biogeographical models that determine vegetation distributions in response to an imposed climate or its changes actually are also biogeochemical models that represent the continental carbon cycle [*VEMAP Members*, 1995; *Cramer et al.*, 2001]. This paper presents a new terrestrial biosphere model, called ORCHIDEE (ORganizing Carbon and Hydrology in Dynamic EcosystEms), which is a SVAT coupled to a biogeochemistry and a dynamic biogeography model. As such, it explicitly simulates the phenomena of the terrestrial carbon cycle that are linked to vegetation and soil decomposition processes, but also changes in vegetation distributions in response to climate change as well as short-timescale interactions between the vegetated land surface and the atmosphere. ORCHIDEE is part of the new IPSL-CM4 Atmosphere-Ocean-Vegetation coupled general circulation model. However, coupled simulations are not presented here. Instead, this paper presents the model, a validation against station data of energy and carbon fluxes at the diurnal and seasonal timescales, and global simulations for which key parameters of simulated equilibrium vegetation distribution and carbon stocks are evaluated against available estimates. The following section describes the basic properties of ORCHIDEE and its principal underlying hypotheses and gives a brief overview of the parameterizations used in the model.

2. Basic Properties and Hypotheses

2.1. General Remarks

[8] ORCHIDEE is based on two different existing models and one newly developed model:

[9] 1. The SVAT SECHIBA [*Ducoudré et al.*, 1993; *de Rosnay and Polcher*, 1998] has been developed as a set of surface parameterizations for the LMD (Laboratoire de Météorologie Dynamique, Paris) atmospheric general circulation models (AGCM). SECHIBA describes exchanges of energy and water between the atmosphere and the biosphere, and the soil water budget. In its standard version, SECHIBA contains no parameterization of photosynthesis. Time step of the hydrological module is of the order of 30 min.

[10] 2. The parameterizations of vegetation dynamics (fire, sapling establishment, light competition, tree mortality, and climatic criteria for the introduction or elimination of plant functional types) have been taken from the dynamic global vegetation model (DGVM) LPJ [*Sitch et al.*, 2003]. The effective time step of the vegetation dynamics parameterizations is 1 year.

[11] 3. The other processes such as photosynthesis, carbon allocation, litter decomposition, soil carbon dynamics, maintenance and growth respiration, and phenology form together a third model called STOMATE (Saclay Toulouse Orsay Model for the Analysis of Terrestrial Ecosystems). STOMATE essentially simulates the phenology and carbon dynamics of the terrestrial biosphere. Treating processes that can be described with a time step of 1 day, STOMATE makes the link between the fast hydrologic and biophysical processes of SECHIBA and the slow processes of vegetation dynamics described by LPJ. Innovative features of STOMATE comprise a completely prognostic plant phenology (leaf out dates, maximum LAI, senescence) and plant tissue allocation including a carbohydrate reserve, and time-variable photosynthetic capacity depending on leaf cohort distribution. This newly developed model is described in section 2.3, and in more detail in Appendix A.

[12] SECHIBA will be referred to as the "hydrological module" in the following, while STOMATE and the included parameterizations of vegetation dynamics will be referred to as the "carbon module."

[13] ORCHIDEE can be run in different configurations, depending on the type of problem to be addressed. These are as follows:

[14] 1. In the hydrology only case, the carbon module is entirely deactivated and leaf conductance is calculated as by *Ducoudré et al.* [1993] without using any parameterizations of photosynthesis. Vegetation distribution is prescribed, and LAI is either prescribed (using satellite observations) or diagnostically calculated as a function of temperature [*Polcher*, 1994].

[15] 2. In the hydrology and photosynthesis case, the parameterizations of photosynthesis (following *Farquhar et al.* [1980] and *Collatz et al.* [1992]) and stomatal conductance (following *Ball et al.* [1987]) are activated,

Table 1. PFTs and PFT-Specific Parameters in ORCHIDEE[a]

PFT	$V_{cmax,opt}$	T_{opt}	λ_{max}	z_{root}	α_{leaf}	h	A_c	T_s	H_s
TrBE	50	37	10	1.25	0.12	25	910	-	0.3
TrBR	60	37	10	1.25	0.14	25	180	-	0.3
TeNE	37.5	27	5	1.	0.14	15	910	-	-
TeBE	37.5	32	5	1.25	0.14	15	730	-	-
TeBS	37.5	28	5	1.25	0.14	15	180	12.5	-
BoNE	37.5	25	4.5	1.	0.14	10	910	-	-
BoBS	37.5	25	4.5	1.	0.14	10	180	5	-
BoNS	35	25	4	1.25	0.14	10	180	7	-
NC3	70	$27.5 + 0.25T_l$	2.5	0.25	0.20	0.2	120	4	0.2
NC4	70	36	2.5	0.25	0.20	0.2	120	5	0.2
AC3	90	$27.5 + 0.25T_l$	6	0.25	0.18	0.4	150	10	0.2
AC4	90	36	3	0.25	0.18	0.4	120	10	0.2

[a]The PFts are: tropical broadleaf evergreen trees (TrBE), tropical broadleaf raingreen trees (TrBR), temperate needleleaf evergreen trees (TeNE), temperate broadleaf evergreen trees (TeBE), temperate broadleaf summergreen trees (TeBS), boreal needleleaf evergreen trees (BoNE), boreal broadleaf summergreen trees (BoBS), boreal needleleaf summergreen trees (BoNS), natural C_3 grass (NC3), natural C_4 grass (NC4), agricultural C_3 grass (AC3), and agricultural C_4 grass (AC4). $V_{cmax,opt}$: Optimal maximum rubisco-limited potential photosynthetic capacity (μmol m^{-2} s^{-1}); T_{opt}: Optimum photosynthetic temperature (°C), function of multiannual mean temperature T_l (°C) for C_3 grasses; λ_{max}: Maximum LAI beyond which there is no allocation of biomass to leaves; z_{root}: exponential depth scale for root length profile (m); α_{leaf}: prescribed leaf albedo; h: prescribed height (m) of vegetation (calculated if LPJ is activated); A_c: critical leaf age for leaf senescence (days); T_s: weekly temperature (°C) below which leaves are shed if seasonal temperature trend is negative; H_s: weekly moisture stress below which leaves are shed. Other PFT-specific parameters used in ORCHIDEE are given by *Sitch et al.* [2003].

but vegetation distribution is prescribed and LAI is either prescribed or diagnosed as a function of temperature.

[16] 3. In the case of hydrology and carbon cycle with static vegetation, the carbon cycle is fully activated. Soil, litter, and vegetation carbon pools (including leaf mass and thus LAI) are prognostically calculated as a function of dynamic carbon allocation. However, LPJ is deactivated; instead, the vegetation distribution is prescribed after *Loveland et al.* [2000].

[17] 4. In the case of hydrology and carbon cycle with dynamic vegetation, all three submodels are fully activated and the model makes no use of satellite input data that would force the vegetation distribution, so that vegetation cover, with its seasonal and interannual variability and dynamics, is entirely simulated by the model.

[18] Global simulations using the latter two configurations will be presented later in this article. In any of these configurations, ORCHIDEE can be run in stand-alone mode, that is, forced by climatological or experimental data (global or local), or it can be run coupled to an AGCM.

[19] Like LPJ, ORCHIDEE builds on the concept of plant functional types (PFT) to describe vegetation distributions. This concept allows grouping of species with similar characteristics into functional types in ways which maximize the potential to predict accurately the responses of real vegetation with real species diversity [*Smith et al.*, 1997]. ORCHIDEE distinguishes 12 PFTs (of which 10 are natural and two agricultural; see Table 1), for which Table 1 gives the values of the most important pertinent biogeochemical parameters (except those already defined by *Sitch et al.* [2003]).

[20] The different PFTs can coexist in every grid element. The fraction of the element occupied by each PFT is either calculated (and thus variable in time) or prescribed when LPJ is deactivated. The fractional area occupied by agricultural PFTs can be fixed such that vegetation dynamics does not act on the agricultural fraction of the grid element. Stomatal resistances are calculated separately for each PFT (and so is the resistance of bare soil). Water reservoirs are calculated for each PFT separately, but the lower soil reservoirs are mixed instantaneously [*de Rosnay and Polcher*, 1998].

[21] In ORCHIDEE grasses cannot grow below trees. This idealized assumption simplifies several parameterizations, for example, photosynthesis, transpiration, and light competition.

[22] Carbon dynamics is described through the exchanges of carbon between the atmosphere and the different carbon pools in plants and soils. There are eight biomass pools: leaves, roots, sapwood above and below ground, heartwood above and below ground, "fruits" (plant parts with reproductive functions: flowers, fruits, etc.), and a plant carbohydrate reserve; four litter pools: structural and metabolic litter, above and below the surface; and three soil carbon pools: active, slow, and passive soil carbon. Turnover time for each of the soil carbon and litter pools depends on temperature, humidity, and quality. The relatively high number of biomass pools is necessary because, first, ORCHIDEE distinguishes aboveground and belowground litter, which induces the need for distinguishing aboveground and below ground biomass; second, the cost of reproductive processes, which represents about 10% of the global NPP [*Sitch et al.*, 2003], needs to be taken into account and therefore requires a corresponding carbon pool; and third, the plant carbohydrate reserve is needed to represent carbon translocation at leaf onset. The litter and soil carbon pools are treated separately on the agricultural and natural part of each grid cell because of the large differences in soil carbon dynamics on agricultural and natural ground. Within each of these two parts of a grid cell (agricultural and natural) the PFTs are supposed to be well mixed so that the soil carbon is not calculated separately below each PFT. The parameterizations of litter decomposition and soil carbon dynamics essentially follow *Parton et al.* [1988].

[23] The basic state variables in the carbon modules of ORCHIDEE are the various carbon reservoirs and the density of individuals ρ (in m^{-2}) of each PFT. The maximum fractional cover v_{max} of each PFT is calculated from these state variables through

$$v_{max} = \rho c, \tag{1}$$

where crown area c (in m^2) of an individual plant is obtained using allometric relationships between c and the biomass of an individual [*Huang et al.*, 1992]. The density of individuals ρ is the result of plant death (through "natural" mortality, competition, and disturbances) and sapling establishment when the vegetation dynamics is activated; it is calculated such that $\rho c = v_{max}$ if v_{max} is prescribed (that is, if the vegetation dynamics is not activated). Note that v_{max}, which represents the part of the grid cell that is covered by the crowns of a given PFT, does

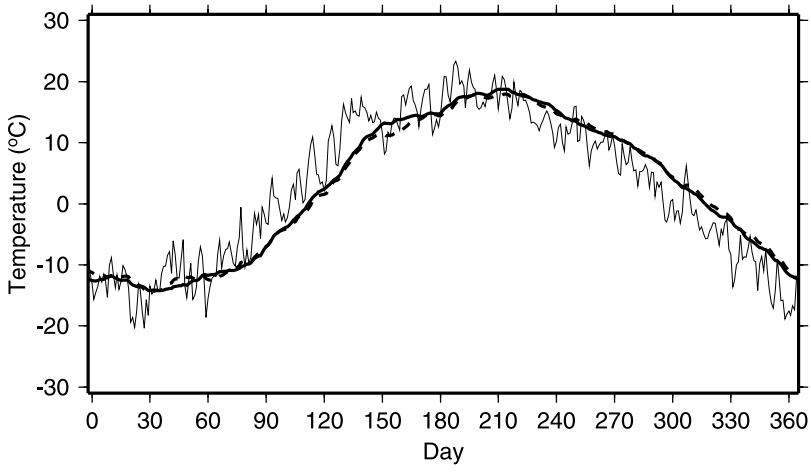

Figure 1. An example presenting the linear relaxation method used to calculate long-term "mean" temperatures in ORCHIDEE. Temperature time series at a model grid point in Siberia: daily mean temperatures (thin solid line); arithmetic average over the preceding 30-day period (thick solid line); "monthly" mean temperature using the relaxation method presented here with $\tau = 18$ days (thick dashed line).

not depend on the leaf mass. For herbaceous PFTs, an individual is defined as a tuft of $c = 1\ \mathrm{m}^2$.

[24] The foliage projective cover v (i.e., the fraction of the ground effectively covered by the leaves of the PFT) is calculated through

$$v = v_{\max}\left(1 - e^{-k\lambda}\right). \tag{2}$$

Here $k = 0.5$ is the extinction coefficient within the canopy [*Monsi and Sæki*, 1953] and λ is the leaf area index (LAI), defined as the ratio between the PFT's total leaf surface and $v_{\max}$. The total leaf surface of a PFT is calculated from the amount of leaf biomass, which is a prognostic variable of the model, and the prescribed specific leaf area. For high leaf area indices, $\lim_{\lambda\to\infty} v = v_{\max}$.

[25] The role of nitrogen is represented implicitly in the photosynthesis (section 2.3.1) and carbon allocation (section 2.3.3) parameterizations. In ORCHIDEE, fires are the main disturbance affecting the terrestrial vegetation, but a simple parameterization of regular herbivory following *McNaughton et al.* [1989] is included in ORCHIDEE. Other natural disturbances (such as wind throw) are not taken into account.

[26] Unlike the original formulation in LPJ, where the time step of vegetation dynamics is 1 year, these calculations are carried out in ORCHIDEE with the time step ($\Delta t =$ 1 day) of the other parts of the carbon module, and the corresponding variables are updated at this time step. However, in most cases, slowly (i.e., annually) varying input variables are used in these slow vegetation dynamics processes in order to maintain consistency with the basic hypotheses of the parameterizations of LPJ (the following paragraph describes how these variables, such as monthly or seasonal air temperatures, are calculated efficiently in ORCHIDEE). Therefore, for most of the parameterizations of vegetation dynamics in ORCHIDEE, the effective temporal resolution, determined by the temporal inertia of the parameterizations' input variables, is still 1 year. This procedure guarantees a smooth temporal evolution of the variables affected by vegetation dynamics and prevents sometimes dramatic, instantaneous changes which could occur if the LPJ parameterizations were only called once per year. The increase of computational cost corresponding to the higher frequency of vegetation dynamics calculations is very weak. The computationally most expensive part of the model remains the hydrology, which is calculated at a time step of 30 min. The time step of the "slower processes," leading to a daily update of the corresponding variables seen by the hydrology (primarily LAI and fractional vegetation cover), is also sufficiently small to allow a smooth temporal evolution of the hydrological variables.

[27] In order to reduce the computer memory requirements, short-term variables X_s (e.g., daily temperatures) are not kept in memory in order to sum them up to obtain long-term variables X_l (e.g., monthly temperatures). Instead, long-term variables X_l are updated at every time step Δt using a linear relaxation method,

$$X_l \leftarrow \frac{(\tau - \Delta t)X_l + \Delta t X_s}{\tau}, \tag{3}$$

where τ is a time constant depending on, and generally somewhat shorter than, the length of the period which X_l is to represent. For example, arithmetic mean temperatures over the preceding 30-day period are best approximated with this relaxation method when $\tau = 18$ days (see Figure 1); weekly arithmetic means are best approximated with $\tau =$ 5 days. Of course the "long-term" variable X_l with a given τ will not be exactly the same as the running mean of X_s over the corresponding period, particularly in cases where there is a strong high-frequency variability. For this reason, some parameterizations had to be retuned for the inclusion in the model. Compared to the running mean method, it is possible that this way of calculating long-term variables

might in many cases actually be more suitable for parameterizing the physiological processes in plants.

2.2. Hydrology

[28] ORCHIDEE builds on the version of SECHIBA as described by *de Rosnay and Polcher* [1998]. In land-surface models which include the vegetation dynamics, the surface parameters can not be read from an observationally based data set and need to be calculated. In ORCHIDEE, surface roughness and surface albedo were identified as the key variables which need to be computed from the simulated state of the vegetation. In both cases the grid-box average value is obtained by averaging the properties of each PFT (see Table 1). The roughness is based on the simulated height of the trees, and the averaging method is chosen such that the grid-box mean momentum flux is preserved. For albedo, the values of all PFTs are averaged and combined with the bare soil albedo which is determined on the basis of the soil color classification by *Wilson and Henderson-Sellers* [1985] and a function of dry soil height as determined by the hydrology module.

[29] The introduction of formulations of stomatal conductance [*Ball et al.*, 1987] and of photosynthesis [*Farquhar et al.*, 1980; *Collatz et al.*, 1992], similar to *Viovy* [1997], is a major modification. It ensures consistency between the treatment of the hydrological processes, in particular transpiration, and the treatment of stomatal conductance and photosynthesis, both being intimately linked. Stomatal conductance and photosynthesis, although informatically included in the hydrology package and calculated at the same time step as the other hydrological processes, are actually a part of the carbon module and are therefore presented in the following section.

2.3. Carbon Module: Physiological and Seasonal Processes

[30] This section describes briefly the main characteristics of the carbon module. The formulations are presented in more detail in Appendix A. Figure 2 shows the basic structure of ORCHIDEE, that is, the different subprocesses treated in the carbon module and their interactions.

2.3.1. Photosynthesis and Stomatal Conductance

[31] The formulation of stomatal conductance follows *Ball et al.* [1987]. C_3 and C_4 photosynthesis is calculated following *Farquhar et al.* [1980] and *Collatz et al.* [1992], respectively. Vertical variations in photosynthetic capacity are conditioned by leaf nitrogen content [*Johnson and Thornley*, 1984; *Sellers et al.*, 1986]. Photosynthetic capacity is thus parameterized as an exponentially decreasing function of canopy depth with an asymptotic minimum limit of 30% of the maximum efficiency after *Johnson and Thornley* [1984]. Water stress is taken into account following *McMurtrie et al.* [1990].

[32] Maximum rubisco-limited potential photosynthetic capacity (that is, unstressed photosynthetic capacity at optimum temperature) is parameterized as a function of leaf age, increasing from a relatively low initial value to a prescribed optimum $V_{cmax,opt}$ (see Table 1) during the first days after leaf onset, staying constant at this maximum for a given period (a few months, depending on the PFT), and then decreasing to a lower value for old leaves [*Ishida et al.*, 1999].

[33] Optimum photosynthesis temperature T_{opt} (see Table 1) is prescribed for most PFTs, but calculated for C_3 grasses as a function of the regularly updated multiannual mean temperature because this PFT occurs in a large range of ecosystems (from tropical savannas to tundra) and therefore comprises species adapted to very diverse climatic conditions.

[34] In order to take into account evergreen dormancy in winter, photosynthesis is not allowed when monthly temperatures are below a prescribed PFT-dependent threshold, even if the instantaneous temperature is exceptionally high [*Strand*, 1995; *Strand and Lundmark*, 1995; *Tania et al.*, 2003].

2.3.2. Phenology: Leaf Onset and Senescence

[35] As ORCHIDEE is designed to be included in an atmospheric general circulation model, leaf onset and leaf senescence have to be treated in a completely prognostic way. For every dormant deciduous PFT, the model has to decide regularly (at least once per week or so) whether leaf onset has to occur. This is done by applying warmth and/or moisture stress criteria to the meteorological conditions of the last days or weeks. Length of photoperiod is not considered in this first version of the model, although observations [e.g., *Nizinski and Saugier*, 1988] clearly show that this can be important in determining the moment of leaf onset. The leaf onset parameterizations in ORCHIDEE are based on the work of *Botta et al.* [2000]. The applied criteria for leaf onset depend on the PFT that is considered. For boreal needleleaf summergreen trees (i.e., *Larix*) the number of growing days over a given period has to exceed a predefined threshold. For broadleaf summergreen trees (both boreal and temperate), the number of growing degree-days g over a given period has to exceed a limit that is determined as a function of the number of chilling days (days with mean temperature below a certain threshold) n during the winter season [*Murray et al.*, 1989]. The growing season of tropical broadleaf raingreen trees begins a predefined number of days after the dry season's (simulated) moisture availability minimum. Grass phenology depends on the climate zone. In ''tropical'' regions (multiannual mean temperature $\overline{T} > 20°C$), the applied criterion is very similar to the one described for tropical deciduous trees. In ''cool'' regions ($\overline{T} < 10°C$), a simple formulation is used where the number of growing degree days during the past few weeks has to exceed a prescribed threshold. In intermediate regions, both criteria have to be fulfilled.

[36] On leaf onset, the plant will use its carbohydrate reserve (which was accumulated during the previous year) to grow a minimum quantity of leaves and roots, and the plant will be declared to be in its growing season. If the carbohydrate reserve is empty, leaf onset cannot occur, and the PFT will disappear from the grid element.

[37] Senescence of leaves and fine roots (plus stalks and ''fruits'' for grasses) is treated in a rather simple way. Two different criteria are used separately to calculate the fraction of leaves and roots that dies at the given time step. The first criterion is meteorological, depending on recent temperature and water stress. For example, summergreen trees essen-

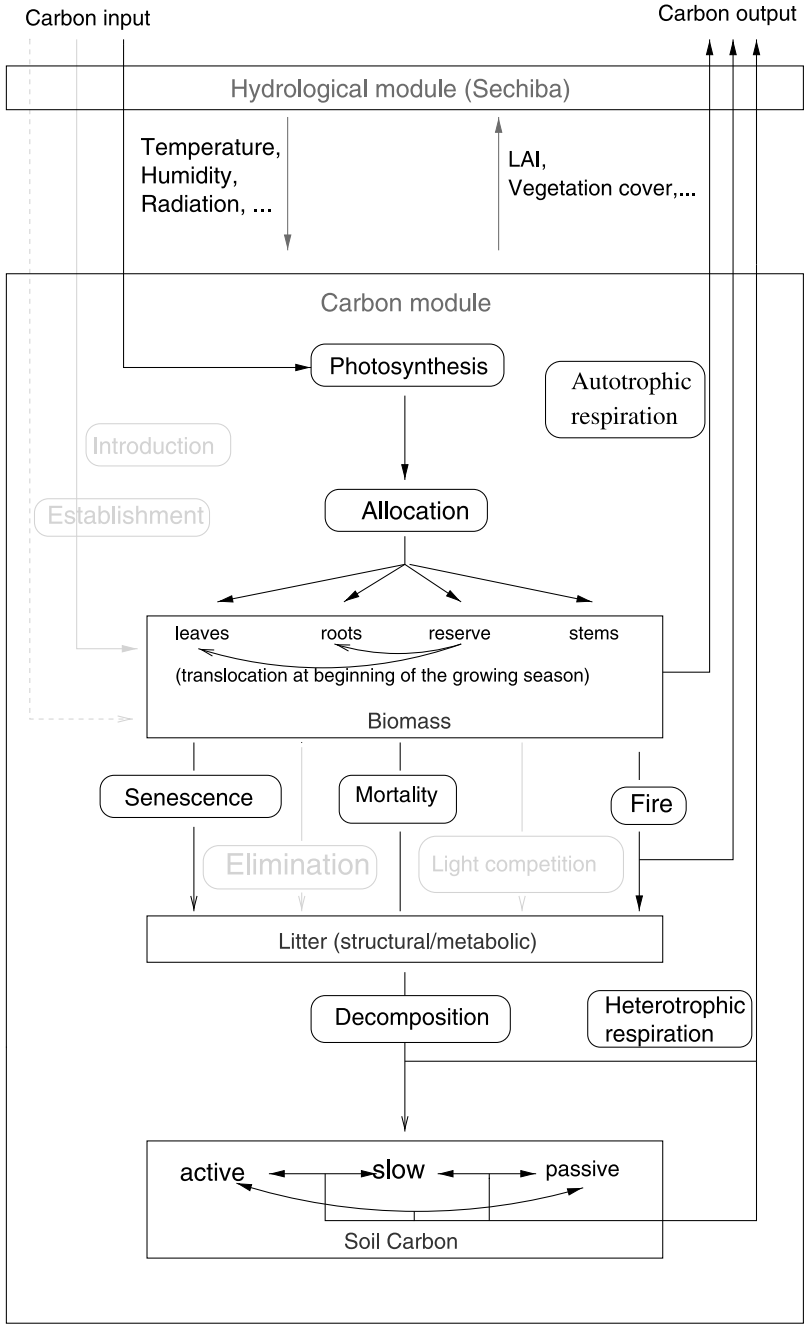

Figure 2. Basic structure of ORCHIDEE. Vegetation dynamics processes (taken from LPJ) show up in green. Within the carbon module box, processes are marked by rounded rectangles, while carbon reservoirs are indicated by normal rectangles (with the corresponding basic state variables in blue). The subprocesses simulated in the carbon module are linked through carbon fluxes (black and green arrows). The exchange of energy and information with the atmosphere passes through the surface scheme (that is, the hydrological module). Eventual biomass increases through PFT introduction and sapling establishment are taken into account as carbon flux from the atmosphere such that the total carbon in atmosphere plus biosphere is conserved. See color version of this figure at back of this issue.

tially shed their leaves and fine roots within some 2 weeks after the monthly temperature has fallen below a given limit (see Table 1). This criterion is also applied to tropical evergreen trees; as these have no carbohydrate reserve, total leaf shed leads to their death. This allows correct modeling of the transition between regions dominated by these two PFTs. Furthermore, for all PFTs, the leaf age itself is used to determine a fraction of leaves (and fine roots, plus stalk and "fruits" for grasses) that is shed. The fraction that is shed is very small when the leaves are young and increases very

strongly when a critical leaf age A_c (see Table 1) is approached. The critical leaf age is of course dependent on the PFT, being up to 2.5 years for evergreen PFTs and 6 months or so for seasonal PFTs [*Schoettle and Fahey*, 1994]. Note that in this parameterization of leaf senescence, the same fraction of leaves and fine roots is shed by the plant. This is certainly a fairly crude simplification.

[38] When during senescence the LAI falls below 0.2, all the remaining leaves are shed, and the plant is declared dormant. The beginning of a new phenological cycle can then occur. This means that several phenological cycles can theoretically occur in 1 year (for example, spring and autumn greening of grasses in Mediterranean-type climates [*Moulin et al.*, 1997]).

[39] In this version of ORCHIDEE, phenology of C3/C4 crops is simply treated in very similar manner to that of their natural counterparts, with adapted maximum possible LAI and slightly modified critical temperature and humidity parameters for phenology (see Table 1). Work is currently being carried out to couple ORCHIDEE to a crop model [*de Noblet-Ducoudré et al.*, 2004].

2.3.3. Carbon Allocation

[40] Carbon allocation is treated following *Friedlingstein et al.* [1998]. The basic hypothesis is that the plant will allocate carbon to its different tissues essentially in response to external limitations: water, light, and nitrogen availability. In reality, carbon allocation is constrained by the need that leaf biomass has to be supported by a sufficient quantity of transport tissue [e.g., *Shinozaki et al.*, 1964a, 1964b; *Berninger and Nikinmaa*, 1994]. This constraint is not taken into account in ORCHIDEE. However, no gross inconsistencies between sapwood and leaf mass appear in ORCHIDEE.

[41] Water availability is calculated supposing an exponential root length profile decreasing with depth, independent of the fine root mass, although parameterizations of root distribution as a function of root biomass exist [*Arora and Boer*, 2003]. For natural plants, light limitation is a function of the weighted mean LAI of the natural PFTs present in the grid box. This is based on the idea that a plant will "see" around itself the LAI of the other plants present in the grid box and will have to compete against these in the struggle for light (although the photosynthesis model considers the PFTs to be spatially separated). For agricultural PFTs, light limitation is calculated as a function of the PFT's own LAI, as agricultural PFTs are spatially separated from each other because they grow on well-defined areas reserved for them (fields).

[42] Nitrogen limitation is parameterized as a function of monthly soil humidity and monthly soil temperature, as in the work of *Friedlingstein et al.* [1998]. The basic idea is that plant available nitrogen will depend on microbial activity in the soil, which itself depends on humidity and temperature.

[43] The three different availabilities are then used to calculate preliminary allocation fractions for leaves, roots, and sapwood. The principal idea is that the stronger a given stress, the more carbon will be allocated to the corresponding tissue (e.g., roots in the case of drought). No carbon is allocated to leaves when the LAI is above a PFT-specific limit fixed somewhat above typically observed annual maximum LAI values (e.g., 10 for tropical evergreen trees). In this case, the carbon is attributed to the sapwood (i.e., the stalks in the case of grasses).

[44] The scheme of *Friedlingstein et al.* [1998] was modified to allow for carbon allocation toward a carbohydrate reserve, not present in the original scheme and needed here because of the fully prognostic phenological cycle. The quantity of photosynthate allocated to the carbohydrate reserve is a prescribed fraction of the preliminary leaf and root allocation factors given by the formulation of *Friedlingstein et al.* [1998], which are then recalculated. However, no biomass is allocated to the carbohydrate reserve if the content of the latter exceeds the biomass equivalent of the prescribed PFT-specific maximum LAI. Conversely, no carbon is allocated to leaves and fine roots during seasonal senescence. At this period of the year, the biomass which would normally be attributed to leaves and roots is stored in the carbohydrate reserve instead. Translocation from the carbohydrate reserve toward leaves and roots occurs at the beginning of the growing season in order to attain rapidly a relatively dense leaf cover. This allows the plant to photosynthesize efficiently at the beginning of the growing season. Observational data to fine-tune the allocation to and translocation from the carbohydrate reserve are missing [*Le Roux et al.*, 2001]. However, our scheme enables ORCHIDEE to represent the well-known basic dynamics of this pool [*Le Roux et al.*, 2001]: rapid depletion at the beginning of the growing season, reserve deposition in summer and fall, and partial depletion in winter through maintenance respiration.

[45] A further modification applied to the original allocation scheme is the fixed allocation of 10% of the photosynthates [*Sitch et al.*, 2003] to reproductive plant tissues, except during senescence. There is no allocation to tree heartwood because the latter is produced by the slow conversion of sapwood.

2.3.4. Autotrophic Respiration

[46] The formulation of autotrophic respiration is based on work by *Ruimy et al.* [1996]. The maintenance respiration R_m for living plant compartments is basically calculated as a function of temperature and biomass, and as a function of the (prescribed) nitrogen/carbon ratio of each tissue. The maintenance respiration coefficient (i.e., the fraction of biomass that is lost during a given time interval) increases linearly with temperature (air temperature for aboveground plant tissues; root-zone temperature for belowground tissues). Observations indicate that respiration of tropical plants is less sensitive to temperature than that of temperate or boreal plants [*Ruimy et al.*, 1996]. This is a problem for grasses in ORCHIDEE, as tropical, temperate, and boreal C_3 grasses are represented by only one generic PFT (see list of PFTs in Table 1). To overcome this problem, the slope of the temperature dependence of the maintenance coefficient (and some other parameters, such as critical temperature values for the phenological cycle) for this PFT is parameterized as a function of a reference temperature T_{ref} at the given grid point. Note that thermal acclimation of autotrophic respiration has actually been observed for a number of different plant functional types, not only for C_3 grasses

[*Loveys et al.*, 2003]. When the vegetation distribution is calculated dynamically, T_{ref} is actually the (simulated) multiannual mean temperature (with an integration constant of several years; see section 2.1). This can be interpreted as a faculty of grasses to adapt to changing environmental conditions, or, in the case of strong climate shifts, as the replacement of unadapted grass species by species that are well adapted to the new climate. This formulation is therefore an implicit representation of vegetation dynamics, which is actually quite fast for grasses, as can be observed in reality as early succession after major disturbances [*Sitch et al.*, 2003]. When the vegetation distribution is prescribed, these parameters are calculated as a function of a prescribed reference temperature (which should be close to the simulated or prescribed annual mean temperature) at each grid point. This allows, for example, comparison of interannual variations of carbon balance in forests and grasslands without any simulated additional adaptation of grasses to changing environmental conditions.

[47] Up to 80% of the photosynthates produced during a time step can be used for maintenance respiration without being allocated to the respiring plant tissues beforehand. If maintenance respiration is higher than this threshold, then the additional carbon needed for maintenance respiration is taken from the respective plant tissues themselves. In other words, at least 20% of the biomass assimilated at each time step can be immediately allocated to the plant tissues. This rather heuristic formulation has been introduced to allow the plants to allocate biomass even under rather severe environmental stress, and therefore to compensate for limitations. A prescribed fraction (28%) of the allocatable assimilates (i.e., assimilates available for tissue growth) is lost to the atmosphere as growth respiration [*McCree*, 1974], and the remaining assimilates are distributed among the various plant organs using the allocation fractions calculated beforehand (section 2.3.3).

2.3.5. Heterotrophic Respiration

[48] The treatment of heterotrophic respiration follows *Parton et al.* [1988]. Prescribed fractions of each type of plant tissue go to the metabolic and structural litter pools whenever one of the numerous litter-forming processes takes place (e.g., natural plant mortality, leaf senescence, fire, light competition; see Figure 2).

[49] The decay of metabolic and structural litter is controlled by temperature and soil or litter humidity. The rate of the decay of structural litter also depends on its lignin content (high lignin fractions decrease the decay rate). Lignin content of the individual plant tissues is prescribed, and lignin content in the structural litter pools is then updated with litterfall and decay.

[50] For each of the litter types, the fraction of the decomposed biomass that goes into the slow, passive, and active soil carbon pools is prescribed, the rest being lost to the atmosphere as heterotrophic respiration. Thus the carbon resulting from the decomposition of the lignin fraction of structural litter goes partially into the slow soil carbon pool and partially into the atmosphere as CO_2, while the carbon from the non-lignin fraction goes partially into the active soil carbon pool and again partially into the atmosphere. The decomposition of metabolic litter results in an increase both of the active carbon pool and of atmospheric CO_2.

[51] Metabolic activity in the soil results in carbon fluxes within the three carbon pools (active, slow, and passive). Time constants for these fluxes are prescribed, but again, temperature and moisture inhibition functions are used to parameterize the decrease of soil metabolic activity under cold, dry, or anaerobic conditions. The fractions of these fluxes that are attributed to the other carbon pools and, as CO_2 flux, to the atmosphere, are again prescribed following *Parton et al.* [1988].

2.4. Vegetation Dynamics

[52] The parameterizations of vegetation dynamics have been taken from the model LPJ [*Sitch et al.*, 2003] with minor modifications. A brief description of the minor modifications applied to these parameterizations is given here. The reader is referred to *Sitch et al.* [2003] for a description of LPJ.

[53] The basic vegetation dynamics parameterizations included in ORCHIDEE are the introduction/elimination of PFT using climatic criteria, sapling establishment, light competition, fire occurrence and impact on vegetation, and tree mortality. A PFT is declared adapted to a given climate if the instantaneous minimum surface air temperature during the last 12 months has not fallen below a PFT-specific threshold (some PFTs, for example, boreal needleleaf summergreen trees, have no such threshold and are thus regarded as totally insensitive to frost). In this case, the PFT can be introduced if it is not already present. In the opposite case, it will be eliminated. In the original version of LPJ the instantaneous minimum temperature was parameterized as a function of the mean temperature of the coldest month. In ORCHIDEE, with its time step of 30 min for the processes involving surface energy exchanges, the actual instantaneous minimum temperature is taken. This means that the meteorological input data have to capture nighttime minimum temperatures; that is, they must have at least a temporal resolution of a few hours. A further difference to LPJ is that warm season temperatures T_{ws} (T_{ws} is the ''seasonal'' surface air temperature calculated with the relaxation method presented in section 2.1 using τ = 60 days) must exceed 7°C for trees to be declared adapted to the given climate (no such criterion is applied in LPJ). The motivation for applying this criterion is the observed strong correlation between warm season isotherms and treeline position, which is thought to be due to growth limitation of tree-specific tissue types at low temperatures [*Körner*, 1998]. However, *Kaplan et al.* [2003] argued that the use of NPP as a limit on tree growth might be more mechanistic. In any case, the inclusion of the warm season temperature criterion allows ORCHIDEE to simulate correctly the present boreal treeline.

[54] Sapling establishment increases the density of individuals ρ of a PFT, but in ORCHIDEE, unlike LPJ, no increase of biomass is associated with sapling establishment except if the number of newly established saplings is not negligible compared to the number of already present individuals (in the latter case, this biomass increase is taken into account as carbon flux from the atmosphere to the

biosphere such that the total mass of carbon in atmosphere plus biosphere is conserved). Biomass is redistributed between the existing and the newly established plants, and the plant characteristics (LAI, height, etc.) are then recalculated.

[55] The formulation of fire occurrence [*Thonicke et al.*, 2001] in LPJ follows an intermediate approach between the fire history concept (using statistical relationships between the length of the fire season and the area burnt) and a process-oriented methodology (estimation of fire conditions based on litter quantity and moisture): the length of the fire season is first calculated from daily litter quantity and moisture and is then used to determine the area burnt in 1 year. As in the other parameterizations of LPJ, the time step of the original formulation of fire occurrence [*Thonicke et al.*, 2001] is 1 year. However, in ORCHIDEE it is desirable to dispose of a formulation that explicitly simulates the seasonal variations of fire occurrence, including human-induced fires, as the effect of fires on radiative properties of the atmosphere (via aerosol injection) or on surface conditions during the dry season can be regionally important when large areas burn in short periods [e.g., *Hobbs et al.*, 1997; *Ross et al.*, 1998]. A good simulation of this seasonality is particularly desirable as ORCHIDEE is coupled to an atmospheric GCM. However, due to the strong nonlinearity of the formulations of *Thonicke et al.* [2001], it is not possible to simply increase the effective temporal resolution of the LPJ fire parameterizations above 1 per year without obtaining unrealistic fire fractions. The solution that was adopted was to increase the effective temporal resolution of the fire parameterizations to 1 month while introducing a corrective term in the calculated fire extents which ensures that the effective annual mean fire extent calculated in this way is equal to the annual mean fire extent that would have been obtained with the original formulation. Using this approach, calculated fire occurrence does exhibit a clear seasonality as a function of drought and litter, and simulated fire return times are reasonable. A parameterization of the transformation of biomass into black carbon, which can be regarded as totally inert at the timescales ORCHIDEE is designed for (a few thousand years at most), has been introduced into the fire subroutine following the work of *Kuhlbusch et al.* [1996].

3. Validation Against FluxNet Data

3.1. Rationale

[56] This section first presents a validation of ORCHIDEE using eddy covariance flux data from FluxNet, a global network of biosphere-atmosphere flux measurement sites [*Baldocchi et al.*, 2001]. At each location, CO_2, water, and energy half-hourly fluxes are measured above vegetation, along with ancillary data, such as climate forcing, leaf area index, soil properties, litterfall, or maximum photosynthetic capacity. At present, over 140 sites are operating on a long-term and continuous basis. However, this study is limited to a subset of sites where climate forcing and flux data were both available in nearly continuous data sets. Table 2 shows the main characteristics for these 28 sites. Nearly all PFTs of ORCHIDEE are represented, except boreal needleleaf summergreen (i.e., *Larix*) and tropical broadleaf raingreen forests. A total of 87 years of half-hourly flux data is used here.

[57] Data such as LAI, photosynthetic capacity, or soil carbon were not used for model calibration or initialization in order to allow for a global validation of ORCHIDEE. Only climate data and vegetation distribution at each site were used to force the model. The preparation of the climate forcing and the initialization of the model at each site is described in Appendix B. Model testing was then performed on the fluxes of CO_2, water vapor, sensible heat, and net radiation at different timescales, from half-hourly to monthly values. Half-hourly and monthly timescales were retained here because they correspond to the diurnal and seasonal cycles, respectively. Note that the onset and termination of the growing season at each site are calculated by ORCHIDEE in a prognostic mode (see section 2.3.2) and therefore the FluxNet data can also be used to check the model performance for phenology.

3.2. Results and Discussion

[58] The slope and intercept of the linear regressions between modeled and measured fluxes have been computed at each site, along with other statistical quantities, for half-hourly and monthly values. Detailed results are given in tables as supporting material on the AGU web site.[1]

3.2.1. Example: Aberfeldy

[59] As an example, measured and modeled fluxes at AB (the first site in alphabetic order, a temperate evergreen needleleaf forest in Scotland) are shown in Figure 3. At this particular site, ORCHIDEE correctly reproduces the diurnal cycles of net radiation and, except for a few peaks caused by forcing problems, of latent and sensible heat fluxes. In contrast, it systematically underestimates the daily amplitude of the net CO_2 flux. A systematic overestimation of the nighttime sensible heat flux explains the disagreement on accumulated values, while the disagreement between measured and modeled net CO_2 fluxes at a half-hourly timescales tends to vanish at greater timescales. This illustrates the importance of performing model tests on different fluxes and at different timescales. In the following, the results at sites belonging to the same PFT were aggregated in order to perform a PFT-by-PFT rather than a site-by-site analysis.

3.2.2. Diurnal Cycle

[60] In order to simplify the analysis, a seasonal mean diurnal cycle rather than series of 10-day bin-averaged diurnal cycles are presented here. Figure 4 displays the measured and modeled "summer" diurnal cycles for each flux and each PFT. This corresponds to the averaged diurnal cycle over the period from 1 June to 31 August because all sites in this study are located in the Northern Hemisphere. The analysis of this figure is given in the following.

[61] 1. For net radiation, ORCHIDEE performs quite well for all PFTs, except for temperate evergreen broadleaf forests (SKy, SKo, CP) where the model predicts too small a daily amplitude. Inspection of the results at these three sites shows that this feature mainly occurs at CP and

[1] Auxiliary material is available at ftp://ftp.agu.org/apend/gb/2003GB002199.

Table 2. Characteristics of the 28 FluxNet Sites Retained for Testing ORCHIDEE[a]

Code	Site Name	Location	Altitude	Selected Years	Age	LAI
		Boreal Deciduous Broadleaf Forest (DBF)				
GU	Gunnarsholt[b]	63°50N 20°13W	78	1996–1998	5	1.4 to 2.5
		Boreal Evergreen Needleleaf Forest (ENF)				
FL	Flakaliden	64°07N 19°27E	225	1996–1998	31	2
HY	Hyytiala[c]	61°51N 24°17E	170	1996–2000	35	2 to 3
NB	BOREAS NSA-OBS[d]	55°52N 98°28W	259	1994–1998	old	4.5
NO	Norunda	60°05N 16°13E	45	1996–1998	100	4 to 5
		C3 Agriculture				
BVS	Bondville soybean	40°00N 88°18W	300	1998	-	0 to 3.8
PO	Ponca city	36°46N 97°08W	310	1997	-	0 to 5
		C4 Agriculture				
BVC	Bondville corn	40°00N 88°18W	300	1997 and 1999	-	0 to 3.8
		C3 Grass				
LW	Little Washita	34°57N 97°59W	30–60	1997–1998	-	2 to 3
UP	Upad[e]	70°16N 148°53W	5	1994	-	1 to 1.5
		C4 Grass				
FI	FIFE	39°07N 95°29W	320–450	1987	-	1 to 3.6
SH	Shidler	36°56N 96°41W	350	1997	-	0 to 2.9
		Temperate Deciduous Broadleaf Forest (DBF)				
HE	Hesse	48°40N 7°04E	300	1996–2000	30	0 to 6
HV	Harvard Forest[f]	42°32N 72°11W	180–490	1992–1999	90	0 to 5.5
SO	Soroe	55°29N 11°38E	40	1997–1999	78	0 to 4.8
VI	Vielsam[f]	50°18N 6°00E	450	1996–1998	60–90	0 to 5.1
WB	Walker Branch[g]	35°57N 84°17W	365–380	1995–1998	58	0 to 6
		Temperate Evergreen Broadleaf Forest (EBF)				
CP	Castelpoziano	41°45N 12°22E	3	1997–1998	50	3.5
SKo	Sky Oaks (old)	33°22N 116°37W	1420	1997–2000	78	1.6
SKy	Sky Oaks (young)	33°22N 116°37W	1420	1997–2000	4	0.6
		Temperate Evergreen Needleleaf Forest (ENF)				
AB	Aberfeldy[c]	56°36N 3°48E	340	1997–1998	14	7 to 8
BR	Brasschaat[h]	51°19N 4°31E	16	1996–1998	67	2 to 3
BX	Bordeaux[b]	44°43N 0°46W	60	1997–1998	30	2.6 to 3.2
LO	Loobos[i]	52°10N 5°44E	25–52	1996–2000	80	1.7 to 3
ME	Metolius	44°27N 121°33W	1310	1996–1997	90	3
TH	Tharandt[i]	50°58N 13°34E	380	1996–2000	140	6
WE	Weiden Brunnen[i]	50°10N 11°53E	765–780	1996–1999	40	5 to 6.5
		Tropical Evergreen Broadleaf Forest (EBF)				
MA	Manaus	2°36S 60°07W	120	1996	-	5 to 6

[a]Altitude in meters above sea level, stand age in years.
[b]With 30% C3 grass.
[c]With 10% C3 grass.
[d]Boreal mixed forest (70% boreal ENF, 30% boreal DBF).
[e]Tundra (50% bare soil, 50% C3 grass).
[f]Temperate mixed forest (70% temperate DBF, 30% temperate ENF).
[g]Temperate mixed forest (80% temperate DBF, 20% temperate ENF).
[h]Temperate mixed forest (40% temperate DBF, 60% temperate ENF).
[i]With 20% C3 grass.

throughout the year, suggesting that ORCHIDEE does not simulate the correct albedo at this particular site, due to a poor representation of the phenological cycle. The simulated diurnal cycle is longer than the measured one at C3 agriculture sites. This is because, in the present version, ORCHIDEE assumes that all C3 agriculture is a perennial grassland and does not account for harvest, while at BVS it is a summer crop (soybean) and at PO the winter wheat is harvested in spring.

[62] 2. For sensible heat flux, ORCHIDEE simulates almost systematically, and especially at night, a diurnal cycle with higher values compared to measurements. This overestimate of the sensible heat flux by ORCHIDEE has already been shown in Figure 3. ORCHIDEE calculates one single energy budget for both the vegetation and the soil, leading to a unique surface temperature value. However, at night, a stable stratification often develops between the height at which fluxes and scalars are measured and the surface. This cannot be correctly represented in the calculation of surface drag with a simple flux formulation based on bulk formulae for sensible and latent heat fluxes. Note that the only ecosystem for which the nighttime sensible

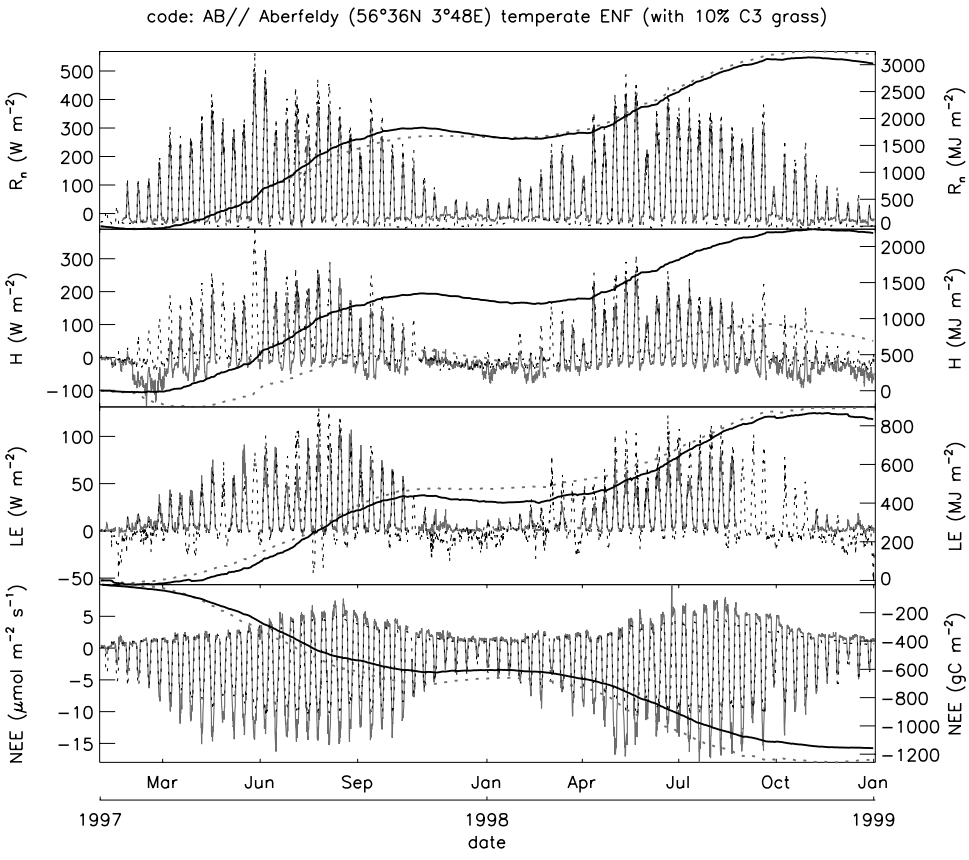

Figure 3. Ten-day bin-averaged and accumulated measured (red) and modeled (black) fluxes at AB (see Table 2). From top to bottom: net radiation (R_n), sensible heat flux (H), latent heat flux (LE), and net CO_2 flux (NEE). See color version of this figure at back of this issue.

heat flux is not overestimated is tropical evergreen forest; this ecosystem is characterized by particularly high vegetation leading to strong surface drag.

[63] 3. For latent heat flux, the simulated summer daily cycle is in good agreement with the measured one at most forest sites. However, mostly at Mediterranean-type ecosystems (SKy, SKo, CP), the modeled diurnal cycle peaks in the afternoon, i.e., later than the measured one. This peak occurs when the air vapor pressure deficit is maximum, which suggests that the stomatal control on water loss in ORCHIDEE is not strong enough at high vapor pressure deficits for this type of ecosystems. The problem could also be due to the buildup of hydrological stress in the plant or rhizosphere, which is negated during the night as the water pathway re-equilibrates. This is not represented in the model. For grasslands and crops, results are not so good. At C3 agriculture sites, ORCHIDEE cannot behave realistically (see item 1 in this list). At other sites, ORCHIDEE seems to simulate either a strong soil water deficit (LW, BVC) or a thick snow cover (UP) that strongly affect the latent heat flux in summer. A more thorough inspection of the results reveals that ORCHIDEE is also unable to reproduce the daily amplitude of the latent heat flux observed at some specific forest sites (e.g., LO), while at other sites among the same PFT, the model behaves quite well.

[64] 4. For net CO_2 fluxes, the peak in the simulated diurnal cycle is also delayed in the afternoon compared to the measured one. In addition, ORCHIDEE simulates an amplitude that is smaller than the measured one at needleleaf forest sites (see also Figure 3) and greater at broadleaf forest sites. At broadleaf forest sites, we also notice an overestimation of nighttime respiration. These differences of amplitude between needleleaf and broadleaf forests might be caused by the way photosynthesis is computed in ORCHIDEE, i.e., for one single big-leaf, whereas there is increasing evidence that diffuse radiation is used by plants more efficiently than direct radiation [*de Pury and Farquhar*, 1997].

3.2.3. Seasonal Cycle

[65] Figure 5 shows the measured and modeled seasonal cycles for each flux and each PFT. This gives a rather precise idea of how ORCHIDEE behaves for each PFT on a monthly basis. Our main conclusions are given below.

[66] 1. At all seasons, ORCHIDEE overestimates the sensible heat flux, especially at night. This disagreement should be compensated by a strong underestimation of the storage terms in the soil and the vegetation. Unfortunately, measurements of these storage terms are sparse or not available at most FluxNet sites. In addition, a direct comparison with what is called storage in ORCHIDEE seems difficult, as the model performs only one single energy budget.

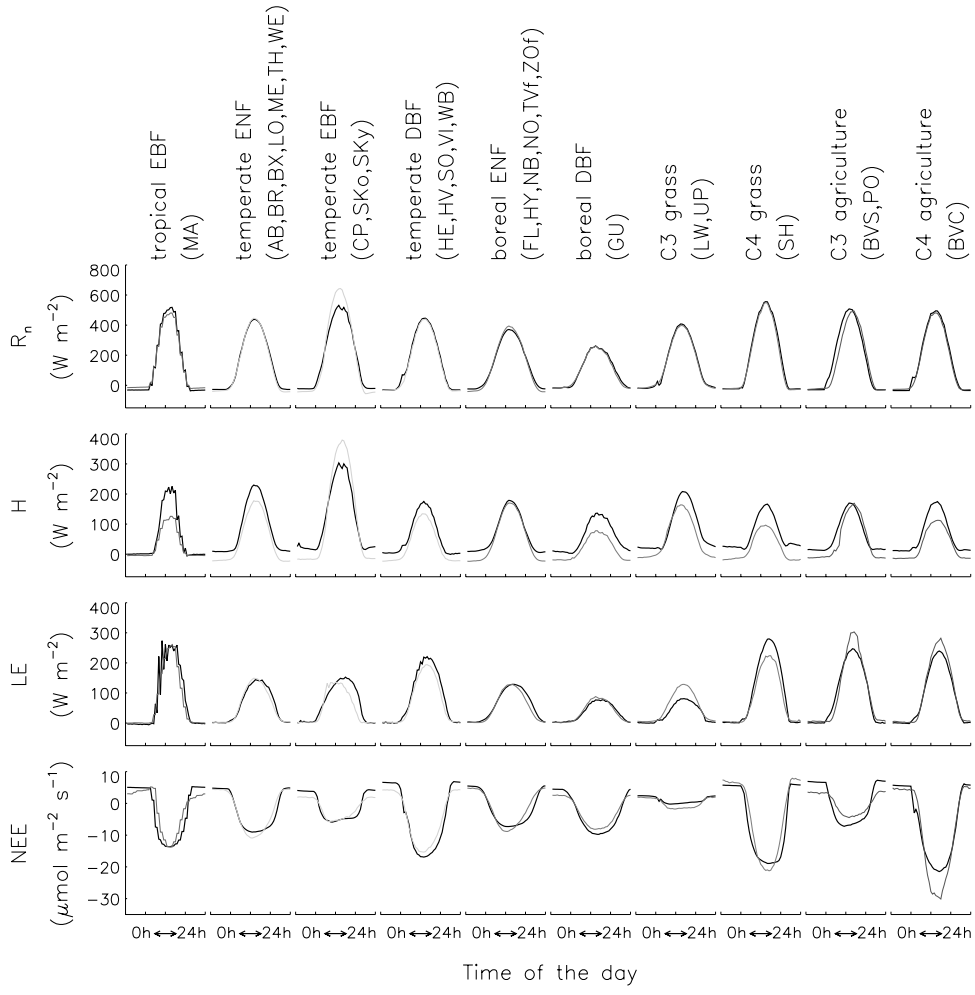

Figure 4. Measured (colored) and modeled (black) "summer" diurnal cycle for each flux and each PFT (see text). From top to bottom: net radiation (R_n), sensible heat flux (H), latent heat flux (LE), and net CO_2 flux (NEE). See color version of this figure at back of this issue.

[67] 2. The discrepancies noticed in Figure 4 in the diurnal cycle of latent heat and net CO_2 fluxes between model and measurements tend to compensate partly on seasonal timescales. Indeed, at needleleaf forests, the smaller amplitude of the CO_2 assimilation rates can be partly compensated by a longer diurnal cycle that peaks in the afternoon. Also, at broadleaf forests, the greater amplitude of the CO_2 assimilation rates can be partly compensated by higher respiration rates at night. The stomatal response to air vapor pressure deficit or the fact that photosynthesis is not computed separately for sunlit and shaded leaves are possible explanations for these discrepancies in the diurnal cycle.

[68] 3. Some model-data discrepancies on the carbon or water fluxes, not visible in Figure 4, appear in Figure 5 because they do not occur in summer. For example, in Mediterranean-type ecosystems, ORCHIDEE simulates strong soil water deficits at the end of the summer, which causes a rapid decrease of LE and NEE compared to measured values. Also, at boreal deciduous broadleaf forests (GU), ORCHIDEE simulates very high rates of respiration and evaporation in winter, but this seems to be a problem of forcing (partitioning between rain and snowfall).

[69] 4. The overall phasing of each flux is rather well simulated in ORCHIDEE. This gives us confidence in the way leaf onset and senescence are calculated.

[70] For nonforest sites, the seasonal results are not so good. For C3 grasslands, ORCHIDEE simulates strong soil water deficits in summer. In addition, the phenology in winter and spring does not seem correct. The model performance seems better for C4 grasslands, but more observations are needed to verify it. For agricultural sites, both the diurnal and seasonal variations of the CO_2 flux are very badly reproduced by ORCHIDEE. This was expected because, as mentioned in section 3.2.2, the model assumes that all C3 agriculture is a perennial prairie and does not account for harvest.

[71] At this point, it must be pointed out that most eddy-flux towers among the FluxNet network are located in young or middle-aged healthy stands with a controlled disturbance. Using these data to validate a global model

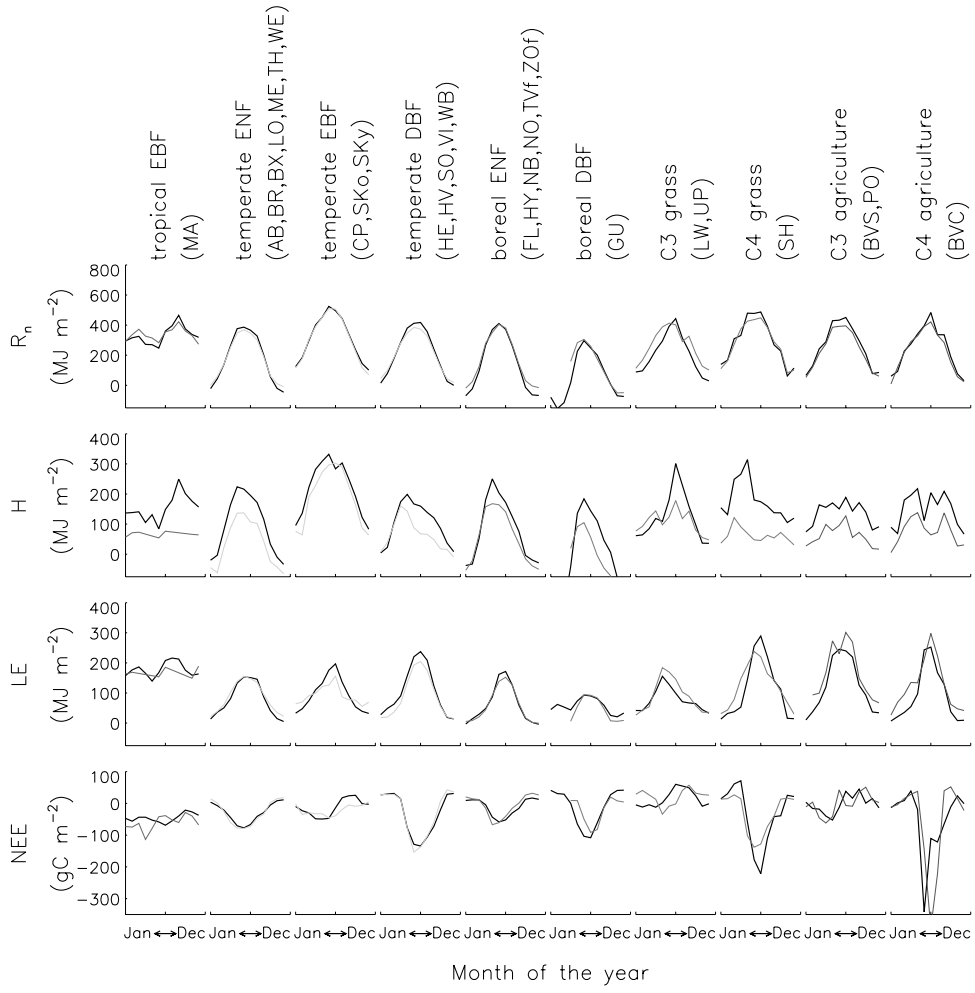

Figure 5. Measured (colored) and modeled (black) seasonal cycle for each flux and each PFT (see text). From top to bottom: net radiation (R_n), sensible heat flux (H), latent heat flux (LE), and net CO_2 flux (NEE). See color version of this figure at back of this issue.

such as ORCHIDEE is necessary but not sufficient, because the model is aimed also to describe the water and carbon cycles of ecosystems undergoing disturbance.

4. Global Simulations

[72] Two global simulations are presented in this section. In the first simulation, referred to as "STAT," vegetation distribution is prescribed ("static"). In the second simulation, called "DYN," vegetation dynamics is activated. Plant phenology and the carbon cycle are explicitly simulated in both simulations (see the description of possible configurations of ORCHIDEE in section 2.1).

[73] STAT used the *Loveland et al.* [2000] global vegetation data. As described by *Vérant et al.* [2004], a correspondence matrix was used to map the initial vegetation classes to ORCHIDEE's PFTs. DYN was started from bare soil in the nonagricultural part of each grid cell, while the fractions of agricultural C_3 and C_4 plants were prescribed as in STAT. Both simulations were run at a horizontal resolution of 4° (zonal) × 2.5° (meridional). This fairly low resolution was chosen for several reasons. First, when coupled to the LMDz atmospheric GCM, ORCHIDEE will generally be run with a similar grid spacing. Second, due to the absence of dynamic interactions between adjacent grid points, no significant increase in large-scale model performance was observed in simulations at varying horizontal resolutions during the development phase (at least as far as global vegetation characteristics are concerned; for regional scale studies, high spatial resolution is of course necessary). Therefore, running the model at higher horizontal resolution would be an unnecessary use of computer resources (at the chosen resolution, 1 year of simulation with the complete model takes 6 min of CPU time on a 3-GHz PC). The model was forced at its half-hourly time step by meteorological parameters obtained from a Richardson-type weather generator [*Richardson and Wright*, 1984; *Friend*, 1998; J. A. Foley, personal communication, 1999] using monthly climatological data for 1961–1990 produced by *New et al.* [1999], using a CO_2 concentration of 350 ppmv. The half-hourly forcing data from the weather generator exhibit a diurnal cycle and variability from synoptic to interannual timescales, the latter of which has been shown to play an important role in shaping certain ecosystems [*Zeng and*

Neelin, 2000]. To accelerate convergence, the following procedure was used iteratively until an equilibrium state was obtained. The whole model was run for 2 years. The daily mean meteorological data and hydrological state of the model from this first run were then used to drive the carbon module and vegetation dynamics parameterizations for about 10 years. From this second run, the pertinent model state variables were saved at a monthly time step and then used to drive the soil carbon submodel for about 1000 years. After about 30 iterations, soil and plant carbon stocks and vegetation distribution (in the case vegetation dynamics is activated) were close to equilibrium. At equilibrium, mortality is compensated by sapling establishment and plant growth, and the calculated mean plant age attains a constant value. By definition, simulated equilibrium NEE is close to zero, as the net primary productivity is compensated by heterotrophic respiration and carbon loss to the atmosphere by biomass burning, the small remainder being sequestrated as black carbon.

[74] As stated before, running the model to equilibrium in order to evaluate the simulated soil carbon stocks is problematic, but inevitable in particular in global applications because the state of the global soil carbon stock is not well known. There is no impact of this initialization method on simulated global NPP or GPP. These attain near-equilibrium values within a few tens of years (a few years for GPP), as nutrient cycles are not modeled in the model. Once the model was in equilibrium, it was run for five final years. The results presented in this section are mean values over this final period.

4.1. Seasonal Leaf Cover

[75] Seasonal LAI λ is evaluated by comparing modeled and MODIS satellite products [*Myneni et al.*, 2002]. Since $\lambda \geq 0$, the quality of modeled monthly LAI over a whole annual cycle at each grid point can be evaluated using the following definition of a figure of merit in time (*FMT* [*Hourdin et al.*, 1999]):

$$FMT = 100\% \frac{\sum_i \min\left(\lambda_{mod,i}, \lambda_{sat,i}\right)}{\sum_i \max\left(\lambda_{mod,i}, \lambda_{sat,i}\right)}. \quad (4)$$

Here i indicates the time axis (e.g., from 1 to 12 for monthly time series). The FMT varies from 0 to 100%. A FMT of 0% indicates the two time series differ widely (no overlap between the time series), while FMT = 100% means that the observed and simulated LAI match exactly over the whole year. To give the reader a feeling for how good or bad the agreement between two LAI time series with a given FMT is, Figure 6 shows an example of simulated and satellite-derived LAI time series for which FMT = 64% (which is close to the global mean FMT, as shown below).

[76] Because both snow cover and low solar angles lead to large errors in the satellite LAI, the FMT is evaluated using only satellite data for snow-free months during which the sun is more than 30° above the horizon at local noon. This means that only the beginning of the growing season (about 3 months around the summer solstice) is evaluated in polar regions. For desert regions, defined as regions in which both simulated and satellite-derived LAI are permanently lower than 0.5, the FMT is not evaluated because very small absolute errors in the model LAI would yield a misleadingly low FMT.

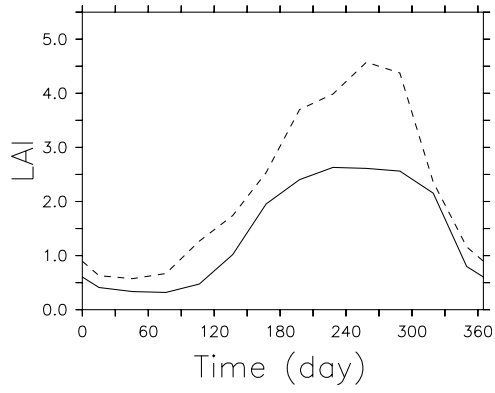

Figure 6. Simulated (solid line) and satellite-derived (dashed line) LAI for 10°E, 10°N in STAT. For these two specific time series, FMT is 64%.

[77] Figure 7 displays the FMT of the simulated LAI for both global simulations. Global mean FMT for both simulations is 63% (it is interesting to note in this respect that an alternative satellite vegetation cover data set [*Tucker et al.*, 2001] has, with respect to the data used here, a global mean FMT of 64%, just as much as the score obtained by ORCHIDEE), and the global patterns are very similar, with generally high values in regions with predominantly woody vegetation and lower values in (semi)arid and tundra regions. As one would expect the prescribed vegetation distribution in STAT to be more realistic than the calculated distribution in DYN, it is surprising that the global mean FMT is the same in DYN and STAT. However, the fact that the FMT in DYN and STAT are very similar might also be due to error compensation in DYN (a misfit in the simulated LAI of individual PFTs being fortuitously compensated by a misfit in the calculated PFT distribution, yielding a relatively correct total grid-scale LAI). This occurs, for example, in the Eurasian forest belt, where the percentage of herbaceous vegetation is underestimated in DYN (see section 4.2), while the tree LAI is underestimated in both simulations. Increased tree fractions in DYN compensate for the underestimate of the LAI of the individual plants. The generally lower FMT in regions where photosynthesis is water-limited [*Nemani et al.*, 2003] is in part due to the previously mentioned fact that when the LAI is low, even fairly small absolute errors of the simulated LAI lead to a rather low FMT. On the other hand, modeled LAI in these regions is consistently too low, indicating a clear systematic error of ORCHIDEE. In fact, the modeled LAI is generally too low outside the equatorial belt, not only in (semi)arid regions. This can be seen in Figure 8, which displays the simulated and satellite-derived zonal mean LAI. The underestimate is particularly strong in the Northern Hemisphere middle and high latitudes in summer, partly because absolute LAI errors can be larger where absolute LAI values are large (in this context, note that, because satellite LAI estimates are subject to fairly large uncertainties for dense canopies [*Carlson and Riplay*, 1997], this low LAI bias

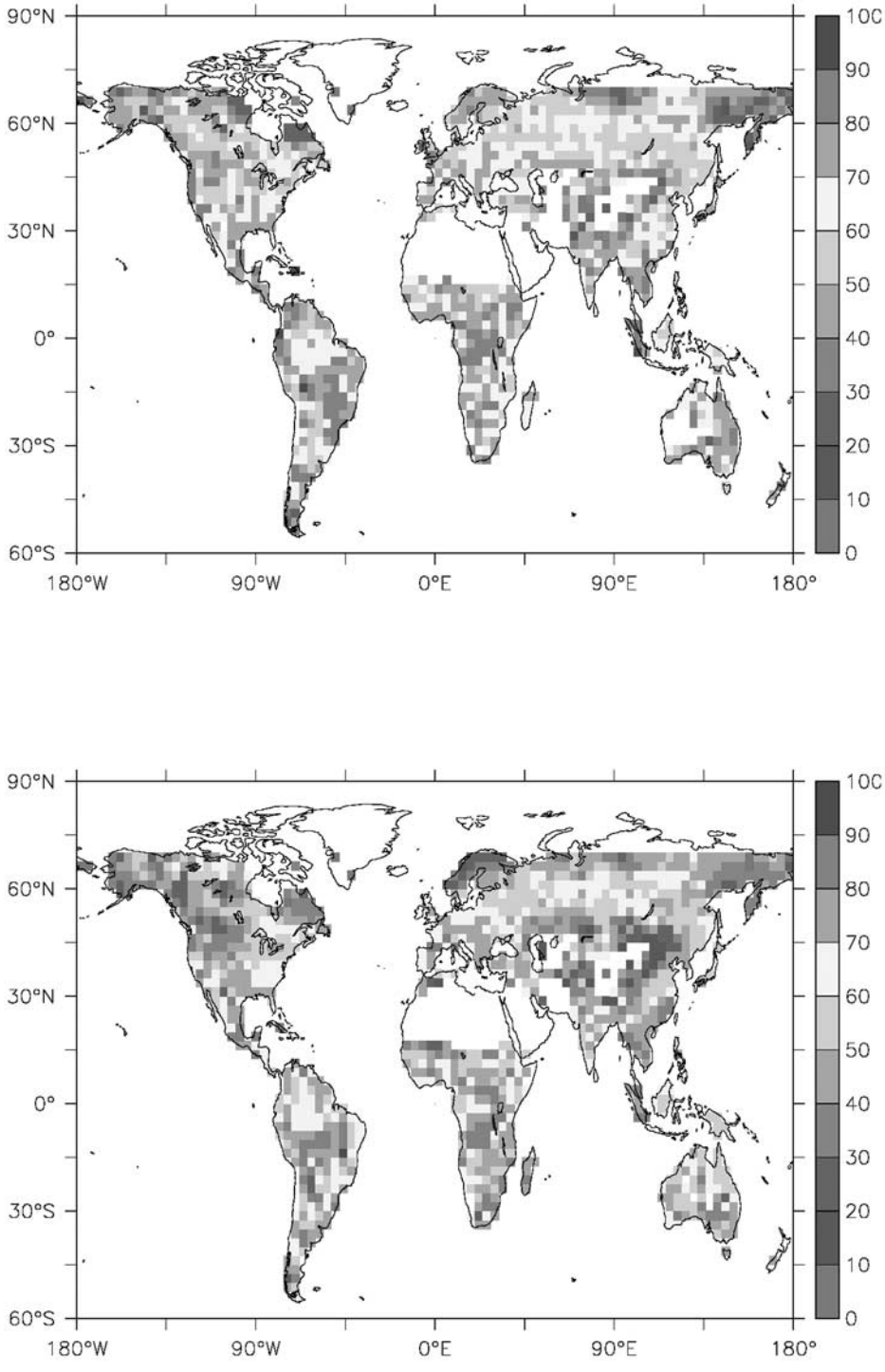

Figure 7. FMT (in %) of the simulated LAI from (top) STAT and (bottom) DYN. See color version of this figure at back of this issue.

might, at least in part, be due to problems in the satellite data set). In both simulations, the maximum LAI is reached about 6 weeks too late. As the onset of the growing season seems to occur with the right timing, this delay might be due to insufficient carbon translocation from the carbohydrate reserves toward leaves and fine root at the beginning of the season, or to the fact that winter crops, which grow early in the season, are frequent in the Northern Hemisphere extra-

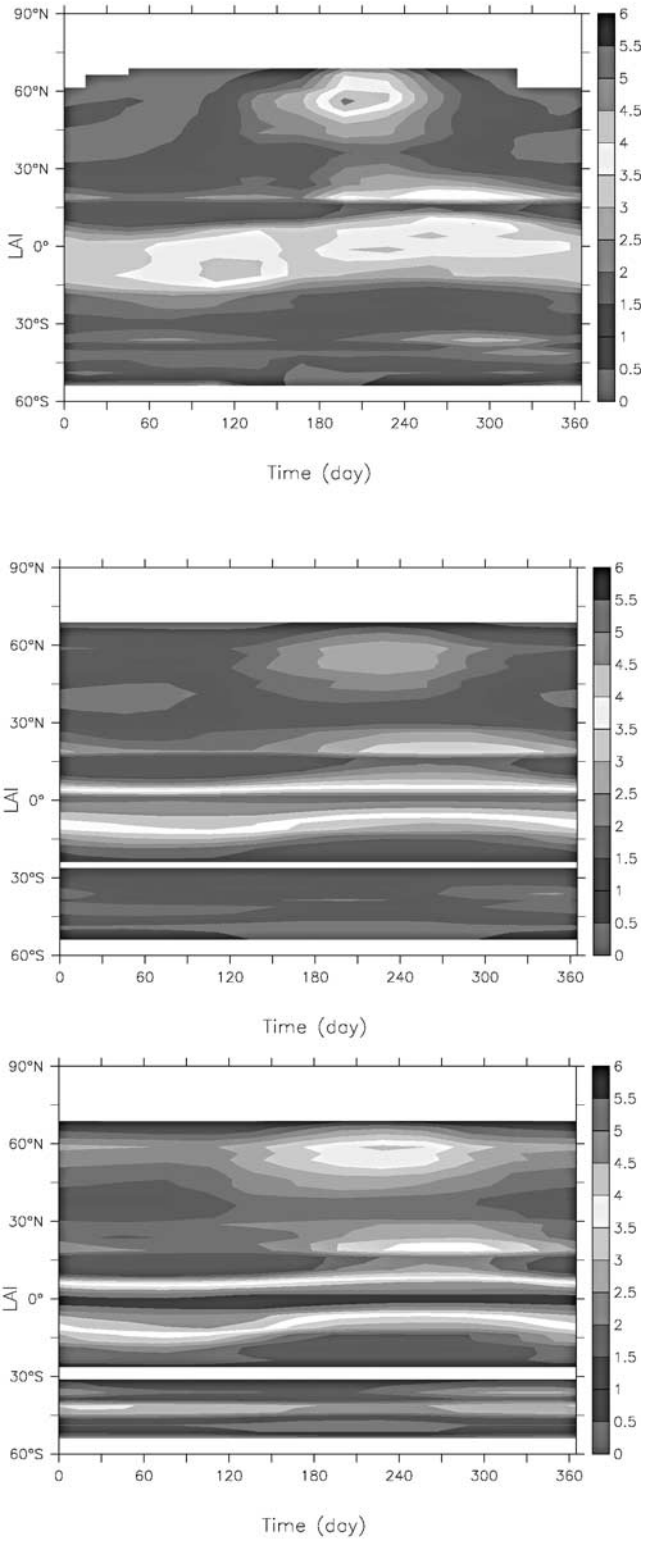

Figure 8. (top) Observed and ((middle) STAT and (bottom) DYN) simulated zonal mean LAI. See color version of this figure at back of this issue.

tropics, and their phenology is poorly represented in ORCHIDEE.

4.2. Present-Day Vegetation Distribution

[78] The modern potential natural vegetation distribution calculated in DYN is shown in Figures 9 and 10. Figure 9 shows a Red-Green-Blue (RGB) composite-color map of the annual maximum foliage projective cover (equation (2)) in STAT and DYN partitioned according to vegetation phenology between evergreen woody, deciduous woody and herbaceous plants, while Figure 10 displays the partitioning according to vegetation morphology between needleleaf woody, broadleaf woody, and herbaceous plants. As STAT uses prescribed vegetation distribution (that is, v_{max} in equation (2) is prescribed), any misfits in the simulated foliage projective cover v in STAT are caused by errors in the simulated LAI λ of the PFTs present in the grid box (see equation (2)). Furthermore, comparing the foliage projective cover between DYN and STAT allows evaluation of the vegetation distribution simulated in DYN directly, because LAI errors of the individual PFTs will be similar; a comparison between the foliage projective cover simulated in DYN and observed foliage projective cover would yield less direct information because misfits in DYN are a combined result of errors in LAI and vegetation distribution. In regions where a large fraction of the total space is agricultural (e.g., Europe), the figures are necessarily very similar, as even in DYN, agricultural vegetation fractions were prescribed. ORCHIDEE reproduces well the position of the limits of the Earth's forest belts in the Northern Hemisphere extratropics and in the equatorial regions, as well as the boundary between tundra and taiga in the boreal regions and the transition from equatorial forests to grasslands in the tropics. Figure 9 shows that the partitioning between evergreen and deciduous woody PFTs is generally well reproduced, for example in Eastern Siberia where the *Larix*-dominated space is correctly simulated. However, the model does not reproduce the predominance of deciduous woody PFTs in New England and Québec. Similarly, the partitioning between needleleaf and broadleaf woody PFTs is globally well reproduced, except in eastern North America.

[79] The main weaknesses of the simulated vegetation distribution are the following:

[80] 1. The global extent of evergreen woody PFTs is overestimated, as these PFTs occupy 35% of the global nonagricultural surface in DYN compared to only 19% in STAT. By contrast, the global extents of deciduous woody PFTs (14% of the global nonagricultural surface in DYN versus 12% in STAT) and herbaceous vegetation (18% in DYN versus 17% in STAT) are quite well captured by ORCHIDEE. This model bias leads to an overestimate of the simulated global extents of broadleaf woody PFTs (30% in DYN versus 22% in STAT) and needleleaf woody PFTs (19% in DYN versus only 8% in STAT). Understanding the reasons for this bias is the object of ongoing studies.

[81] 2. Globally, fractional vegetation coverage is higher in DYN than in STAT. This can be seen in Figures 9 and 10, and in Figure 11 which displays, as an example, the simulated annual maximum fractions of tropical evergreen trees, tropical deciduous trees, and grass in a meridional cut

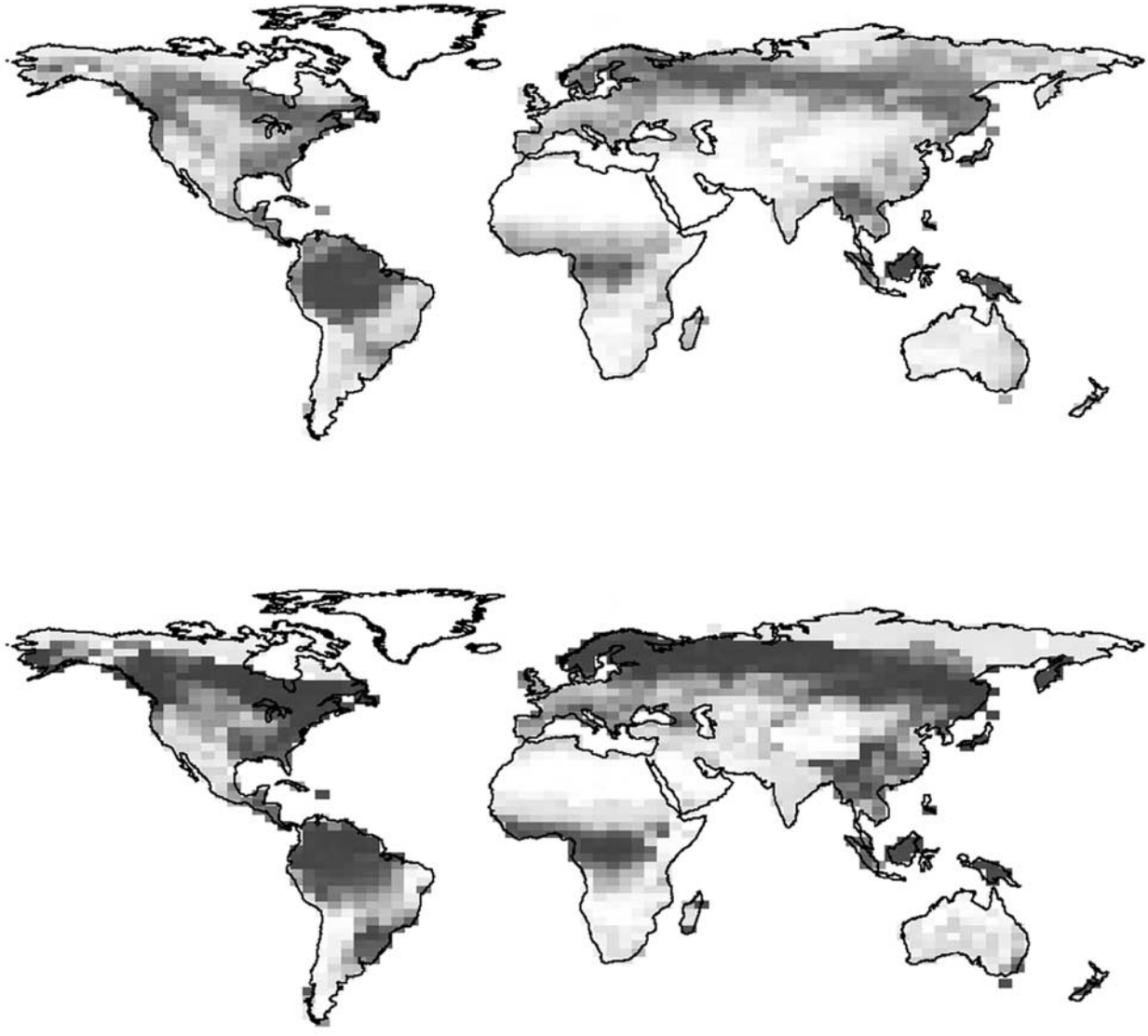

Figure 9. Composite-color map of the simulated annual maximum foliage projective cover (v) in (top) STAT and (bottom) DYN, partitioned according to phenology. STAT uses the observed vegetation distribution; therefore, differences between STAT and DYN are due to vegetation dynamics in DYN. Color coding is such that saturation indicates total grid-scale annual maximum v, while hue indicates the relative v of the following three PFT groups: evergreen woody (blue), deciduous woody (red), and herbaceous (green) plants. See color version of this figure at back of this issue.

through Africa at 20°E. The overestimate of vegetation density is surely, at least in part, linked to the fact that in DYN, the model freely chooses what it "thinks" to be the most productive vegetation assembly, unlike in STAT, where the PFT fractions are prescribed. However, this might also point to an underestimation of plant mortality and/or of the impact of external disturbances (e.g., fire, herbivory, or windthrow, the latter not being taken into account in ORCHIDEE), in particular for trees, as their fractional coverage is overestimated in the Earth's forest belts at the expense of bare soil or grass.

[82] 3. ORCHIDEE tends to exaggerate the dominance of the most adapted PFT or PFT group. Again, this can be seen in Figures 9 and 10, and more clearly in Figure 11. The model captures very well the latitudinal transitions between the regions dominated by the different PFTs, but within each of these regions, the fractional cover of the dominant PFT is overestimated, while the surface fraction of the nondominant PFTs is too low. This might also point to an underestimation of plant mortality and/or of the impact of external disturbances. Additional space liberated by such processes could be colonized equally by young individuals of all PFTs present in the grid cell, thereby favoring the nondominant PFTs. Part of this discrepancy might be due to the fact that pasture or degraded forest areas do not exist in the model.

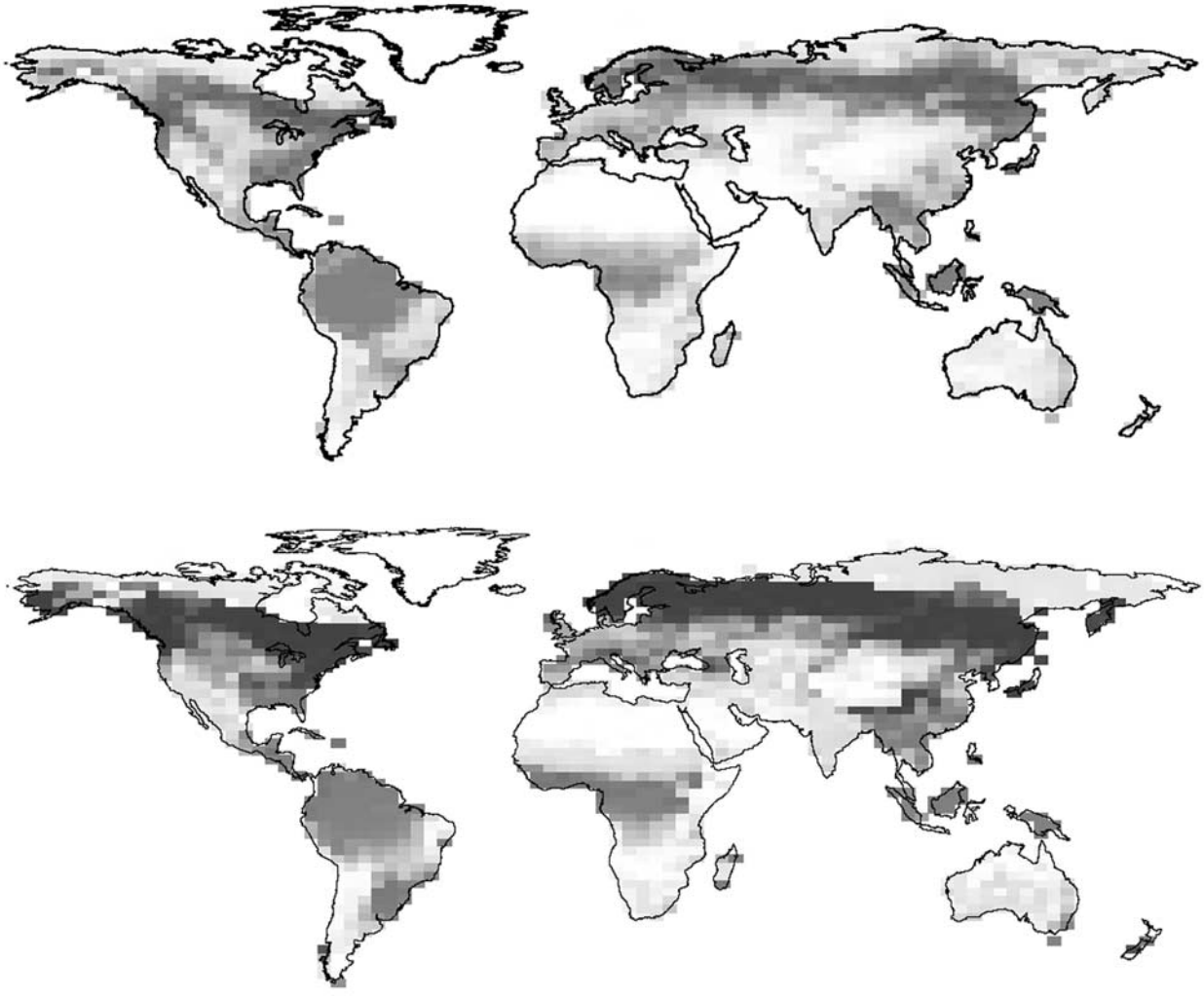

Figure 10. Composite-color map of the simulated annual maximum foliage projective cover (v) in (top) STAT and (bottom) DYN, partitioned according to vegetation morphology. STAT uses the observed vegetation distribution; therefore, differences between STAT and DYN are due to vegetation dynamics in DYN. Color coding is such that saturation indicates total grid-scale annual maximum v, while hue indicates the relative v of the following three PFT groups: needleleaf woody (blue), broadleaf woody (red), and herbaceous (green) plants. See color version of this figure at back of this issue.

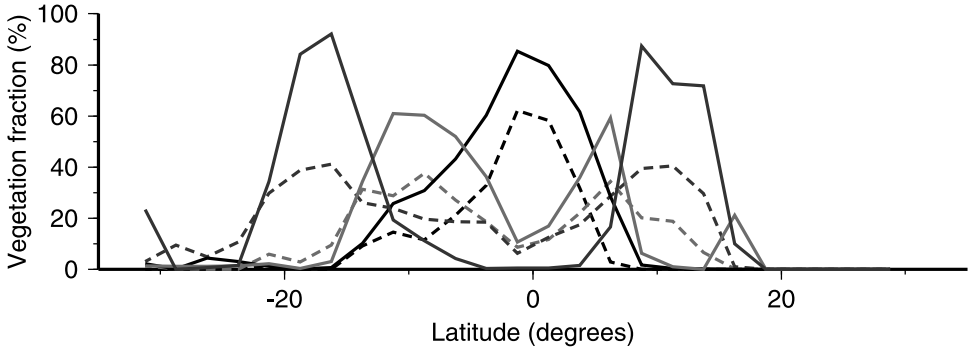

Figure 11. Simulated annual maximum foliage projective cover (v) of tropical evergreen trees (black), tropical deciduous trees (red), and grass (blue) in a meridional cut through Africa at 20°E. Solid lines: DYN; dotted lines: STAT. See color version of this figure at back of this issue.

[83] There is an apparent inconsistency between the tendency of ORCHIDEE to underestimate leaf area index (compared to satellite observations) reported in section 4.1 and the overestimate of vegetation density reported here (compared to the vegetation density in STAT, obtained using prescribed vegetation distribution). This might be due to errors in the translation of the original vegetation map [*Loveland et al.*, 2000] into the PFT fractional coverage input data; it is possible that bare soil fractions have been overestimated in STAT. For example, it is not clear whether the "warm semi desert shrubs" vegetation type of *Loveland et al.* [2000] should really be translated into 70% of bare soil in ORCHIDEE, or whether a higher vegetation density should be prescribed, knowing that under a semi-desert climate, the simulated LAI of the prescribed plants is likely to be low anyway.

[84] It is noteworthy that some clear differences exist between the vegetation structure simulated by ORCHIDEE and that obtained with the original LPJ code, although the parameterizations of vegetation dynamics in ORCHIDEE have been taken from LPJ [*Sitch et al.*, 2003] with little modification. For example, *Sitch et al.* [2003] report that LPJ tends to overestimate the extent of broadleaf woody vegetation, while ORCHIDEE simulates too much evergreen (in particular, needleleaf evergreen) woody vegetation. It is probable that these differences are due to the fact that the processes on short and intermediate timescales (photosynthesis, autotrophic respiration, carbon allocation, phenology, etc.) are calculated differently in LPJ and in ORCHIDEE, but it is also possible that more indirect effects or the use of different meteorological forcing data influence the simulated vegetation dynamics.

4.3. Carbon Stocks and Fluxes

4.3.1. Primary Productivity

[85] Global mean net primary productivity (NPP) from STAT and DYN is displayed in Figure 12. Global mean NPP in STAT is 64.0 GtC yr^{-1}. It is somewhat higher in DYN (73.7 GtC yr^{-1}) because of the reasons discussed at the beginning of section 4.2. The carbon stocks and fluxes of DYN will not be discussed any further in the following. The simulated global NPP in STAT is on the high end of the range of 44.4–66.3 GtC yr^{-1} simulated by the terrestrial biogeochemistry models participating in the Potsdam NPP Intercomparison Project [*Cramer et al.*, 1999]. A reason for part of this difference may be that 1961–1990 climate data and an atmospheric CO_2 concentration of 350 ppmv were used here, while most of the simulations carried out in the NPP model intercomparison exercise used the 1930–1961 climate input, which is slightly cooler in the Northern Hemisphere [*Mann et al.*, 1999], and a slightly lower atmospheric CO_2 concentration (340 ppmv). It might also be in part due to the fact that nitrogen limitation, a key control on productivity in many ecosystems, particularly in the high latitudes [*Vitousek and Howarth*, 1991], is not taken into account in ORCHIDEE (however, most of the models participating in the recent Potsdam NPP Intercomparison Project do not explicitly model the nitrogen cycle either). Indeed, ORCHIDEE overestimates NPP in the Siberian boreal forest, where growth is, as typical for arctic and boreal regions, limited not only by the shortness of the growing season, but also by nitrogen availability [*Hobbie et al.*, 2002]: Mean NPP of Siberian boreal forest in STAT is 453 gC m^{-2} yr^{-1}, while stand-level observations [*Jarvis et al.*, 2001; *Ciais et al.*, 2004] indicate a mean value of 281 ± 94 gC m^{-2} yr^{-1} (supposing a ratio of aboveground to total NPP of 0.4; using a higher ratio would lead to a higher NPP estimate) and extensive forest biomass inventories yield an NPP of 228 ± 14 gC m^{-2} yr^{-1} [*Shvidenko and Nilsson*, 2003; *Ciais et al.*, 2004]. By contrast, in Europe, where there is more nitrogen deposition because of the longer growing season, simulated mean forest NPP (563 gC m^{-2} yr^{-1}) is in better agreement with the 617 ± 182 gC m^{-2} yr^{-1} observed in stand studies [*Schulze et al.*, 2000; *Ciais et al.*, 2004] and the 448 gC m^{-2} yr^{-1} from extensive forest biomass inventories [*Ciais et al.*, 2004]. Similar good agreement is obtained in Amazonia, where forest stand studies indicate an NPP of 820 ± 170 gC m^{-2} yr^{-1} [*Clark et al.*, 2001; *Ciais et al.*, 2004] and forest biomass inventories yield an NPP of 914 ± 255 gC m^{-2} yr^{-1} [*Ciais et al.*, 2004], while ORCHIDEE simulates 932 gC m^{-2} yr^{-1}.

[86] The global gross primary productivity (GPP) is slightly more than twice the global NPP (137.4 GtC yr^{-1} in STAT), with the highest NPP/GPP ratios (up to 70%, not shown) occurring in the high latitudes where autotrophic respiration rates are lowest, and lowest NPP/GPP ratios (locally about 30%) occurring in the equatorial belt. Local maxima (about 50%) occur at ±15° latitude. These are due to the fact that herbaceous vegetation is preponderant in these regions; grasses have a higher ratio between leaf and total biomass, and thus a more favorable NPP/GPP ratio, as autotrophic respiration occurs in all living plant tissues, while photosynthesis occurs in the leaves.

4.3.2. Carbon Stocks

[87] Simulated global totals for equilibrium vegetation, litter, and organic soil carbon are 641, 356, and 1177 PgC, respectively. Concerning vegetation carbon (Figure 13), this is similar to previously published model estimates [e.g., *Foley et al.*, 1996; *Kucharik et al.*, 2000; *Sitch et al.*, 2003]. However, compared to regional estimates of forest biomass [*Dixon et al.*, 1994], ORCHIDEE simulates too much vegetation carbon in the low latitudes. This can be seen in Table 3 which displays a regional breakdown of simulated forest biomass compared to these estimates. The overestimate is particularly high in Amazonia. However, it is noteworthy in this respect that *Houghton et al.* [2001] have shown that estimates of forest biomass in the Amazon region vary by more than a factor of 2.

[88] The overestimate of vegetation mass in the low latitudes is linked to an overestimate of C residence time, itself due to an underestimate of tree mortality in these regions. Carbon residence time τ in vegetation, defined as the ratio between living biomass and net primary productivity in equilibrium and displayed in Figure 14, locally exceeds 60 years in the heart of Amazonia and in Indonesia, while *Whittaker and Likens* [1975] report carbon residence times of about 20 years in tropical rain forests. In these regions, simulated mean age of tropical broadleaf evergreen trees exceeds 70 years, which is higher than typical mean tree ages of about 50 years in tropical rain

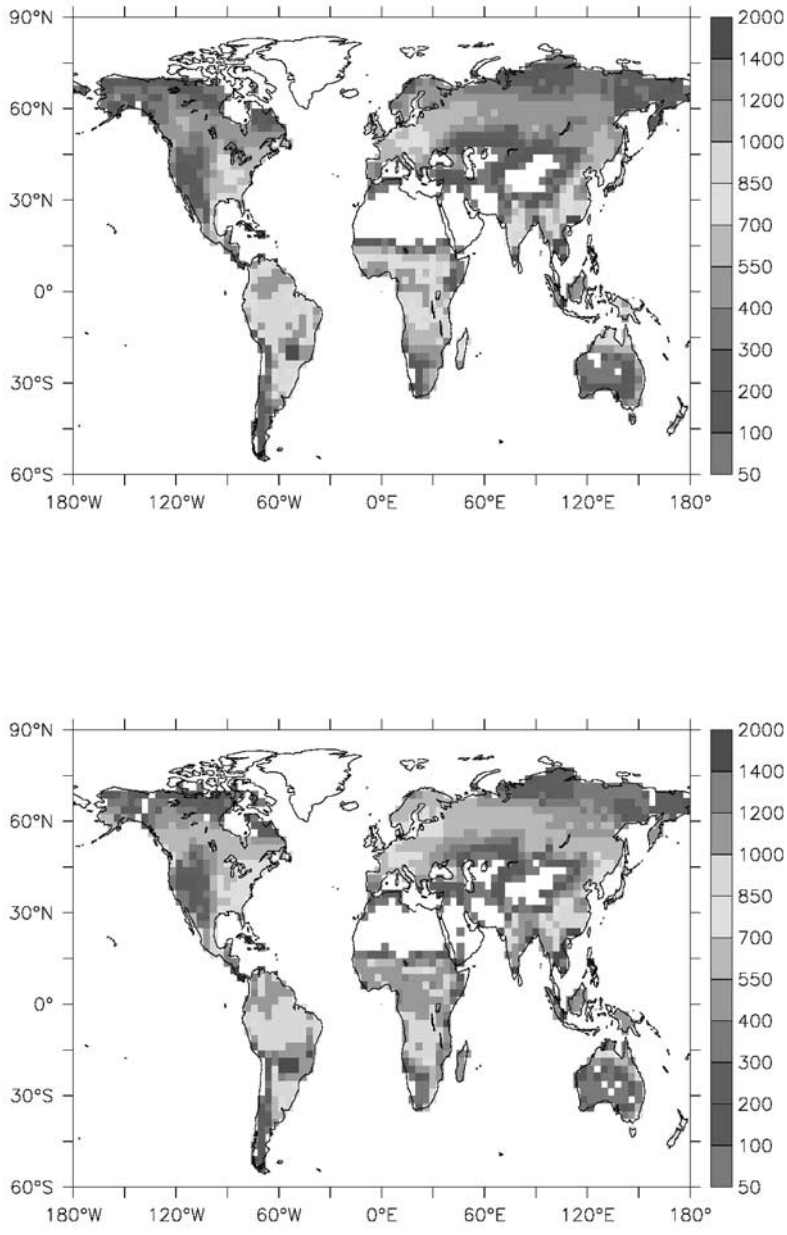

Figure 12. Simulated annual mean NPP (in gC m^{-2} yr^{-1}) for (top) STAT and (bottom) DYN. See color version of this figure at back of this issue.

forests [*Lieberman et al.*, 1985]. The reason might be, as mentioned before, the missing representation of disturbances other than fires, or the overly simplistic representation of gap dynamics. Understorey vegetation, absent in ORCHIDEE, is also typically composed of more short-lived species which reduce the mean carbon residence time in the vegetation of these ecosystems. Herbivory, which could also be seen as a disturbance which should decrease the trees' life span, is taken into account in the model, but a subtle but unrealistic interplay between the formulation of natural mortality and herbivory in the model might actually decrease tree mortality in tropical areas, where herbivory is particularly important. As described in section 2.4, calculated mortality is low when the annual biomass increase, linked to NPP, is large compared to the tree's annual maximum leaf mass. However, herbivory decreases the annual maximum leaf mass and has little impact on the simulated NPP. When herbivory is taken into account, simulated mortality therefore decreases, and mean tree age and thus carbon residence time increase correspondingly.

[89] The size of the litter pool, comprising aboveground and belowground litter, appears overestimated, both with respect to the size of the vegetation carbon pool and with respect to other model results [e.g., *Kucharik et al.*, 2000; *Sitch et al.*, 2003]. By contrast, total organic soil carbon is on the lower end of current estimates of about 1200–

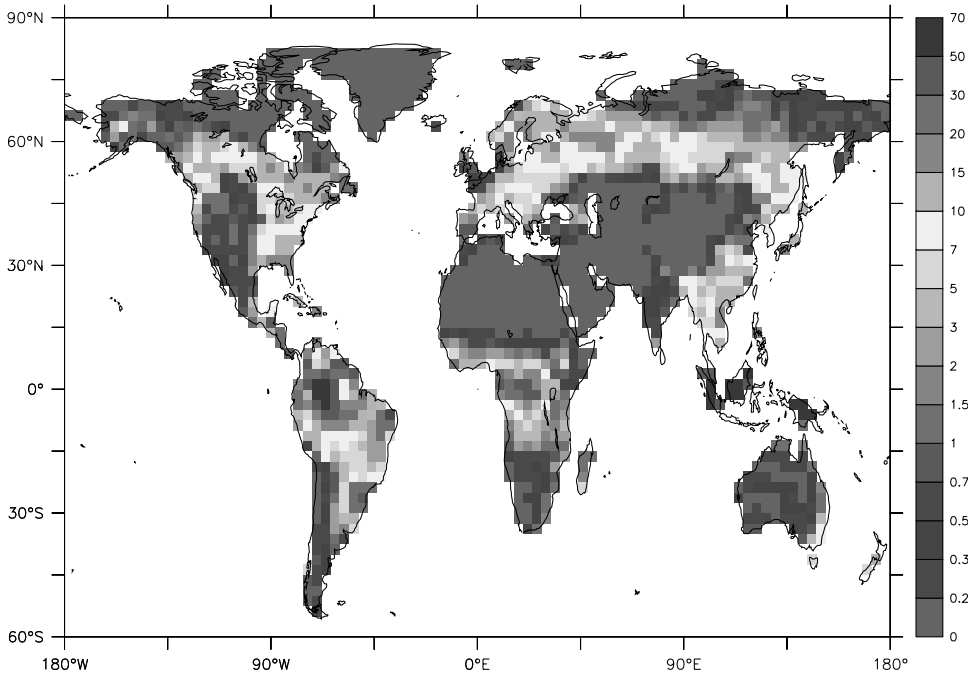

Figure 13. Mean aboveground and belowground biomass of natural vegetation (in kgC/m^2) in STAT. See color version of this figure at back of this issue.

1600 PgC [*Post et al.*, 1982; *Zinke et al.*, 1986; *Schlesinger*, 1991; *Eswaran et al.*, 1993; *Sombroek et al.*, 1993; *Batjes*, 1996]. However, soil C estimates are typically measures of total organic carbon to 1 m depth, with large woody roots removed, and include necessarily all small roots and recent root litter; this might explain the relative overestimate of the litter pool as well as the light underestimate of the soil carbon pool by ORCHIDEE. Figure 15 displays the simulated and observed (N. H. Batjes, Global data set of derived soil properties, 0.5-degree grid (ISRIC-WISE), 2000, Oak Ridge National Laboratory Distributed Active Archive Center available online at http://www.daac.ornl.gov) organic soil carbon. Compared to these observations, the simulated organic soil carbon is globally correct, but too high in east Siberia, and too low in the northern parts of Europe, West Siberia, and North America. The negative biases in North America and West Siberia are mainly located in areas with high wetland fractions [e.g., *Matthews and Fung*, 1987]. High organic soil carbon contents are characteristic for the humid wetland soils [*IPCC*, 2001]. Because ORCHIDEE does not simulate wetlands, the underestimate of organic soil carbon in these regions was expected.

4.4. Global Runoff

[90] Simulated global total runoff in STAT is 39.2 $\times$ 10^{12} m^3 yr^{-1}, which is well within the current range of estimates between 36.5 $\times$ 10^{12} m^3 yr^{-1} [*Chanine*, 1992] and 45.5 $\times$ 10^{12} m^3 yr^{-1} [*Cogley*, 1998]. The simulated global total runoff in DYN (34.9 $\times$ 10^{12} m^3 yr^{-1}) is at the lower boundary of these estimates. As the prescribed observed precipitation is the same in DYN and STAT, this means that there is probably too much evaporation in DYN, which is coherent with the fact that primary productivity is too high and vegetation cover is too dense in this run. In both simulations, zonal mean runoff (Figure 16) is lower than estimates by *Cogley* [1998] in the Southern equatorial region (essentially Amazonia) and in the boreal latitudes. This is consistent with the overestimate of the LAI in equatorial regions (see section 4.1 and Figure 8) and with the overestimate of the NPP in the Earth's boreal forest belt reported in section 4.3.

5. Conclusion and Perspectives

[91] The results presented in the previous sections show that ORCHIDEE is capable of simulating water, energy, and

Table 3. Simulated (STAT) and Estimated [*Dixon et al.*, 1994] Size of Forest Vegetation Carbon Pool[a]

Region	Simulated	Observed
	High Latitudes	
Russia	62	74
Canada	33	12
Alaska	1.5	2
	Midlatitudes	
Continental United States	26	15
Europe	6	9
China	12	17
Australia	3.4	18
	Low Latitudes	
Asia	118	41–54
Africa	82	52
Americas	210	119

[a]Size of forest carbon vegetation pool is given in PgC. High latitudes: between 50°N and 75°N; midlatitudes: between 25° and 50° (north and south); low latitudes: between 25°S and 25°N.

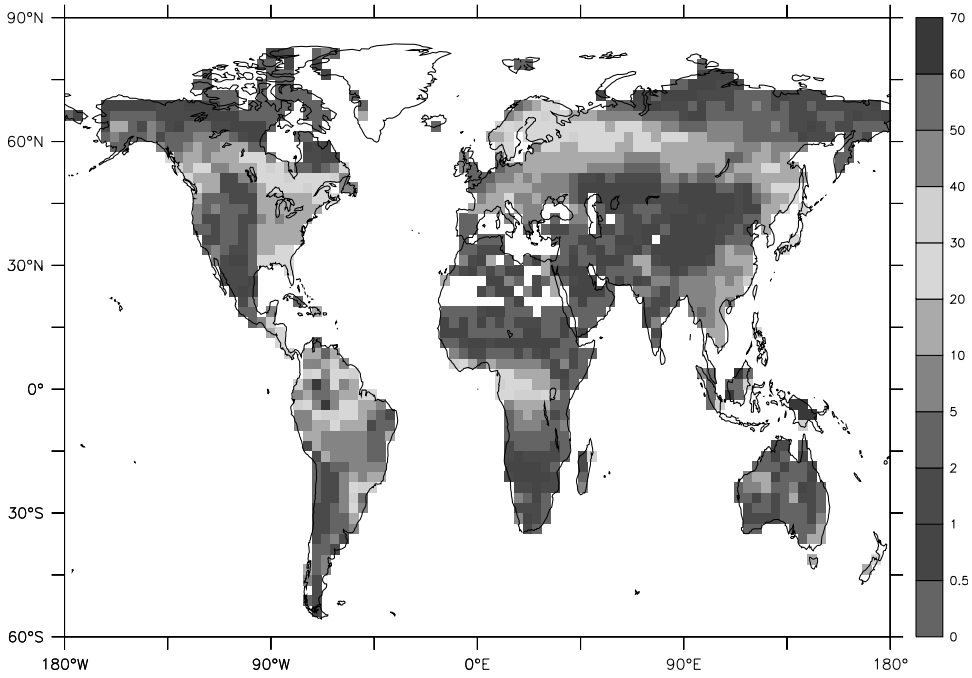

Figure 14. Residence time of carbon in natural vegetation (years) simulated in STAT. See color version of this figure at back of this issue.

carbon exchanges and stocks on the continental surface in line with current best estimates, representing vegetation processes on both short (diurnal cycle) and long (multiannual) timescales, and vegetation-atmosphere exchanges on the local scale as well as global mean vegetation characteristics (extent, morphological properties, carbon stocks, and fluxes). These are important prerequisites for ORCHIDEE to be used as a component of an Earth system model. It is impossible to exactly evaluate the capacity of such a model to correctly simulate the global carbon state, because both the present state and its history, necessary for model initialization, are not well known on the global scale. The diurnal and seasonal dynamics of carbon fluxes are correctly represented by ORCHIDEE. This makes us confident that the model is able to simulate interannual variability of the global carbon fluxes and stocks; this capacity is also important for coupled climate system/carbon cycle studies.

[92] This work shows that fast and slow biogeophysical processes can be treated synchronously in a climate model. The impacts of processes usually not treated on subannual scales in DGVMs coupled to general circulation models, such as fires, which can play an important role in regional-scale air and photochemistry, can in this manner be taken into account in Earth system models. Throughout the development of ORCHIDEE, a main goal was to construct as free a model as possible. For example, the phenological cycle had to be fully prognostic, so that the model can be used for simulations of periods where no satellite observations of LAI are available. This goal was essentially achieved, but the results indicate that more biophysical and physiological processes might have to be explicitly represented to improve model performance.

[93] On the global level, it is interesting that there is a global underestimate of LAI in spite of a probable overestimate of global productivity due to the missing representation of nutrient limitation. Consequently, one of the most important future developments of the model will be the inclusion of a prognostic nitrogen cycle, allowing, among others, an explicit representation of nitrogen limitation in the carbon allocation scheme and, more critically, more realistic simulation of plant productivity in nitrogen-limited environments. This is also necessary in the context of climate change experiments, the results of which may depend critically on the representation of nitrogen limitation [*Hungate et al.*, 2003]. Future pertinent developments of the LPJ dynamic global vegetation model will have to be included in ORCHIDEE. The inclusion of a more detailed soil hydrology [*de Rosnay et al.*, 2002], which hopefully will improve the model behavior in arid regions, will also be an important future development. Further developments will include, among others, a distinction between direct and diffuse solar radiation in the photosynthesis parameterizations. A version of ORCHIDEE coupled to a detailed crop model yields encouraging results in agricultural areas [*de Noblet-Ducoudré et al.*, 2004]. A similar activity has been started for pastures.

Appendix A: Description of STOMATE

A1. Photosynthesis and Stomatal Conductance

A1.1. At the Leaf Level

[94] *Ball et al.* [1987] have derived an empirical expression for stomatal conductance g_s (mol m^{-2} s^{-1}) as a function of assimilation A (μmol m^{-2} s^{-1}), atmospheric

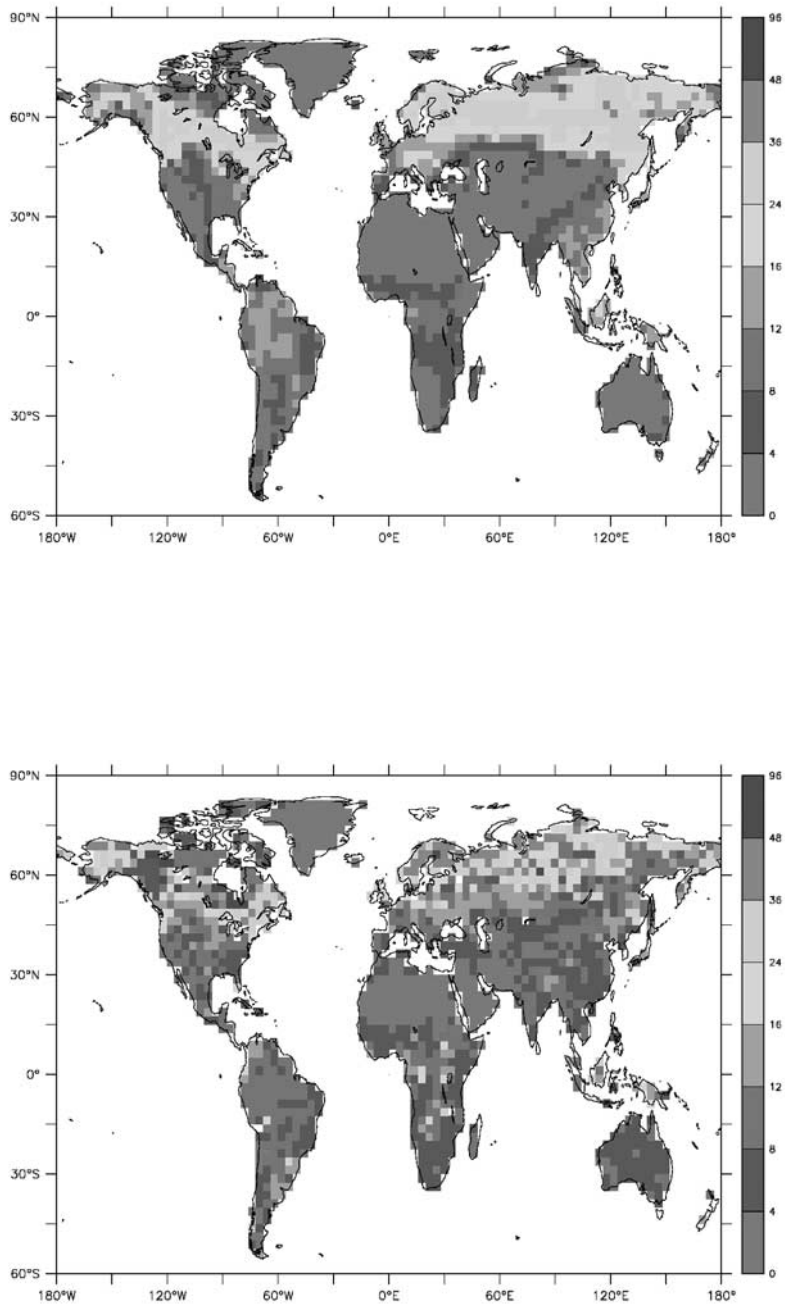

Figure 15. Organic soil carbon in kg m^{-2}: (top) simulated and (bottom) observed (N. H. Batjes, Global data set of derived soil properties, 0.5-degree grid (ISRIC-WISE), 2000, available online at http://www.daac.ornl.gov). The observed soil organic carbon (between 0 and 1 m depth) was interpolated to the model grid. See color version of this figure at back of this issue.

CO_2 concentration C_a (ppm), and relative air humidity h_r(%),

$$g_s = mA\frac{h_r}{C_a} + b. \tag{A1}$$

Here, m and b are derived from laboratory measurements using C_3 species.

[95] Assimilation is calculated from *Farquhar et al.* [1980],

$$A_n = V_c\left(1 - \Gamma*/C_i\right) - R_d. \tag{A2}$$

V_c (μmol $m^{-2}s^{-1}$) is the rate of carboxylation, $\Gamma*$ (ppm) is the CO_2 compensation point when there is no nonphotor-

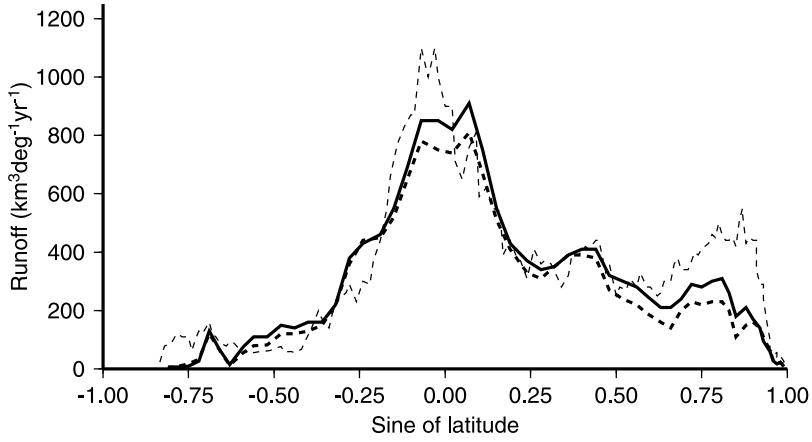

Figure 16. Estimated and simulated zonal mean total annual runoff (in $km^3\ deg^{-1}\ yr^{-1}$). Thin dashed line: estimates after *Cogley* [1998]; thick dashed line: STAT; thick solid line: DYN.

espiratory respiration, R_d ($\mu mol\ m^{-2}\ s^{-1}$) is the rate of nonphotorespiratory respiration, and C_i the CO_2 concentration at the carboxylation site.

[96] The rate of carboxylation is expressed as the more limiting factor of Rubisco activity W_c and RuBP regeneration W_j ($\mu mol\ m^{-2}\ s^{-1}$),

$$V_c = \min(W_c, W_j). \tag{A3}$$

The Rubisco-limited rate is given by

$$W_c = \frac{V_{c\max} C_i}{C_i + K_C(1 + O_i/K_O)}. \tag{A4}$$

$V_{c\max}$ ($\mu mol\ m^{-2}\ s^{-1}$) is the maximum rate of RuBP carboxylation, K_C and K_O are the Michælis-Menten constants for enzyme catalytic activity for CO_2 and O_2, respectively, and O_i is the intercellular concentration of oxygen.

[97] The RuBP-regeneration-limited rate is defined by

$$W_j = \frac{V_j}{1 + 2\Gamma*/C_i}. \tag{A5}$$

V_j is the potential rate of RuBP regeneration. It depends on the incident photon flux I. V_j can be empirically described using a nonrectangular hyperbola,

$$V_j = \frac{1}{2\Theta}\left[\alpha_j I + V_{j\max} - \sqrt{(\alpha_j I + V_{j\max})^2 - 4\Theta\alpha_j I V_{j\max}}\right]. \tag{A6}$$

Here α_j is the quantum yield of RuBP regeneration, $V_{j\max}$ is the maximum potential rate of RuBP regeneration at quantum-saturation, and Θ is the curvature of the quantum response.

[98] An equivalent simplified model of photosynthesis has been developed for C_4 plants by *Collatz et al.* [1992]. The photosynthesis is in this case defined by a pair of nested quadratic functions. The first one is expressed as

$$\Phi M^2 - M(V_T + \alpha Q) + V_T \alpha_T Q = 0, \tag{A7}$$

where V_T is the temperature-dependent, substrate-saturated, Rubisco capacity (equivalent of $V_{j\max}$ in the C_3 model), α_T is the quantum efficiency, and M is the flux determined by the Rubisco and light limited capacities. The second quadratic function is given by

$$\beta A^2 - A(M + k_T C_i) + M k_T C_i = 0, \tag{A8}$$

where k_T is the temperature-dependent pseudo-first-order rate constant of assimilation response to CO_2, and Φ, β are the curvatures of the two quadratics. The smaller roots are the appropriate solutions for both equations, and A_n is defined as for C_3 by

$$A_n = A - R_T. \tag{A9}$$

Here R_T is the temperature-dependent nonphotosynthetic respiration.

[99] Equation (A1) gives the stomatal conductance g_s as a function of assimilation A. Equations (A2) and (A9) compute A as a function of C_i. A third equation is introduced in order to relate assimilation and stomatal conductance to the gradient of CO_2 between the atmosphere and the carboxylation site,

$$A_n = g_s(C_a - C_i)/1.6. \tag{A10}$$

The value of 1.6 represents the ratio of water vapor diffusivity to the CO_2 diffusivity. The system formed by equations (A1), (A2) (or (A9)), and (A10) is solved using a simple iterative method that converges very rapidly in most cases.

[100] It is well known that if soil moisture decreases, stomatal resistance will increase through both a direct and an indirect effect, as reviewed by *Farquhar and Sharkey* [1982]. The direct effect involves chemical mediators such as abscisic acid [*Willmer*, 1988; *Zhang and Davies*, 1989]. In the indirect effect, assimilation is first decreased and forces the closure of stomata. There is still no universal agreement on the relative importance of both effects. In the model, water stress influences only the photosynthetic

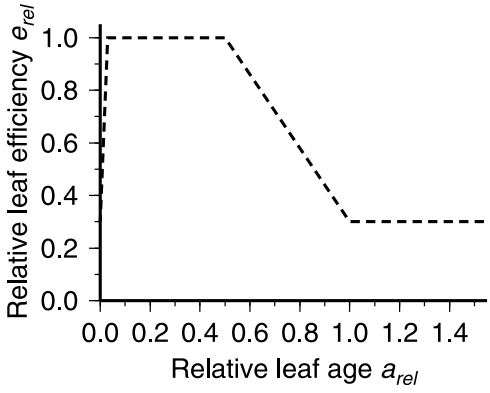

Figure A1. Relative leaf efficiency e_{rel} as a function of relative age a_{rel}.

capacity (i.e., $V_{j\max}$ and $V_{c\max}$). The water stress factor γ_w is defined after *McMurtrie et al.* [1990],

$$\gamma_w = \begin{cases} 1 & \text{if } f_w > f_{w1} \\ 1 - \dfrac{f_w - f_{w0}}{f_{w1} - f_{w0}} & \text{if } f_{w0} < f_w < f_{w1} \\ 0 & \text{if } f_w < f_{w0} \end{cases} \tag{A11}$$

Here f_w is the water fraction available for the plant in the root zone (i.e., $f_w = 0$ at wilting point and $f_w = 1$ at field capacity); $f_{w0} = 0.028$ and $f_{w1} = 0.5$ are the soil water fractions inducing, respectively, closure and maximum opening of the stomata.

[101] The photosynthetic capacity (given through $V_{j\max}$ and $V_{c\max}$, respectively) depends on leaf age through

$$V_{(c,j)\max}(a) = V_{(c,j)\max,opt} e_{rel}(a), \tag{A12}$$

where a is the leaf age, e_{rel} is the relative photosynthetic efficiency, and $V_{(c,j)\max,opt}$ is the PFT-dependent optimum photosynthetic capacity. Figure A1 schematically shows e_{rel} as a function of the relative leaf age a_{rel} (defined as age over the PFT-dependent prescribed mean leaf lifetime), meant to schematically represent the decrease of leaf photosynthetic activity with leaf age [*Ishida et al.*, 1999].

A1.2. At the Canopy Level

[102] Calculation of the equivalent stomatal conductance at the canopy level g_c ($g_c = 1/r_c$) requires the integration of g_s over the canopy depth, that is, over the leaf area index (hereinafter LAI),

$$g_c = \int_0^{LAI} g_s(l)dl, \tag{A13}$$

where l is the cumulative LAI. It increases from the canopy top ($l = 0$) to the canopy bottom ($l = \text{LAI}$).

[103] The assimilation rate ($A_c = \int_0^{LAI} A_n(l)\, dl$) can be integrated in a similar manner. For simplicity, it is assumed that there is no gradient of air humidity, nor of CO_2 within the canopy. Light, on the other hand, decreases with increasing LAI, following Beer-Lambert's law [*Monsi and Sœki*, 1953],

$$I(l) = I_0 e^{-kl},$$

where I_0 is the incident radiation at the top of the canopy, and k is the attenuation coefficient.

[104] Moreover, plants naturally optimize their vertical distribution of nitrogen in order to favor the levels where light is the most abundant. Therefore the maximum rates of RuBP carboxylation ($V_{c\max}$) and regeneration ($V_{j\max}$) also decrease with increasing LAI.

[105] The approach of *Johnson and Thornley* [1984] was used, assuming an exponential decrease of $V_{c\max}$ and $V_{j\max}$ with a nonzero asymptotic limit,

$$V_{(c,j)\max}(l) = V_{(c,j)\max}(0)\left[1 - \lambda\left(1 - e^{-kl}\right)\right]. \tag{A14}$$

For all PFTs, λ is set to 0.7.

A2. Phenology: Leaf Onset

[106] Following *Botta et al.* [2000], different models are applied to the different PFTs in the determination of leaf onset.

[107] 1. In the so-called alternating model [*Murray et al.*, 1989; *Chuine et al.*, 1998], applied to summergreen broadleaf trees, the springtime warmth (sum of growing degree days) g required for leaf onset is a function of the state of chilling, defined as the number of days during which the temperature is under a certain threshold T_c. Springtime warmth g is accumulated after midwinter. "Midwinter" is deemed to have passed when the weekly temperature begins to exceed the monthly temperature (i.e., when temperatures begin to increase). In this case, g is updated if the daily mean temperature T_d exceeds a given threshold T_w,

$$g \leftarrow g + (T_d - T_w)\Delta t \text{ if } T_d/geT_w, \tag{A15}$$

where Δt is STOMATE's time step (one or a few days). The critical warmth g_c to be attained is calculated as

$$g_c = ae^{-bn} - c, \tag{A16}$$

where a, b, and c are positive parameters depending on the PFT and n is the number of chilling days, counted from the moment on when the PFT's weekly net primary productivity (NPP) has fallen below a prescribed fraction (20%) of last year's maximum weekly NPP (i.e., essentially when the plant enters the dormancy season).

[108] 2. A criterion only based on the number of growing days n_g is applied to boreal summergreen needleleaf trees (i.e., *Larix*). The number of growing days n_g is reset to zero when the PFT's weekly net primary productivity is higher than a prescribed fraction (20%) of last year's maximum weekly NPP (see preceding point). It is then updated following

$$n_g \leftarrow n_g + \Delta t \tag{A17}$$

when the daily mean temperature exceeds the threshold $T_c = -5°\text{C}$ and decays exponentially to 0 with a time constant of

50 days (i.e., the number of growing days is counted over 2 months approximately).

[109] 3. A humidity criterion is applied to tropical raingreen trees. Leaf onset occurs a given time after the dry season's moisture availability minimum (the moment of the most severe moisture stress undergone by the plant) has been detected. Plant moisture availability (between 0 for very dry and 1 for very wet conditions) is calculated supposing an exponential root profile decreasing with depth,

$$A_H = \max\left(0.1, \frac{\sum_{i=1}^{n} H_i e^{-z_i/\zeta}\Delta_i}{\sum_{i=1}^{n} e^{-z_i/\zeta}\Delta_i}\right). \tag{A18}$$

Here H_i is the relative soil humidity at the ith soil layer, z_i is the depth of this layer, and Δ_i its thickness. The plant is not limited when $A_H = 1$, and it is under strong stress when $A_H = 0.1$. The root density profile is prescribed by $\zeta = 1.5$ m for trees and $\zeta = 0.3$ m for grasses. A time counter C is set to zero whenever the "monthly" moisture availability $A_{H,m}$ (recalculated at each time step) is lower than the minimum moisture availability $A_{H,m,\min}$ attained up to that date during the dormancy period ($A_{H,m,\min}$ is then set to $A_{H,m}$). The time counter C is updated through

$$C \leftarrow C + \Delta t \tag{A19}$$

when this is not the case. This means that C counts the time that has passed since the moisture minimum (but again only during the dormancy season; see preceding points). When C exceeds a given threshold (50 days for tropical raingreen trees), leaf onset occurs.

[110] 4. Grass phenology depends on the climate zone. In "tropical" regions (multiannual mean temperature $\overline{T} > 20°C$), a moisture criterion very similar to the one described for tropical deciduous trees is applied. In addition, tropical grasses can initiate their growing season simply when the "monthly" moisture exceeds a given threshold (60%), regardless of the timing of the moisture minimum. This allows grasses to react rapidly to soil moisture variations in arid areas, where the temporal evolution of soil moisture can be fairly erratic. In "cool" regions ($\overline{T} < 10°C$), a simple growing degree-day criterion is used. Following *Botta et al.* [2000], the pertinent cutoff temperature for grasses is −5°C, and the growing degree days are counted over the whole dormancy season. The critical sum of growing degree days to be exceeded depends on the PFT and on the multiannual mean temperature $\overline{T}$, as grasses in boreal regions need less warmth to initiate their growth. For C_3 grasses, it is 185° Cd for $\overline{T} = 0°C$ and 400° Cd for $\overline{T} = 30°C$. For C_4 grasses, the critical value is 400° Cd. In the transition zone, both criteria have to be fulfilled. In any case, grass growth is not initiated if there is more than 1 cm of snow (water equivalent).

A3. Phenology: Leafshed

[111] The "meteorological" leaf senescence can be of three types: sensitivity to cold temperatures, to lack of water, or to both. Temperate and boreal deciduous trees in the model shed their leaves when temperatures decrease (i.e., weekly temperatures are lower than monthly temperatures) and the monthly temperatures fall below a given threshold T_s (see table 1). Tropical raingreen trees will shed their leaves when the weekly moisture availability falls below a value A_c given by

$$A_c = \min\left(A_{\min} + x(A_{\max} - A_{\min}), A_p\right), \tag{A20}$$

where $A_{\min}$ and $A_{\max}$ are the last year's moisture availability extrema at that grid point, while $x = 0.5$ and $A_p = 0.3$ are prescribed parameters. A combination of the first two types of "meteorological" leaf senescence is applied to grasses (with different parameters). Additionally, an absolute moisture stress criterion is applied to some PFTs, stipulating that these PFTs will lose their leaves when weekly moisture stress falls below this limit H_s (see Table 1). This allows prevention of extreme situations where leaves would be kept in dry regions and in the absence of clear seasonal moisture variations. Trees are supposed to lose their fine roots at the same rate that they lose their leaves. In grasses, the leaf senescence is extended to the whole plant except its carbohydrate reserve. For the carbon pools affected by senescence, the rate of biomass loss ΔB is prescribed through

$$\Delta B = B\frac{\Delta t}{\tau}, \tag{A21}$$

with $\tau = 10$ days.

[112] Another fraction of the leaves and fine roots (plus stalk and "fruits" for grasses) is lost at every time step as a function of the leaf age. This is based on the fact that even if the meteorological conditions are favorable for leaf maintenance, plants, in particular evergreen trees, have to renew their leaves simply because old leaves become inefficient. The fraction of biomass loss is tentatively prescribed as

$$\Delta B = B\min\left(0.99, \frac{\Delta t}{a_c}\left(\frac{a}{a_c}\right)^4\right), \tag{A22}$$

where a_c is the critical leaf age. For evergreen trees, $a_c = 2.5$ years, while for natural grasses, $a_c = 120$ days. This formulation ensures quite rapid loss of leaves when these approach their critical age. Note that leaf age decreases when new biomass is allocated to the leaves. The turnover formulation based on leaf age is applied separately to each of the leaf age classes (see section A1).

[113] When during senescence the LAI falls below 0.2, the remaining leaves are shed and the plant is declared to be out of its growing season. In that case, a new growing season can be initiated.

A4. Other Turnover Processes

A4.1. Fruit Turnover

[114] Trees simply lose their "fruits" with a time constant of 90 days. The corresponding biomass is converted into litter.

A4.2. Sapwood Conversion

[115] Following LPJ [*Sitch et al.*, 2003], sapwood biomass B_s is converted into heartwood biomass B_h with a time constant τ of 1 year,

$$\Delta B_{s\rightarrow h} = B_s\frac{\Delta t}{\tau}, \tag{A23}$$

with B_s and B_h being updated at every time step.

A4.3. Herbivory

[116] Herbivory affects leaves and fruits as well as stalks (the latter only for grasses, of course). Following *McNaughton et al.* [1989], the probability p_a for a leaf to be eaten in 1 year is parameterized as a linear function of the annual NPP in the surroundings, N: $p_a = bN$. With the model time step Δt of the order of one or a few days, a daily probability p_d is used such that

$$p_d = 1 - (1 - p_a)^{\frac{1}{365 days}}. \tag{A24}$$

The proportionality constant a is such that for values of N typical for tropical rain forests (1000 gC/m^2), the probability for a leaf to be eaten in 1 year is about 30% [*McNaughton et al.*, 1989].

[117] One other important effect of herbivory is the role it plays in favoring grasslands versus woodlands. Herbivory reduces the effective sapling establishment rate, simply because the young plants can be eaten [*van de Koppel and Prins*, 1998]. Supposing conservatively that newly established saplings are particularly vulnerable to herbivory during the first $\Delta t = 6$ months of their existence, this effect can be taken into account by multiplying the annual establishment rate by a factor

$$x = e^{-p_d \Delta t} \leq 1. \tag{A25}$$

A4.4. Leaf Age Classes

[118] The turnover between the n different leaf age classes is determined by a time constant $\tau = a_c/n$, where a_c is the critical leaf age described in section A3. The leaf mass passing from age class i to age class $i + 1$ at each time step is

$$\Delta B_{i \rightarrow i+1} = B_i \frac{\Delta t}{\tau}. \tag{A26}$$

The leaf age in each age class is then recalculated through

$$A_i \leftarrow A_i + \Delta t + \frac{A_{i-1} \Delta B_{i-1 \rightarrow i} + A_i B_i}{B_i + \Delta B_{i-1 \rightarrow i}}. \tag{A27}$$

Afterward, B_i is updated through

$$B_i \leftarrow B_i + \Delta B_{i-1 \rightarrow i}. \tag{A28}$$

For the first age class, $\Delta B_{0 \rightarrow 1}$ represents simply the carbon allocated to leaves after photosynthesis or translocated at the beginning of the growing season, with $A_0 = 0$.

A5. Carbon Allocation

[119] Following *Friedlingstein et al.* [1998], carbon allocation is parameterized as a function of moisture, temperature, and nitrogen availabilities.

[120] Moisture availability is the same as described in section A2. Light availability is a function of the LAI that the plant "sees" around itself (see section 2.3.3),

$$A_l = \max\left(e^{-k\lambda}, 0.1\right), \tag{A29}$$

where λ is the pertinent LAI and k is the extinction coefficient taken to be 0.5 [*Monsi and Sæki*, 1953]. The formulation is such that an increasing LAI means a stronger light limitation (A_l decreases).

[121] Nitrogen availability is parameterized as a function of monthly soil humidity and monthly soil temperature (see section 2.3.3). Both temperature and humidity are calculated by the hydrological module for several layers in the soil. For the parameterization of the microbial activity, it is supposed that the decomposers are distributed in the soil following an exponential profile decreasing with depth. The pertinent soil temperature and humidity, i.e., the temperature T and humidity H which the decomposers feel, is then calculated in the same way as described in equation (A18) with a depth constant of $\zeta = 0.2$ m. The nitrogen availability is then calculated as by *Friedlingstein et al.* [1998] as the product of a soil humidity limitation $A_{N,H}$ and a temperature limitation $A_{N,T}$ on nitrogen availability,

$$A_N = A_{N,H} A_{N,T}, \tag{A30}$$

with

$$A_{N,H} = \min(1, \max(0.5, H)) \tag{A31}$$

$$A_{N,T} = \min\left(1, \max\left(0.1, 2^{\frac{T - T_0}{T_c}}\right)\right). \tag{A32}$$

The belowground availabilities A_N and A_H are then combined to a single belowground availability

$$A_b = \min(A_N, A_H). \tag{A33}$$

[122] The three different availabilities are then used to calculate preliminary allocation fractions for leaves, roots, and sapwood ($\tilde{f}_l, \tilde{f}_r$, and $\tilde{f}_s$, with $\tilde{f}_l + \tilde{f}_r + \tilde{f}_s = 1$),

$$\tilde{f}_r = \max\left(r_{\min}, r_0 \frac{3A_l}{A_l + 2A_b}\right), \tag{A34}$$

$$\tilde{f}_s = s_0 \frac{3A_b}{2A_l + A_b}, \tag{A35}$$

$$\tilde{f}_l = \max\left(a_{\min}, \min\left(a_{\max}, 1 - \tilde{f}_r - \tilde{f}_s\right)\right). \tag{A36}$$

Here $r_{\min} = 0.15$, $a_{\min} = 0.2$, $a_{\max} = 0.5$, and $r_0 = s_0 = 0.3$. The preliminary root allocation fraction is then recalculated,

$$\tilde{f}_r = 1 - \tilde{f}_s - \tilde{f}_l. \tag{A37}$$

This original allocation scheme of *Friedlingstein et al.* [1998], which calculates the allocation fractions for three compartments (leaves, stems, roots), has been modified here as the plants in ORCHIDEE have eight biomass compartments, toward six of which carbon can be allocated (leaves, "fruits," the carbohydrate reserve, fine root, and aboveground and belowground sapwood). The modifications are described below.

[123] If for a given PFT the LAI is higher than a prescribed maximum LAI $\lambda_{\max}$ (e.g., $\lambda_{\max} = 10$ for tropical trees),

then no carbon will be allocated to the leaves no matter what the limitations are. In this case, $\tilde{f}_s \leftarrow \tilde{f}_s + \tilde{f}_l$ and $\tilde{f}_l$ is set to zero.

[124] The final allocation fractions f are then calculated using the preliminary fractions $\tilde{f}$, with some special cases being taken into account. If a plant is at the end of its growing season (i.e., it undergoes "meteorological leaf senescence," see section A3), then there is no point in allocating carbon to leaves or roots. The whole assimilate will then be attributed to the carbohydrate reserve: $f_c = 1$, while all the other allocation fractions are set to zero (leaves, roots, sapwood above and below ground, "fruits"). In the opposite case, the "fruit" allocation f_f is simply set to 10% as in LPJ [*Sitch et al.*, 2003]. The allocation toward the carbohydrate reserve is tentatively parameterized as a function of the sum of the preliminary allocation fractions $\tilde{f}_l$ and $\tilde{f}_r$ (as the biomass will later be translocated toward the leaves and roots),

$$f_c = (1 - C)\left(1 - f_f\right), \tag{A38}$$

where

$$C = \frac{1}{1 + a\left(\tilde{f}_l + \tilde{f}_r\right)} \tag{A39}$$

with a tuning parameter $a = 1$ for seasonal plants and $a = 0$ for evergreen trees. Note that this means that evergreen trees have no carbohydrate reserve in the model, which is not true in reality [*Hansen and Beck*, 1990]. However, in the model, the carbohydrate reserve is only used by seasonal trees and grasses at the beginning of the growing season in order to attain rapidly a reasonable leaf cover. However, if the carbohydrate reserve already contains too much biomass (more than twice the equivalent of λ_{max}), no carbon is allocated to the reserve (that is, C in equation (A39) is set to 1). Tests have shown that the model is not very sensible to the exact formulation of equation (A39), provided that enough carbon is allocated toward the reserve to allow for a rapid increase of leaf and fine root mass at the beginning of the next growing season.

[125] Note that in LPJ the formulation for carbon allocation is such that 1 year's NPP is actually allocated in the following year [*Sitch et al.*, 2003]. In our case, this would correspond to allocating all photosynthate first to the carbohydrate reserve, while attribution to the other plant tissues would occur through carbon translocation from that reserve during the growing season.

[126] The final leaf allocation is then

$$f_l = \tilde{f}_l\left(1 - f_f\right)C. \tag{A40}$$

The final root allocation fraction is calculated in the same way. Sapwood can be located above or below the ground, the former corresponding to stems and the latter to coarse roots. These two carbon reservoirs are distinguished. As a simplification, biomass is evenly allocated to these two reservoirs, although observations and theoretical considerations indicate that stem biomass is generally higher than coarse root mass [*Enquist and Niklas*, 2002],

$$f_{s\uparrow} = f_{s\downarrow} = \frac{1}{2}\tilde{f}_s\left(1 - f_f\right)C. \tag{A41}$$

However, the assimilates are not allocated immediately toward the tissues, but are first partially used up by autotrophic respiration. There is no allocation to tree heartwood as the latter is produced by the slow conversion of sapwood (see section A4).

[127] Furthermore, translocation from the carbohydrate reserve toward leaves and roots at the beginning of the growing season has to be treated. If the plant is at the beginning of its growing season (i.e., if the detection of the beginning of the growing season took place not longer than 60 (30) days ago for trees (grasses)), and if the LAI is lower than $\lambda_{max}/2$, then carbon is translocated from the carbohydrate reserve to the leaves and roots. The quantity translocated is such that without additional photosynthesis, the plant would attain an LAI of $\lambda = \lambda_{max}/2$ within 2 weeks when starting with no leaves at all.

A6. Autotrophic Respiration

[128] Autotrophic respiration is calculated following *Ruimy et al.* [1996]. The maintenance respiration R_m for living plant compartments (except leaves) is calculated as

$$R_{m,i} = c(T)B_i, \tag{A42}$$

where c is a maintenance respiration coefficient (in gC/(gC day)) depending on temperature and B_i is the biomass in the plant compartment i. For leaves, the C/N ratio and thus the maintenance respiration for a given mass of carbon varies within the canopy. Again, following *Ruimy et al.* [1996], the maintenance respiration for leaves is calculated as

$$R_{m,leaf} = c(T)B_{leaf}\frac{0.3\lambda + 1.4\left(1 - e^{-\frac{1}{2}\lambda}\right)}{\lambda}. \tag{A43}$$

The maintenance respiration coefficient is parameterized as

$$c(T) = \max\left(c_{0,i,j}(1 + T/T_0), 0\right), \tag{A44}$$

where c_0 and T_0 are prescribed for each plant part i and PFT j. Once there is an explicit representation of plant nitrogen cycling in the model, c_0 might actually be calculated. For aboveground plant compartments, the temperature used in equation (A44) is the 2-m temperature. For belowground plant compartments (fine roots, sapwood below the ground, and the carbohydrate reserve), ORCHIDEE uses the root temperature which is calculated as in equation (A18) using the prescribed root profile.

[129] Up to $f = 80\%$ of the allocatable biomass B_a (i.e., the biomass produced by photosynthesis during that time step) can be used up for maintenance respiration. If the total maintenance respiration $R_m = \sum R_{m,i}$ is above this threshold, then the missing mass is taken proportionally from the respective plant tissues themselves. In practice, introducing this maximum fraction allows the plant to be able to react to severe stress (that is, in situations where photosynthesis tends to be weak, in particular weaker than respiration) by allocating new biomass to tissues where this is needed. The remaining allocatable biomass is then

$$B'_a = \max(B_a - R_m, (1 - f)B_a). \tag{A45}$$

A fraction $g = 28\%$ of this remaining allocatable biomass B'_a is lost to the atmosphere as growth respiration R_g [*Ruimy et al.*, 1996],

$$R_g = gB'_a. \tag{A46}$$

The remaining definitive allocatable biomass

$$B''_a = (1-g)B'_a \tag{A47}$$

is then used for plant growth using the allocation fractions calculated before (section A5).

A7. Heterotrophic Respiration

[130] The treatment of heterotrophic respiration follows *Parton et al.* [1988]. Dead biomass is attributed to structural (slowly decomposing with high lignin content) and metabolic (rapidly decomposing with low lignin content) litter pools above and below the surface. Soil carbon, resulting from litter decomposition, is present in three different pools: active, passive, and slow. Litter and soil carbon is treated separately on the natural and agricultural fractions of the surface. Therefore the model has altogether eight ($2 \times 2 \times 2$) litter pools and six (2×3) soil carbon pools.

[131] The fraction f_m of dying biomass that is attributed to metabolic litter increases with the lignin to nitrogen ratio of the tissue,

$$f_m = 0.85 - 0.018\frac{L}{C}\frac{C}{N}. \tag{A48}$$

The remaining fraction $f_s = 1 - f_m$ is attributed to the structural litter pool. Both the lignin to carbon (L/C) and the carbon to nitrogen ratio (C/N) of the plant tissues are prescribed in this first version. Whether dying biomass is attributed to a belowground or aboveground litter pool depends on the physical location of the corresponding plant part.

[132] The decay of metabolic and structural litter is controlled by temperature and litter humidity. The fraction of dead biomass in each of the four metabolic litter pools (above/below ground, on natural or agricultural ground) that is decomposed per time step Δt is

$$f = c_T c_H \frac{\Delta t}{\tau}, \tag{A49}$$

where τ is a prescribed time constant, and $0 \le c_T \le 1$ and $0 \le c_H \le 1$ are inhibition factors that represent the slowing down of decomposer activity at low temperatures or in dry (or too wet) soil. The soil temperature T and humidity H used for litter decomposition in the soil are again calculated as in equation (A18). The temperature inhibition factor c_T is parameterized as

$$c_T = 2^{\left(\frac{T-30^\circ C}{10^\circ C}\right)}, \tag{A50}$$

while the soil humidity inhibition factor c_H is

$$c_H = \min\left(0, \max\left(1, aH^2 + bH + c\right)\right), \tag{A51}$$

with $a = -1.1$, $b = 2.4$, and $c = -.29$. The particular optimal form of c_H depends strongly on the assumptions and formulation of the hydrological scheme used.

[133] The fraction of dead biomass in each of the four structural litter pools that is decomposed is

$$f = c_T c_H e^{-3l}\frac{\Delta t}{\tau}, \tag{A52}$$

where l is the lignin fraction in the structural litter. The lignin content of each plant compartment being prescribed, the prognostic lignin fraction l is updated with litterfall at every time step.

[134] For each of the litter types, the fraction of the decomposed biomass that goes into the slow, passive, and active soil carbon pools is prescribed, the remainder being lost to the atmosphere as heterotrophic respiration. Thus the carbon resulting from the decomposition of the lignin fraction of structural litter goes partially into the slow soil carbon pool and partially into the atmosphere as CO_2, while the carbon from the nonlignin fraction goes partially into the active soil carbon pool and again partially into the atmosphere. The decomposition of metabolic litter results in an increase both of the active carbon pool and of atmospheric CO_2.

[135] Metabolic activity in the soil results in carbon fluxes within the three carbon pools (active, slow, and passive). The fraction of each of the carbon pools that is transformed at each time step is again calculated using equation (A49), with the time constant τ being prescribed for each of the carbon pools and the same inhibition function c_T and c_H. The fractions of these fluxes that are attributed to the other carbon pools and, as CO_2 flux, to the atmosphere, are again prescribed following *Parton et al.* [1988].

Appendix B: Preparation of the ORCHIDEE Runs at the FluxNet Sites

B1. Data Origin

[136] Both climate forcing and flux data have been downloaded from the FluxNet website (http://www.daac.ornl.gov/FLUXNET/fluxnet.html), excepted data from two Russian sites (TVf and ZOf in Table 2) that have been studied during the TCOS-Siberia project (http://www.bgc-jena.mpg.de/public/carboeur/web_TCOS).

B2. Preparation of the Climate Forcing

[137] At some sites, such as boreal grasslands, climate forcing and flux data are available only during the growing season. More generally, gaps in the climate data are caused by instrumentation shutdowns that can last up to several weeks. Gap-filling methods had therefore to be developed in order to get continuous half-hourly climate forcing data sets and run ORCHIDEE at each site. Each time gaps were present in the FluxNet climate forcing, data from nearby weather stations and from the ECMWF ERA15 1×1 degree reanalysis were used instead.

[138] Weather stations provide average, minimum, and maximum daily temperature, mean daily dew point temperature, daily precipitation, and mean daily wind speed. The ECMWF ERA15 1×1 degree reanalysis was used to get

the incoming short-wave radiation. Weather stations can be located up to several kilometers from the sites. A linear correction was then applied to these daily data. For each variable, except for rainfall, this correction was computed from the linear regression between all available data at the site and at the weather station. For rainfall, the regression between weather station data and measured forcing data was too poor to be used for scaling the total amount of rainfall given by the weather stations.

[139] For surface air pressure, gaps are filled with the average value at the site. If no pressure at all is available, a constant value of 1015 hPa was taken, regardless of the site elevation. Such an approximation is expected to have little consequence on the behavior of the model.

[140] Because climate forcing in ORCHIDEE is defined at a half-hourly time step, a diurnal cycle for each climate variable from these daily values had to be rebuilt. The diurnal cycle of air temperature was assumed to fit portions of sinusoidal functions with a minimum value at sunrise and a maximum value at 1400 local time. The sinusoidal functions were such that they guaranteed smooth day-to-day variations of the air temperature. Half-hourly air humidity values were given by half-hourly dew point temperature values. The latter were computed from the interpolated air temperature minus the difference between mean daily dew point temperature and mean daily air temperature. The diurnal cycle of the short-wave radiation was assumed to fit a second-order polynomial during daytime with a maximum at noon, and was set to zero before sunrise and after sunset. For precipitation, a mean number of hours of rain per day was calculated at each site, and this mean duration was used to distribute rainfall regularly over the day. The incoming long-wave radiation was computed at a half-hourly time step from air temperature, air humidity, and incoming short-wave radiation according to *Crawford and Duchon* [1999].

B3. Initialization of the Model

[141] ORCHIDEE was run separately at each site. The vegetation dynamics, including fire, was deactivated and the fractional cover of each PFT at a particular site was prescribed according to Table 2. All model parameters were then taken from global tables, and soil water content was initialized at field capacity.

[142] In general, the site history, and thus the initial values for soil and vegetation carbon pools, are not known precisely. To guess these initial values, it is assumed that the soil is entirely mineral at the beginning of the simulation and "seeded" according to the fractional cover of each PFT. The meteorological data for the observation period are used cyclically over a long period until equilibration of the carbon pools is attained. The vegetation carbon pools reach equilibrium within 200 years, but a longer period is required for soil carbon equilibrium (i.e., when litter input compensates soil respiration). The model output of the last iteration is then used for analysis.

[143] One problem in doing so is that one ends up with ecosystems in "equilibrium," which means that the accumulated net carbon exchange with the atmosphere is zero on a yearly or decennial basis. This is a problem one is also faced with in global runs: The exact vegetation and carbon history is not known for most sites, and definitely not on the global scale. Measurements at managed forest and other agricultural sites also have to be considered carefully for the same reason. One therefore has to limit model validation to interannual and seasonal variations of carbon stocks and fluxes using the model at equilibrium. This was also done here, yet it is well established that most FluxNet sites are net carbon sinks [e.g., *Law et al.*, 2002]. Simulated half-hourly CO_2 fluxes were therefore corrected in order to account for these sinks. The procedure is described in the following.

[144] Let NEE_{mod} and $NEE_{mod,cor}$ be the raw and corrected modeled net CO_2 flux, respectively, and let NEE_{obs} be the measured net CO_2 flux. The latter has been measured during N_{obs} time steps over a total of N time steps for the whole period of study (e.g., 17,520 half-hourly values per year). In order to calculate the carbon sink for this period, the measured net CO_2 flux must be interpolated at all time steps. One can write

$$NEE_{obs,int} = \begin{cases} NEE_{obs} & \text{if measurement available} \\ NEE_{mod,cor} & \text{otherwise} \end{cases} \quad \text{(B1)}$$

where $NEE_{obs,int}$ is the measured CO_2 flux interpolated at all time steps. The average measured carbon sink per time step is then given by

$$\sigma_{mes} = \frac{1}{N}\sum_{N} NEE_{obs,int} = \frac{1}{N}\left(\sum_{N_{obs}} NEE_{obs} + \sum_{N-N_{obs}} NEE_{mod,cor}\right). \quad \text{(B2)}$$

The corrected modeled net CO_2 flux is computed according to

$$NEE_{mod,cor} = NEE_{mod} + \sigma_{mes}. \quad \text{(B3)}$$

Combining equations (B2) and (B3) leads to

$$\sigma_{mes} = \frac{1}{N_{obs}}\left(\sum_{N_{obs}} NEE_{obs} + \sum_{N-N_{obs}} NEE_{mod}\right). \quad \text{(B4)}$$

This equation is used in equation (B3) to compute the corrected modeled net CO_2 flux at each time step. Values of $NEE_{mod,cor}$ and $NEE_{obs,int}$ give the same carbon sink only if $\sum_N NEE_{mod} = 0$.

[145] **Acknowledgment.** We sincerely thank Jon Foley for providing us with his weather generator used in the global simulations.

References

Arora, V. (2002), Modeling vegetation as a dynamic component in soil-vegetation-atmosphere transfer schemes and hydrological models, *Rev. Geophys.*, *40*(2), 1006, doi:10.1029/2001RG000103.

Arora, V., and G. Boer (2003), A representation of variable root distribution in dynamic vegetation models, *Earth Interactions*, *7*(6), 1–19.

Baldocchi, D., E. Falge, and L. Gu (2001), FLUXNET: A new tool to study the temporal and spatial variability of ecosystem-scale carbon dioxide, water vapor, and energy flux densities, *Bull. Am. Meteorol. Soc.*, *82*, 2415–2434.

Ball, J., T. Woodrow, and J. Berry (1987), A model predicting stomatal conductance and its contribution to the control of photosynthesis under different environmental conditions, *Prog. Photosynthesis*, *4*, 221–224.

Batjes, N. (1996), Total carbon and nitrogen in the soils of the world, *Eur. J. Soil Sci.*, *47*, 151–163.

Beerling, D., F. Woodward, and A. Jenkins (1997), Testing the responses of a dynamic global vegetation model to environmental change: A comparison of observations and predictions, *Global Ecol. Biogeogr. Lett.*, *6*, 439–450.

Berninger, F., and E. Nikinmaa (1994), Foliage area–sapwood area relationships of scots pine (*pinus sylvestris*) trees in different climates, *Can. J. For. Res.*, *24*, 2263–2268.

Betts, R. (2000), Offset of the potential carbon sink from boreal forestation by decreases in surface albedo, *Nature*, *408*, 187–190.

Bonan, G., D. Pollard, and S. Thompson (1992), Effects of boreal forest vegetation on global climate, *Nature*, *359*, 716–718.

Botta, A., N. Viovy, P. Ciais, and P. Friedlingstein (2000), A global prognostic scheme of leaf onset using satellite data, *Global Change Biol.*, *6*, 709–726.

Bousquet, P., P. Peylin, P. Ciais, C. Le Quéré, P. Friedlingstein, and P. Tans (2000), Regional changes in carbon dioxide fluxes of land and oceans since 1980, *Science*, *290*, 1342–1346.

Carlson, T., and D. Riplay (1997), On the relation between NDVI, fractional vegetation cover and leaf area index, *Remote Sens. Environ.*, *62*, 241–262.

Chanine, M. (1992), The hydrological cycle and its influence on climate, *Nature*, *359*, 373–380.

Chuine, I., P. Cour, and D. Rousseau (1998), Fitting models predicting dates of flowering of temperate-zone trees using simulated annealing, *Plant Cell Environ.*, *21*, 455–466.

Ciais, P., I. Janssens, A. Shvidenko, C. Wirth, Y. Malhi, J. Grace, E. Schulze, M. Heimann, O. Phillips, and H. Dolman (2004), The potential for rising CO_2 to account for the observed uptake of carbon by tropical, temperate and boreal forest biomes, in *The Carbon Balance of Forest Biomes*, edited by H. Griffith and P. J. Jarvis, pp. 109–149, BIOS Sci., Oxford, UK.

Clark, D., S. Brown, D. Kicklighter, J. Chambers, J. Thomlinson, J. Ni, and E. Holland (2001), NPP in tropical forests: An evaluation and synthesis of existing field data, *Ecol. Appl.*, *11*, 371–384.

Cogley, J. (1998), Global hydrographic data, release 2.2, *Tech. Rep. 98-1*, Dep. of Geogr., Trent Univ., Peterborough, Ont., Canada.

Collatz, G., M. Ribas-Carbo, and J. Berry (1992), Coupled photosynthesis-stomatal conductance model for leaves of C_4 plants, *Aust. J. Plant Physiol.*, *19*, 519–538.

Cox, P., R. Betts, C. Jones, S. Spall, and I. Totterdell (2000), Acceleration of global warming due to carbon-cycle feedbacks in a coupled climate model, *Nature*, *408*, 184–187.

Cramer, W., et al. (1999), Comparing global models of terresttrial net primary productivity (NPP): Overview and key results, *Global Change Biol.*, *5*, Suppl. 1, 1–15.

Cramer, W., et al. (2001), Global response of terrestrial ecosystem structure and function to CO_2 and climate change: Results from six dynamic global vegetation models, *Global Change Biol.*, *7*, 357–373.

Crawford, T., and C. Duchon (1999), An improved parameterization for estimating atmospheric emissivity for use in calculating daytime downwelling longwave radiation, *J. Appl. Meteorol.*, *38*, 474–480.

de Noblet-Ducoudré, N., C. Prentice, S. Joussaume, D. Texier, A. Botta, and A. Haxeltine (1996), Possible role of atmosphere-biosphere interactions in triggering the last glaciation, *Geophys. Res. Lett.*, *23*, 3191–3194.

de Noblet-Ducoudré, N., M. Claussen, and C. Prentice (2000), Mid-Holocene greening of the Sahara: First results of the GAIM 6000 yr BP experriment with two asynchronously coupled atmosphere/biome models, *Clim. Dyn.*, *16*, 643–659.

de Noblet-Ducoudré, N., S. Gervois, P. Ciais, N. Viovy, N. Brisson, B. Seguin, and A. Perrier (2004), Coupling the soil-vegetation-atmosphere-transfer scheme ORCHIDEE to the agronomy model STICS to study the influence of croplands on the European carbon and water budgets, *Agronomie*, *24*, doi:10.1051/agro:2004038, 397–407.

de Pury, D., and G. Farquhar (1997), Simple scaling of photosynthesis from leaves to canopies without the errors of big-leaf models, *Plant Cell Environ.*, *20*, 537–557.

de Rosnay, P., and J. Polcher (1998), Modeling root water uptake in a complex land surface scheme coupled to a GCM, *Hydrol. Earth Syst. Sci.*, *2*, 239–256.

de Rosnay, P., J. Polcher, M. Bruen, and K. Laval (2002), Impact of a physically based soil water flow and soil-plant interaction representation for modeling large-scale land surface processes, *J. Geophys. Res.*, *107*(D11), 4118, doi:10.1029/2001JD000634.

Dixon, R., R. Houghton, A. Solomon, M. Trexlier, and J. Wisniewski (1994), Carbon pools and flux of global ecosystems, *Science*, *263*, 185–190.

Douville, H., S. Planton, J. Royer, D. Stephenson, S. Tyteca, L. Kergoat, S. Lafont, and R. Betts (2000), Importance of vegetation feedbacks in doubled-CO_2 climate experiments, *J. Geophys. Res.*, *105*, 14,841–14,861.

Ducoudré, N. I., K. Laval, and A. Perrier (1993), SECHIBA, a new set of parameterizations of the hydrologic exchanges at the land-atmosphere interface within the LMD atmospheric general circulation model, *J. Clim.*, *6*, 248–273.

Enquist, B., and K. Niklas (2002), Global allocation rules for patterns of biomass partitioning in seed plants, *Science*, *295*, 1517–1520.

Eswaran, H., E. Van den Berg, and P. Reich (1993), Organic carbon in soils of the world, *Soil Sci. Soc. Am. J.*, *57*, 192–194.

Fan, S., M. Gloor, J. Mahlmann, S. Pacala, J. Sarmiento, T. Takahashi, and P. Tans (1998), A large terrestrial carbon sink in North America implied by atmospheric and oceanic carbon dioxide data and models, *Science*, *282*, 442–446.

Farquhar, G., and T. Sharkey (1982), Stomatal conductance and photosynthesis, *Ann. Rev. Plant Physiol.*, *33*, 317–345.

Farquhar, G., S. von Caemmener, and J. Berry (1980), A biochemical model of photosynthesis CO_2 fixation in leaves of C_3 species, *Planta*, *149*, 78–90.

Foley, J., J. Kutzbach, M. Coe, and S. Levis (1994), Feedbacks between climate and boreal forests during the Holocene epoch, *Nature*, *371*, 52–54.

Foley, J., I. Prentice, N. Ramankutty, S. Levis, D. Pollard, S. Sitch, and A. Haxeltine (1996), An integrated biosphere model of land surface processes, terrestrial carbon balance, and vegetation dynamics, *Global Biogeochem. Cycles*, *10*, 603–628.

Foley, J. A., S. Levis, C. Prentice, D. Pollard, and S. L. Thompson (1998), Coupling dynamic models of climate and vegetation, *Global Change Biol.*, *4*, 561–579.

Friedlingstein, P., G. Joel, C. B. Field, and I. Fung (1998), Toward an allocation scheme for global terrestrial carbon models, *Global Ch. Biol.*, *5*, 755–770.

Friedlingstein, P., L. Bopp, P. Ciais, J.-L. Dufresne, L. Fairhead, H. LeTreut, P. Monfray, and J. Orr (2001), Positive feedback between future climate change and the carbon cycle, *Geophys. Res. Lett.*, *28*, 1543–1546.

Friend, A. (1998), Parameterisation of a global daily weather generator for terrestrial ecosystem modelling, *Ecol. Modell.*, *109*, 121–140.

Hansen, J., and E. Beck (1990), The fate and path of assimilation products in stem of 8-year-old Scots pine (*Pinus sylvestris L.*) trees, *Trees*, *4*, 16–21.

Henderson-Sellers, A., and K. McGuffie (1995), Global climate models and "dynamic" vegetation changes, *Global Change Biol.*, *1*, 63–75.

Henderson-Sellers, A., K. McGuffie, and A. Pitman (1996), The project for intercomparison of land-surface schemes: 1992 to 1995, *Clim. Dyn.*, *12*, 849–859.

Hobbie, S., K. J. Nadelhoffer, and P. Högberg (2002), A synthesis: The role of nutrients as constraints on carbon balances in boreal and arctic regions, *Plant Soil*, *242*, 163–170.

Hobbs, P., J. Reid, R. Kotchenruther, R. Ferek, and R. Weiss (1997), Direct radiative forcing by smoke from biomass burning, *Science*, *275*, 1776–1778.

Houghton, R., K. Lawrence, J. Hackler, and S. Brown (2001), The spatial distribution of forest biomass in the Brazilian Amazon: A comparison of estimates, *Global Change Biol.*, *7*, 731–746.

Hourdin, F., J.-P. Issartel, B. Cabrit, and A. Idelkadi (1999), Reciprocity of atmospheric transport of trace species, *C. R. Acad. Sci.*, *329*, 623–628.

Huang, S., S. Titus, and D. Wiens (1992), Comparison of nonlinear height-diameter functions of major Alberta tree species, *Can. J. For. Res.*, *22*, 1297–1304.

Hungate, B., J. Dukes, M. Shaw, Y. Luo, and C. Field (2003), Nitrogen and climate change, *Science*, *302*, 1512–1513.

Intergovernmental Panel on Climate Change (2001), *IPCC Third Assessment Report: Climate Change 2001—The Scientific Basis*, 944 pp., Cambridge Univ. Press, New York.

Ishida, A., A. Uemura, N. Koike, Y. Matsumoto, and A. Lai Hoe (1999), Interactive effects of leaf age and self-shading on leaf structure, photosynthetic capacity and chlorophyll fluorescence in the rain forest tree, *dryobalanops aromatica*, *Tree Physiol.*, *19*, 741–747.

Jarvis, P., B. Saugier, and E. Schulze (2001), Productivity of boreal forests, in *Terrestrial Global Productivity*, edited by J. Roy, B. Saugier, and H. Mooney, pp. 211–244, Academic, San Diego, Calif.

Johnson, I. R., and J. Thornley (1984), A model of instantaneous and daily canopy photosynthesis, *J Theor. Biol.*, *107*, 531–545.

Kaplan, J. O., et al. (2003), Climate change and arctic ecosystems: 2. Modeling, paleodata-model comparisons, and future projections, *J. Geophys. Res.*, *108*(D19), 8171, doi:10.1029/2002JD002559.

Kirilenko, A. P., and A. M. Solomon (1998), Modeling dynamic vegetation response to rapid climate change using bioclimatic classification, *Clim. Change*, *38*, 15–49.

Körner, C. (1998), A re-assessment of high elevation treeline positions and their explanation, *Oecologia*, *115*, 445–459.

Kucharik, C., J. Foley, C. Delire, V. Fisher, M. Coe, J. Lenters, C. Young-Molling, N. Ramankutty, J. Norman, and S. Gower (2000), Testing the performance of a dynamic global ecosystem model: Water balance, carbon balance, and vegetation structure, *Global Biogeochem. Cycles*, *14*, 795–825.

Kuhlbusch, T., M. Andreae, H. Cachier, J. Goldammer, J.-P. Lacaux, R. Shea, and P. Crutzen (1996), Black carbon formation by savanna fires: Measurements and implications for the global carbon cycle, *J. Geophys. Res.*, *101*, 23,651–23,665.

Kutzbach, J., G. Bonan, J. Foley, and S. Harrison (1996), Vegetation and soil feedbacks on the response of the African monsoon to orbital forcing in the early to middle Holocene, *Nature*, *384*, 623–626.

Law, B., et al. (2002), Environmental controls over carbon dioxide and water vapor exchange of terrestrial vegetation, *Agric. For. Meteorol.*, *113*, 97–120.

Le Roux, X., A. Lacointe, A. Escobar-Gutiérrez, and S. Le Dizès (2001), Carbon-based models of individual tree growth: A critical appraisal, *Ann. For. Sci.*, *58*, 459–506.

Lieberman, D., M. Lieberman, G. Hartshorn, and R. Peralta (1985), Mortality patterns and stand turnover rates in a wet tropical forest in Costa Rica, *J. Ecol.*, *73*, 915–924.

Loveland, T., B. Reed, J. Brown, D. Ohlen, Z. Zhu, L. Yang, and J. Merchant (2000), Development of a global land cover characteristics database and IGBP DISCover from 1 km AVHRR data, *Int. J. Remote Sens.*, *21*, 1303–1330.

Loveys, B., L. Atkinson, D. Sherlock, R. Roberts, A. Fitter, and O. Atkin (2003), Thermal acclimatation of leaf and root respiration: An investigation comparing inherently fast- and slow-growing plant species, *Global Change Biol.*, *9*, 895–910.

Mann, M., R. Bradley, and M. Hughes (1999), Northern Hemisphere temperatures during the past millennium: Inferences, uncertainties, and limitations, *Geophys. Res. Lett.*, *26*, 759–762.

Matthews, E., and I. Fung (1987), Methane emission from natural wetlands: Global distribution, area, and environmental characteristics of sources, *Global Biogeochem. Cycles*, *1*, 61–86.

McCree, K. (1974), Equation for the rate of dark respiration of white clover as a function of dry weight, photosynthesis rate and temperature, *Crop Sci.*, *14*, 509–514.

McMurtrie, R., D. Rook, and F. Kelliher (1990), Modelling the yield of *pinus radiata* on a site limited by water and nitrogen, *For. Ecol. Manage.*, *30*, 381–413.

McNaughton, S., M. Oesterheld, D. Franck, and K. Williams (1989), Ecosystem-level patterns of primary productivity and herbivory in terrestrial habitats, *Nature*, *341*, 142–144.

Monsi, M., and T. Sæki (1953), Über den Lichtfaktor in den Pflanzengesellschaften und seine Bedeutung für die Stoffproduktion, *Jpn. J. Bot.*, *14*, 22–52.

Moulin, S., L. Kergoat, N. Viovy, and G. Dedieu (1997), Global scale assessment of vegetation phenology using NOAA/AVHRR satellite measurements, *J. Clim.*, *10*, 1154–1170.

Murray, M., M. Cannell, and R. Smith (1989), Date of budburst of fifteen tree species in Britain following climatic warming, *J. Appl. Ecol.*, *26*, 693–700.

Myneni, R., S. Hoffman, J. Glassy, Y. Zhang, P. Votava, R. Nemani, S. Running, and J. Privette (2002), Global products of vegetation leaf area and fraction absorbed PAR from year one of MODIS data, *Remote Sens. Environ.*, *83*, 214–231.

Nemani, R., C. Keeling, H. Hashimoto, W. Jolly, S. Piper, C. Tucker, R. Myneni, and S. Running (2003), Climate-driven increases in global terrestrial net primary production from 1982 to 1999, *Science*, *300*, 1560–1563.

New, M., M. Hulme, and P. Jones (1999), Representing twentieth-century space-time climate variability: I. Development of a 1961–90 mean monthly terrestrial climatology, *J. Clim.*, *12*, 829–856.

Nizinski, J. J., and B. Saugier (1988), A model of leaf budding and development for a mature *quercus* forest, *J. Appl. Ecol.*, *25*, 643–652.

Parton, W., J. Stewart, and C. Cole (1988), Dynamics of C, N, P, and S in grassland soil: A model, *Biogeochemistry*, *5*, 109–131.

Polcher, J. (1994), Etude de la sensibilité du climat tropical à la déforestation, Thèse de doctorat, Univ. Pierre et Marie Curie, Paris.

Post, W., W. Emanuel, P. Zinke, and A. Stangenberger (1982), Soil carbon pools and world life zones, *Nature*, *258*, 156–159.

Richardson, C., and D. Wright (1984), A model for generating daily weather variables, technical report, U.S. Dep. of Agric, Agric. Res. Serv., Washington, D. C.

Ross, J., P. Hobbs, and B. Holben (1998), Radiative characteristics of regional hazes dominated by smoke from biomass burning in Brazil: Closure tests and direct radiative forcing, *J. Geophys. Res.*, *103*, 31,925–31,941.

Ruimy, A., G. Dedieu, and B. Saugier (1996), TURC: A diagnostic model of continental gross primary productivity and net primary productivity, *Global Biogeochem. Cycles*, *10*, 269–285.

Schlesinger, W. (1991), *Biogeochemistry*, 443 pp., Academic, San Diego, Calif.

Schoettle, A., and T. Fahey (1994), Foliage and fine root longevity of pines, *Ecol. Bull.*, *43*, 136–153.

Schulze, E., H. Högberg, H. Van Oene, T. Persson, A. Harrison, D. Read, A. Kjoller, and G. Matteucci (2000), A synopsis of a study along a north-south transect through Europe, in *Carbon and Nitrogen Cycling in European Forest Ecosystems*, edited by U. Sommer, pp. 468–491, Springer-Verlag, New York.

Sellers, P. J., Y. Mintz, Y. Sud, and A. Dalcher (1986), A simple biosphere model (SiB) for use with general circulation models, *J. Atmos. Sci.*, *43*, 505–531.

Shinozaki, K., K. Yoda, K. Hozumi, and T. Kira (1964a), A quantitative analysis of plant form—The pipe model theory I, *Jpn. J. Ecol.*, *14*, 97–105.

Shinozaki, K., K. Yoda, K. Hozumi, and T. Kira (1964b), A quantitative analysis of plant form—The pipe model theory II: Further evidence of the theory and its application in forest ecology, *Jpn. J. Ecol.*, *14*, 133–139.

Shvidenko, A., and S. Nilsson (2003), A synthesis of the impact of Russian forests on the global carbon budget for 1961–1998, *Tellus, Ser. B*, *55*, 391–415.

Sitch, S., et al. (2003), Evaluation of ecosystem dynamics, plant geography and terrestrial carbon cycling in the LPJ dynamic vegetation model, *Global Change Biol.*, *9*, 161–185.

Smith, T., H. Shugart, and F. Woodward (Eds.) (1997), *Plant Functional Types: Their Relevance to Ecosystem Properties and Global Change*, Cambridge Univ. Press, New York.

Sombroek, W., F. Nachtergaele, and A. Hebel (1993), Amounts, dynamics and sequestering of carbon in tropical and subtropical soils, *Ambio*, *22*, 417–429.

Strand, M. (1995), Inhibition of photosynthesis in current-year needles of unfertilized and fertilized Norway spruce (*Picea abies* (L.) Karst.) during autumn and early winter, *Trees*, *9*, 332–340.

Strand, M., and T. Lundmark (1995), Recovery of photosynthesis in 1-year-old needles of unfertilized and fertilized norway spruce (*Picea abies* (L.) Karst.) during spring, *Tree Physiol.*, *15*, 151–158.

Tania, S., et al. (2003), Air temperature triggers the recovery of evergreen boreal forest photosynthesis in spring, *Global Change Biol.*, *9*, 1410–1426.

Thonicke, K., S. Venevsky, S. Sitch, and W. Cramer (2001), The role of fire disturbance for global vegetation dynamics: Coupling fire into a Dynamic Global Vegetation Model, *Global Ecol. Biogeogr.*, *10*, 661–677.

Tucker, C., D. Slayback, J. Pinzon, S. Los, R. Myneni, and M. Taylor (2001), Higher northern latitude NDVI and growing season trends from 1982 to 1999, *Int. J. Biometeorol.*, *45*, 184–190.

van de Koppel, J., and H. Prins (1998), The importance of herbivore interactions for the dynamics of African savanna woodlands: An hypothesis, *J. Trop. Ecol.*, *14*, 565–576.

VEMAP Members (1995), Vegetation/ecosystem modeling and analysis project: Comparing biogeography and biogeochemistry models in a continental-scale study of terrestrial ecosystem responses to climate change and CO_2 doubling, *Global Biogeochem. Cycles*, *9*, 407–437.

Vérant, S., K. Laval, J. Polcher, and M. De Castro (2004), Sensitivity of the continental hydrological cycle to the spatial resolution over the Iberian Peninsula, *J. Hydrometeorol.*, *5*, 267–285.

Viovy, N. (1997), Interannuality and CO_2 sensitivity of the SECHIBA-BGC coupled SVAT-BGC model, *Phys. Chem. Earth*, *21*, 489–497.

Vitousek, P., and R. Howarth (1991), Nitrogen limitation on land and in the sea: How can it occur?, *Biogeochemistry*, *13*, 87–115.

Whittaker, R. H., and G. E. Likens (1975), The biosphere and man, in *Primary Productivity of the Biosphere*, *Ecol. Stud.*, vol. 14, edited by H. Lieth and R. H. Whittaker, pp. 305–328, Springer-Verlag, New York.

Willmer, C. (1988), Stomatal sensing of environment, *Bot. J. Linn. Soc.*, *34*, 205–217.

Wilson, M., and A. Henderson-Sellers (1985), A global archive of land cover and soils data for use in general circulation models, *J. Climatol.*, *5*, 119–143.

Zeng, N., and J. Neelin (2000), The role of vegetation-climate interaction and interannual variability in shaping the African savanna, *J. Clim.*, *13*, 2665–2670.

Zhang, J., and W. J. Davies (1989), Sequential response of whole plant water relations to prolonged soil drying in the regulation of stomatal behaviour of sunflower plants, *New Phytol.*, *113*, 167–174.

Zinke, P., A. Stangenberger, W. Post, W. Emanuel, and J. Olson (1986), Worldwide organic carbon and nitrogen data, *Tech. Rep. ORNL/TM-8857*, Oak Ridge Nat. Lab., Oak Ridge, Tenn.

P. Ciais, N. de Noblet-Ducoudré, P. Friedlingstein, and N. Viovy, Laboratoire des Sciences du Climat et de l'Environnement, CEA/CNRS, Saclay, F-91191 Gif sur Yvette, France. (ciais@lsce.saclay.cea.fr; noblet@lsce.saclay.cea.fr; pierre@lsce.saclay.cea.fr; viovy@lsce.saclay.cea.fr)

G. Krinner, Laboratoire de Glaciologie et Géophysique de l'Environnement/CNRS, BP 96, F-38402 St. Martin d'Hères, France. (krinner@ujf-grenoble.fr)

J. Ogée, Ecologie Fonctionelle et Physique de l'Environnement (Ephyse), INRA Bordeaux, Domaine de la Grande Ferrade BP 81, F-33883 Villenave d'Ornon, France. (ogee@pierroton.inra.fr)

J. Polcher, Laboratoire de Météorologie Dynamique/CNRS, Université de Paris 6, Case Postale 99, 4 place Jussieu, F-75252 Paris, France. (polcher@lmd.jussieu.fr)

I. C. Prentice, Department of Earth Sciences, University of Bristol, Wills Memorial Building, Queen's Road, Bristol BS8 1RJ, UK. (colin.prentice@bris.ac.uk)

S. Sitch, Met Office (JCHMR), Maclean Building, Crowmarsh-Gifford, Wallingford OX10 8BB, UK. (stephen.sitch@metoffice.gov.uk)

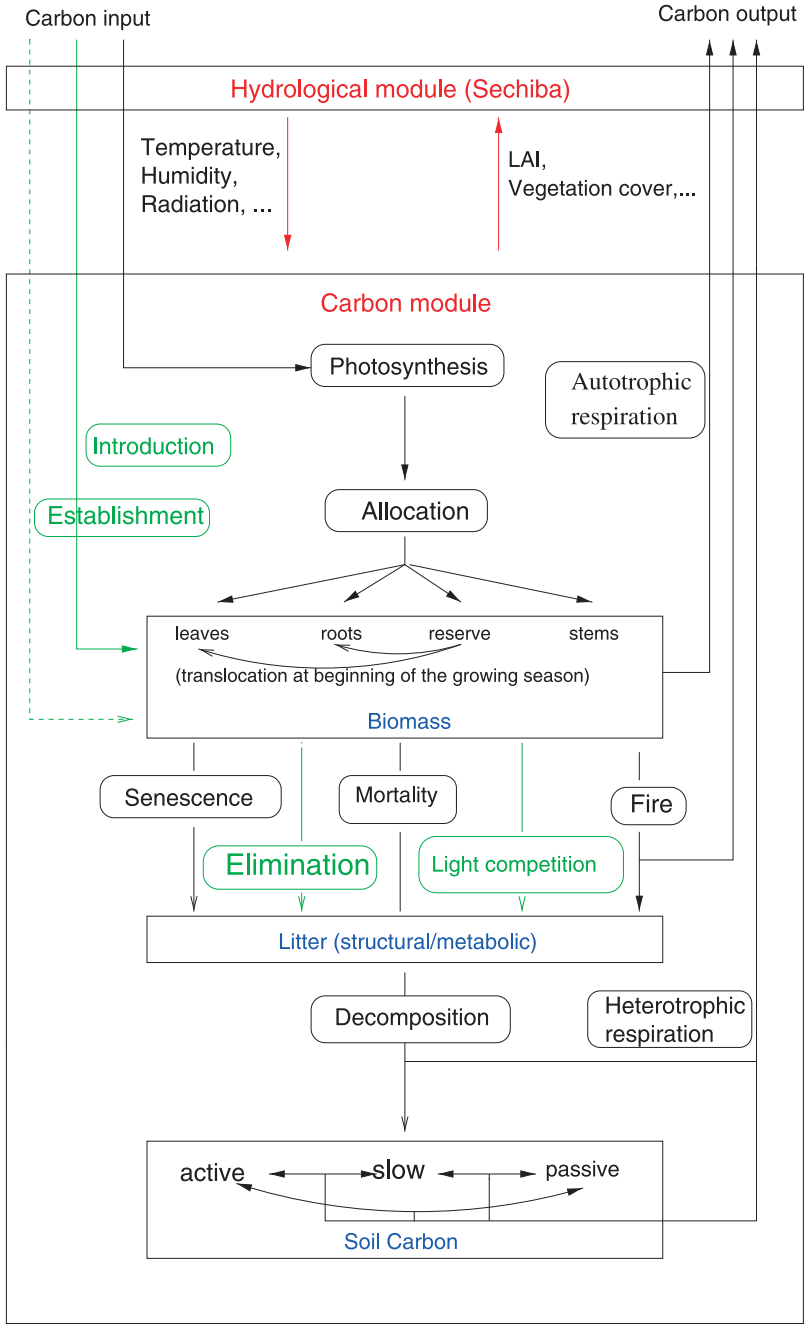

Figure 2. Basic structure of ORCHIDEE. Vegetation dynamics processes (taken from LPJ) show up in green. Within the carbon module box, processes are marked by rounded rectangles, while carbon reservoirs are indicated by normal rectangles (with the corresponding basic state variables in blue). The subprocesses simulated in the carbon module are linked through carbon fluxes (black and green arrows). The exchange of energy and information with the atmosphere passes through the surface scheme (that is, the hydrological module). Eventual biomass increases through PFT introduction and sapling establishment are taken into account as carbon flux from the atmosphere such that the total carbon in atmosphere plus biosphere is conserved.

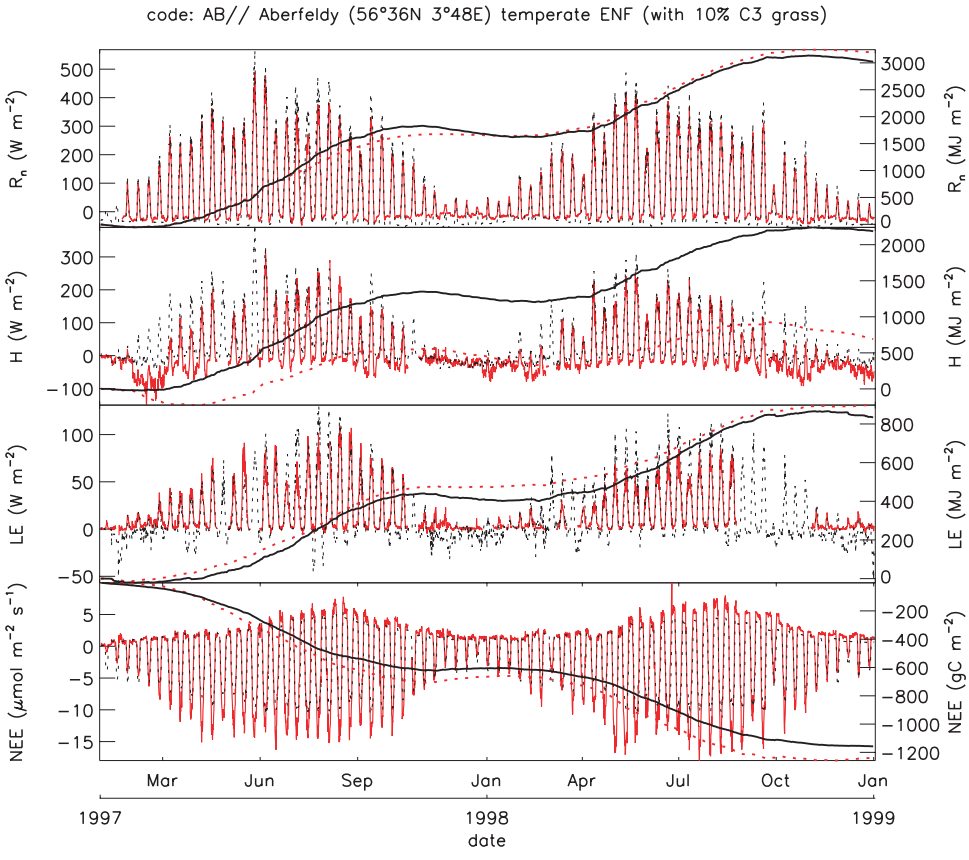

Figure 3. Ten-day bin-averaged and accumulated measured (red) and modeled (black) fluxes at AB (see Table 2). From top to bottom: net radiation (R_n), sensible heat flux (H), latent heat flux (LE), and net CO_2 flux (NEE).

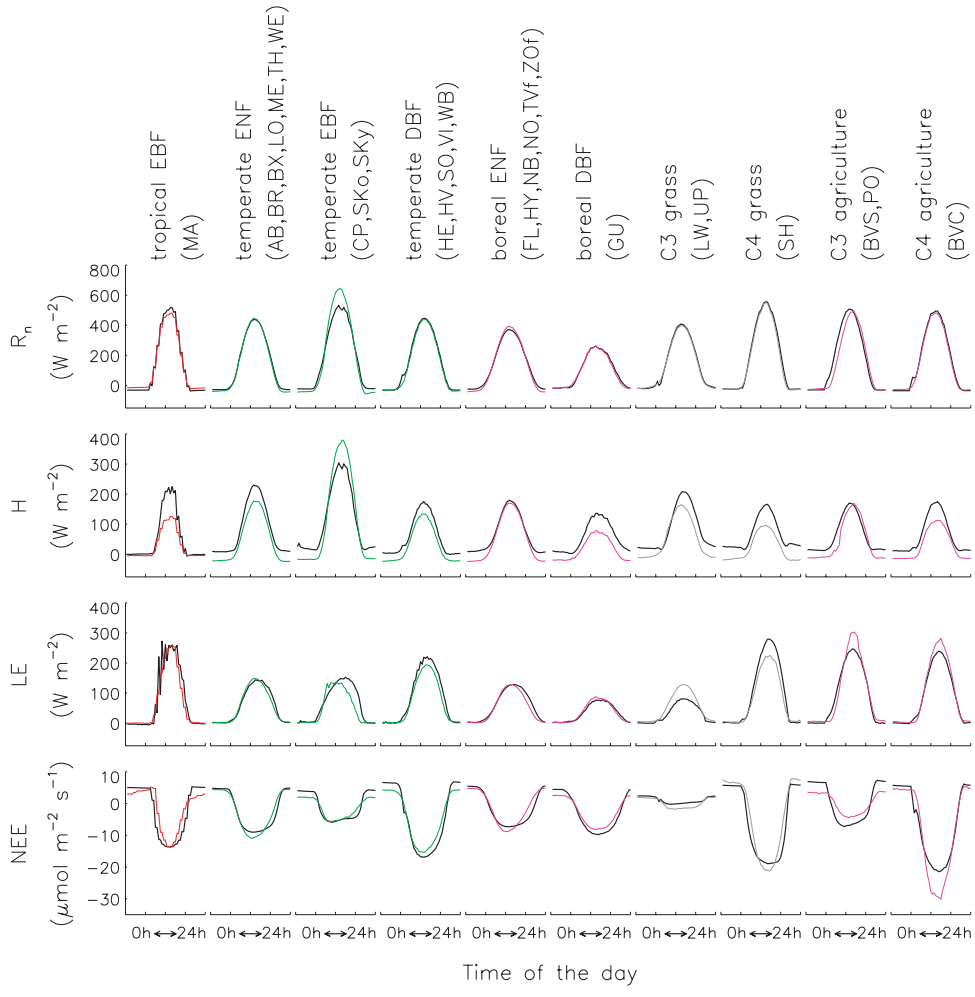

Figure 4. Measured (colored) and modeled (black) "summer" diurnal cycle for each flux and each PFT (see text). From top to bottom: net radiation (R_n), sensible heat flux (H), latent heat flux (LE), and net CO_2 flux (NEE).

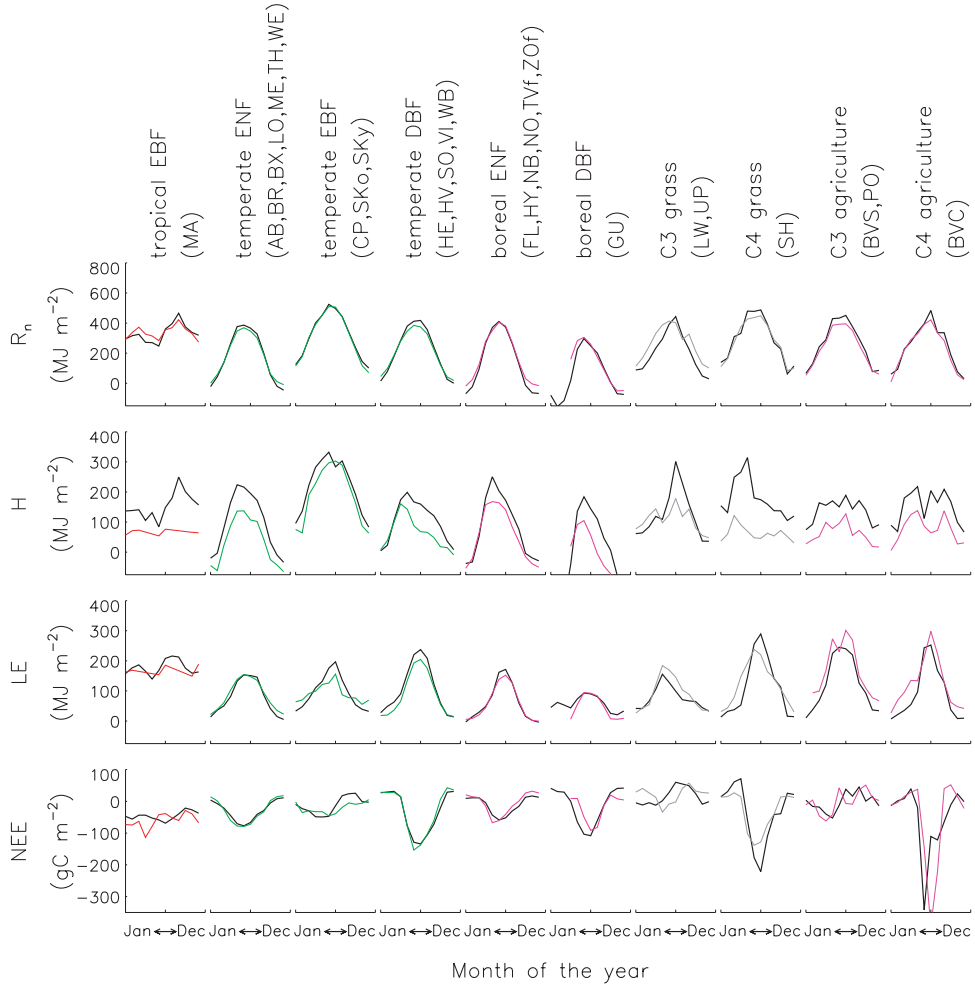

Figure 5. Measured (colored) and modeled (black) seasonal cycle for each flux and each PFT (see text). From top to bottom: net radiation (R_n), sensible heat flux (H), latent heat flux (LE), and net CO_2 flux (NEE).

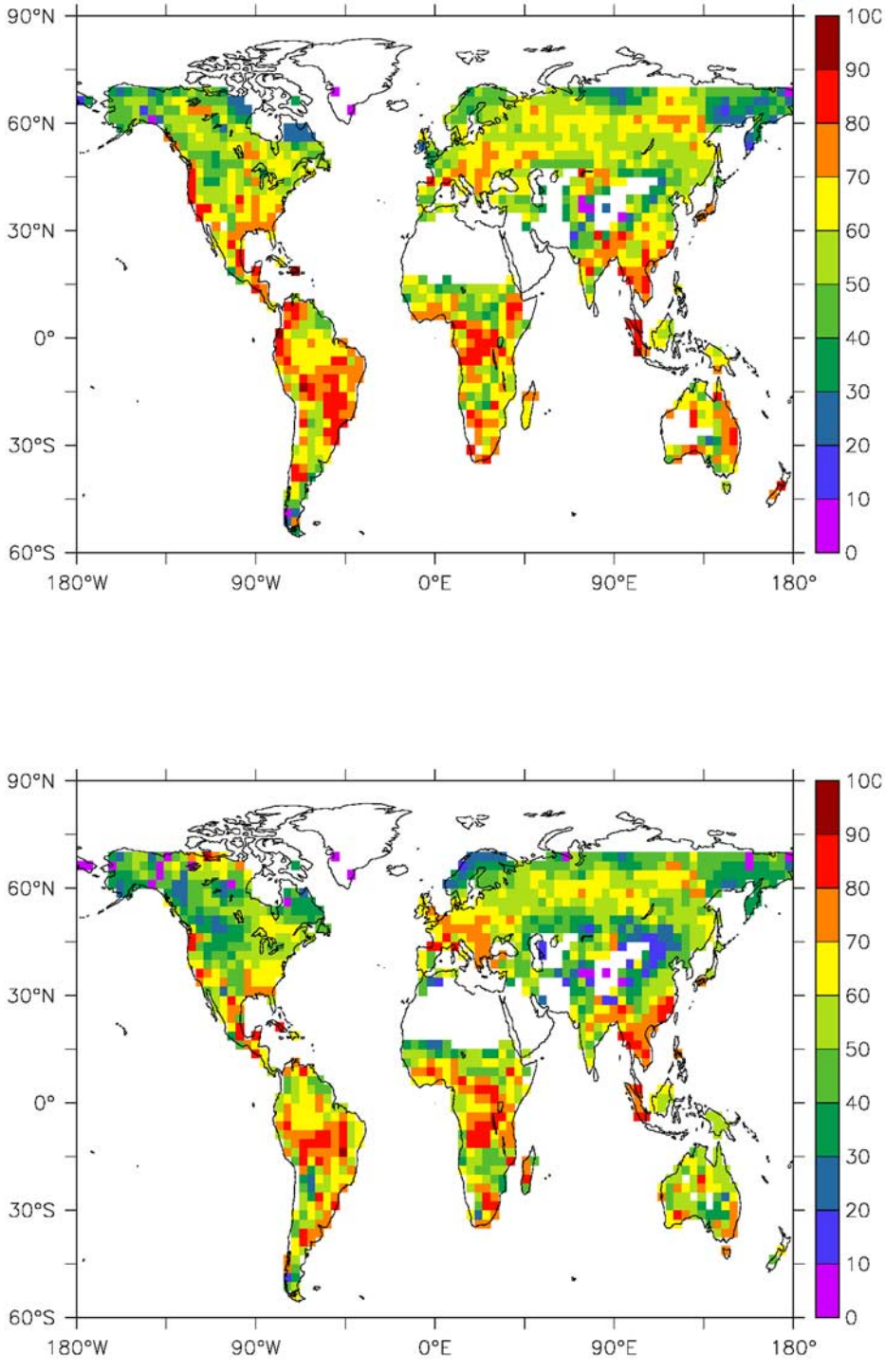

Figure 7. FMT (in %) of the simulated LAI from (top) STAT and (bottom) DYN.

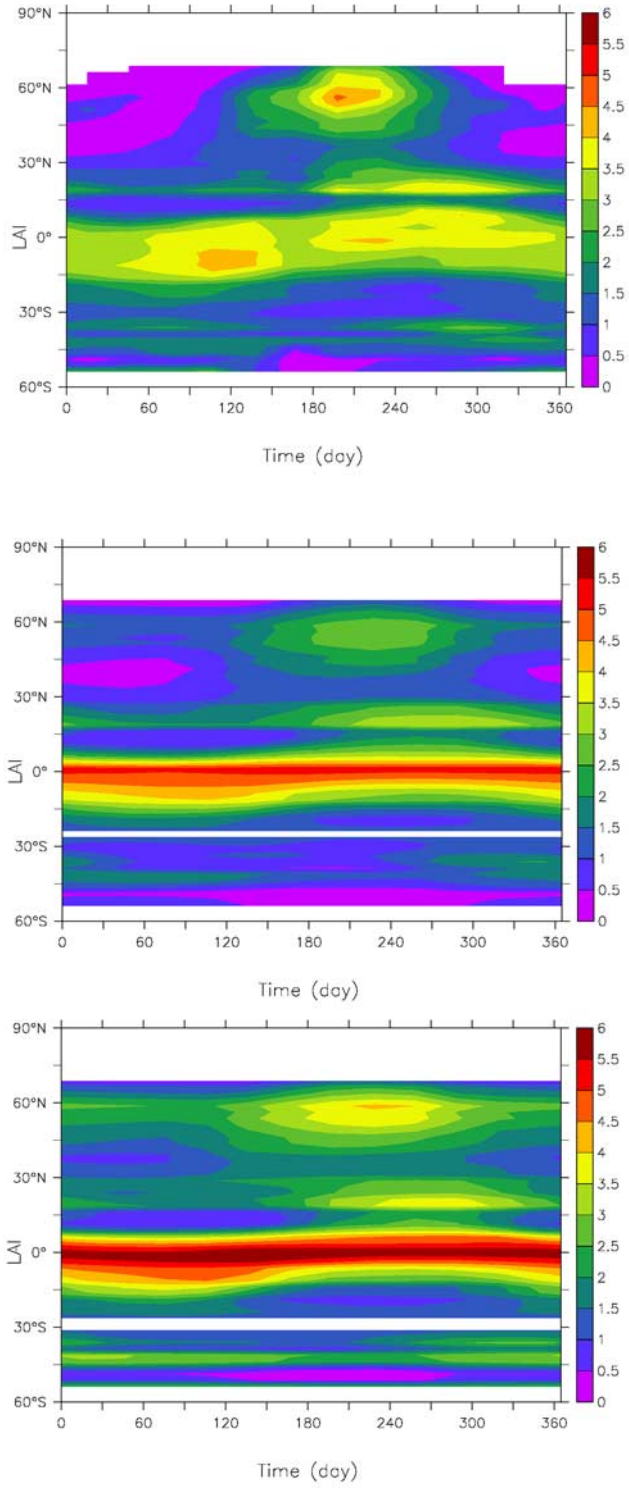

Figure 8. (top) Observed and ((middle) STAT and (bottom) DYN) simulated zonal mean LAI.

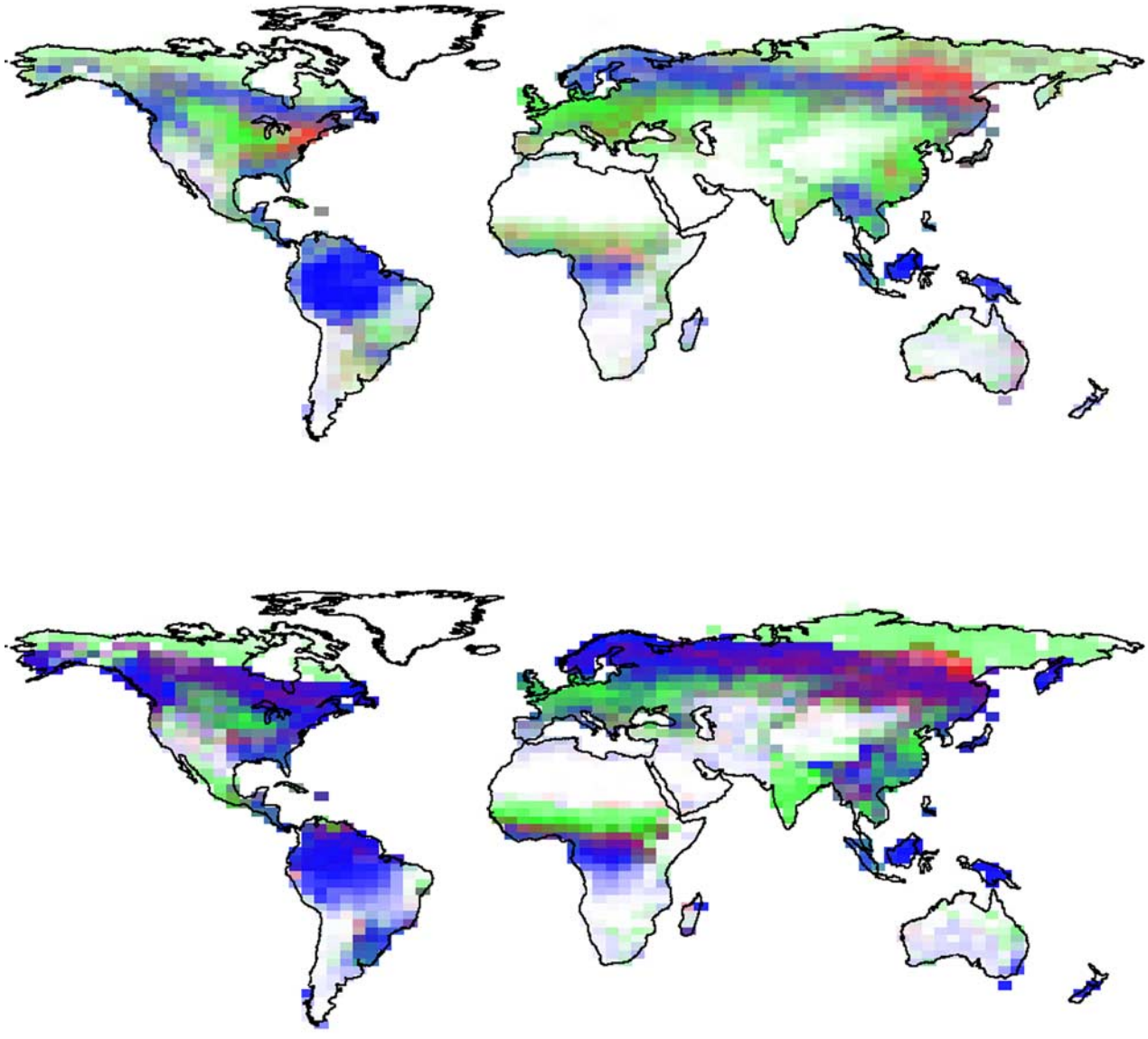

Figure 9. Composite-color map of the simulated annual maximum foliage projective cover (v) in (top) STAT and (bottom) DYN, partitioned according to phenology. STAT uses the observed vegetation distribution; therefore, differences between STAT and DYN are due to vegetation dynamics in DYN. Color coding is such that saturation indicates total grid-scale annual maximum v, while hue indicates the relative v of the following three PFT groups: evergreen woody (blue), deciduous woody (red), and herbaceous (green) plants.

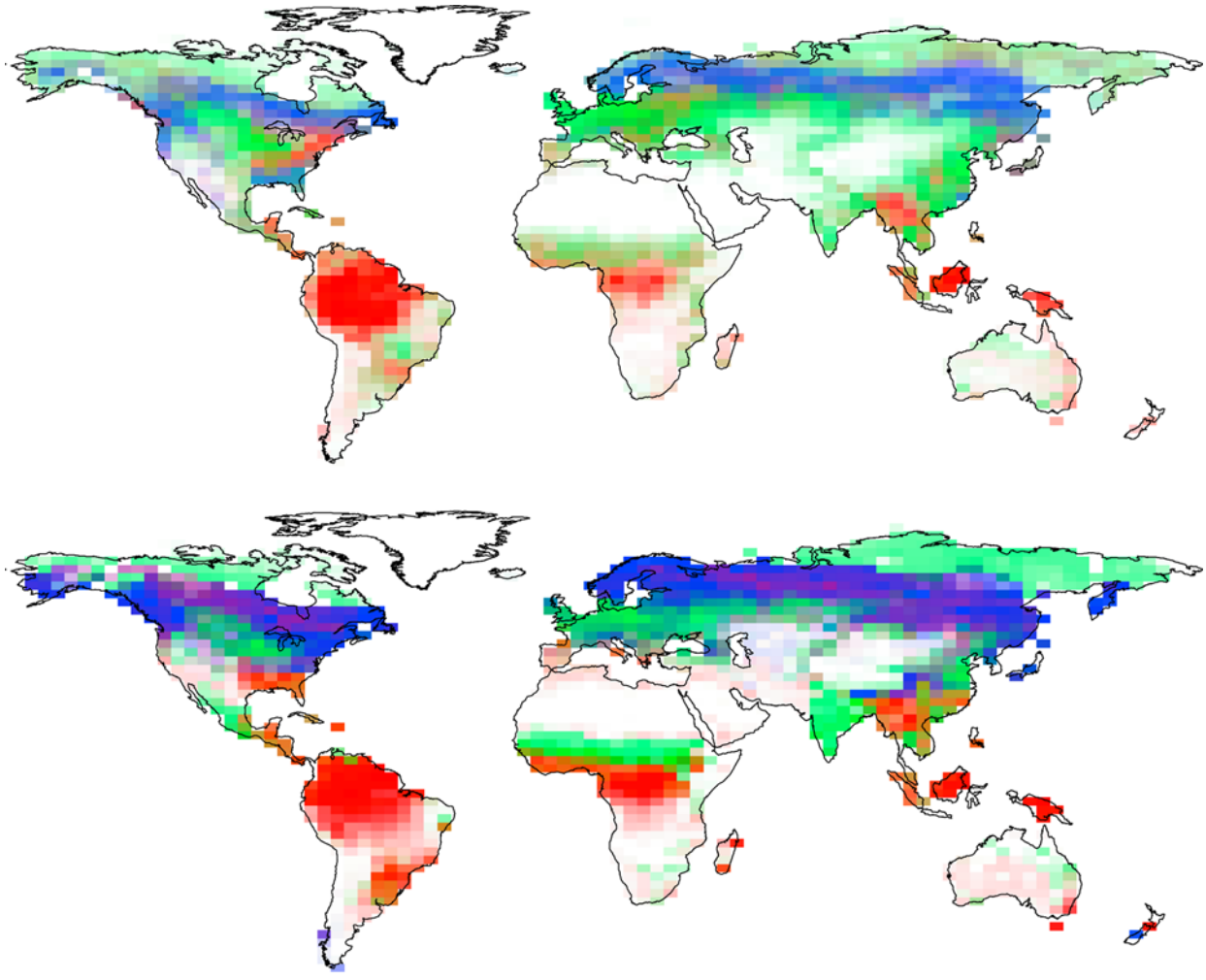

Figure 10. Composite-color map of the simulated annual maximum foliage projective cover (v) in (top) STAT and (bottom) DYN, partitioned according to vegetation morphology. STAT uses the observed vegetation distribution; therefore, differences between STAT and DYN are due to vegetation dynamics in DYN. Color coding is such that saturation indicates total grid-scale annual maximum v, while hue indicates the relative v of the following three PFT groups: needleleaf woody (blue), broadleaf woody (red), and herbaceous (green) plants.

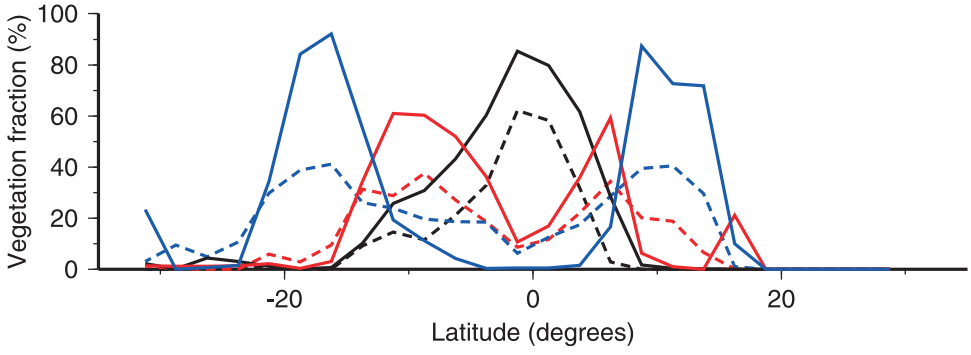

Figure 11. Simulated annual maximum foliage projective cover (v) of tropical evergreen trees (black), tropical deciduous trees (red), and grass (blue) in a meridional cut through Africa at 20°E. Solid lines: DYN; dotted lines: STAT.

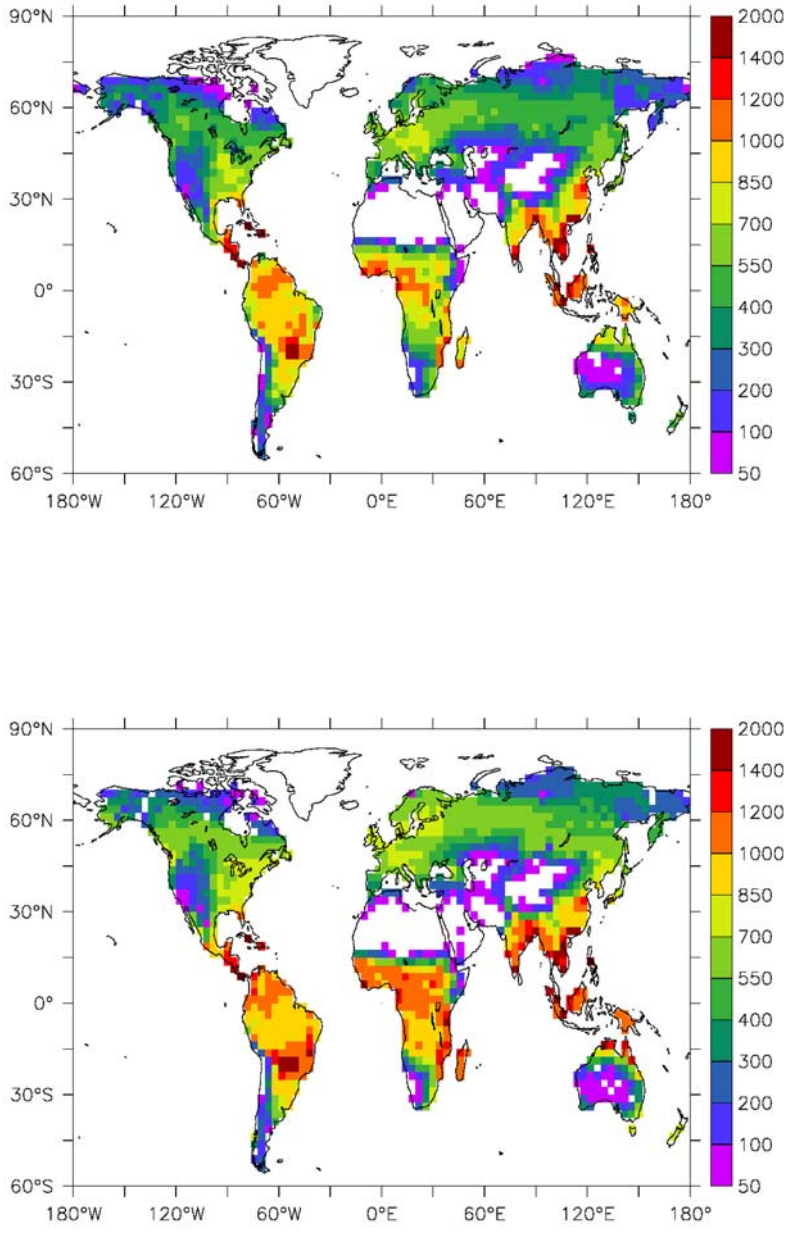

Figure 12. Simulated annual mean NPP (in gC m^{-2} yr^{-1}) for (top) STAT and (bottom) DYN.

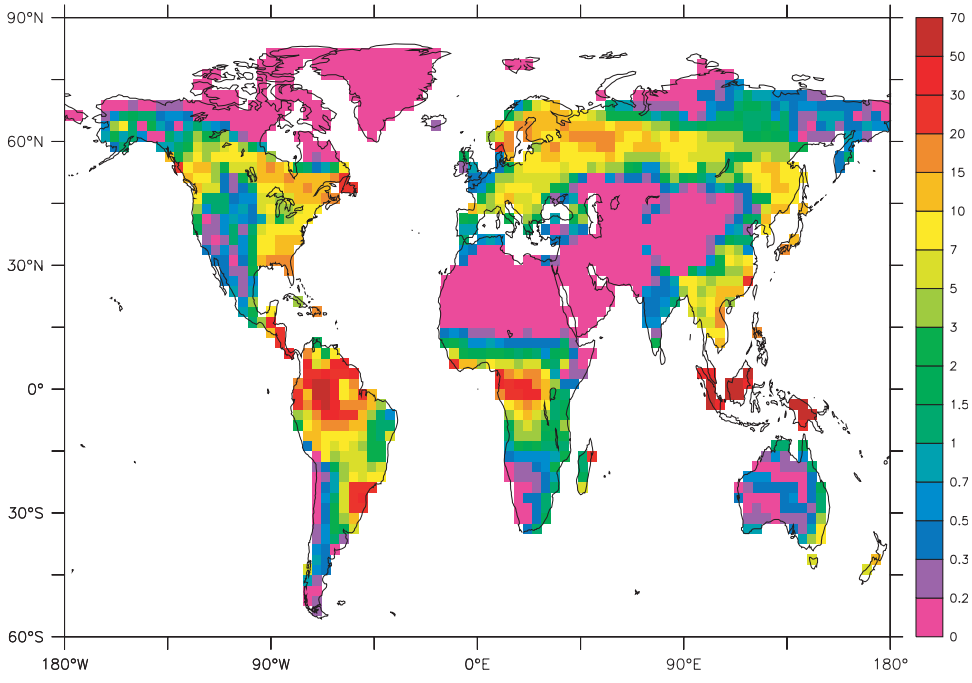

Figure 13. Mean aboveground and belowground biomass of natural vegetation (in kgC/m^2) in STAT.

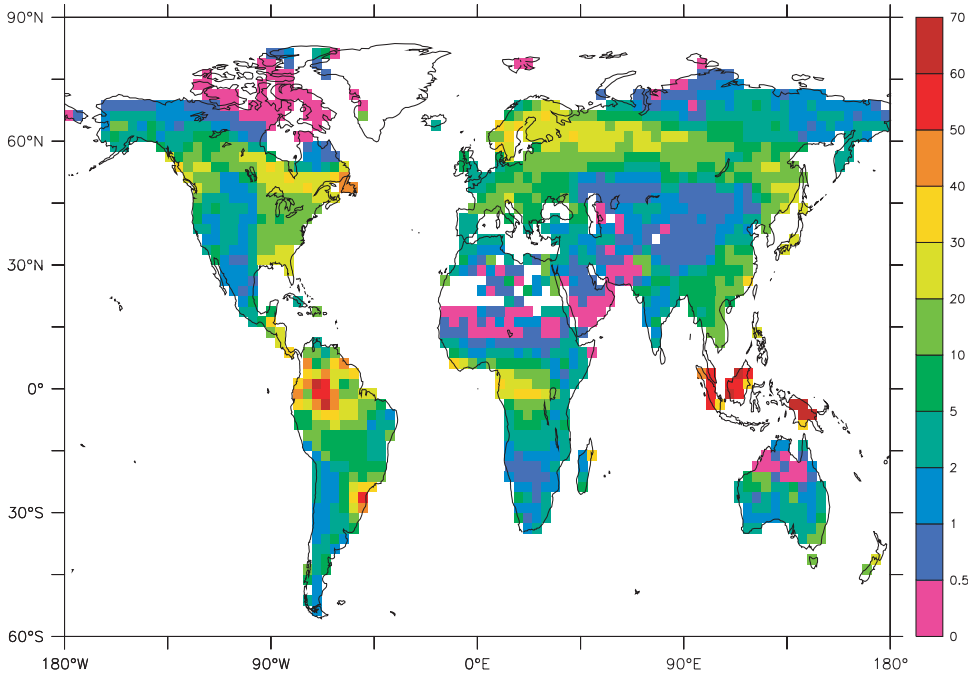

Figure 14. Residence time of carbon in natural vegetation (years) simulated in STAT.

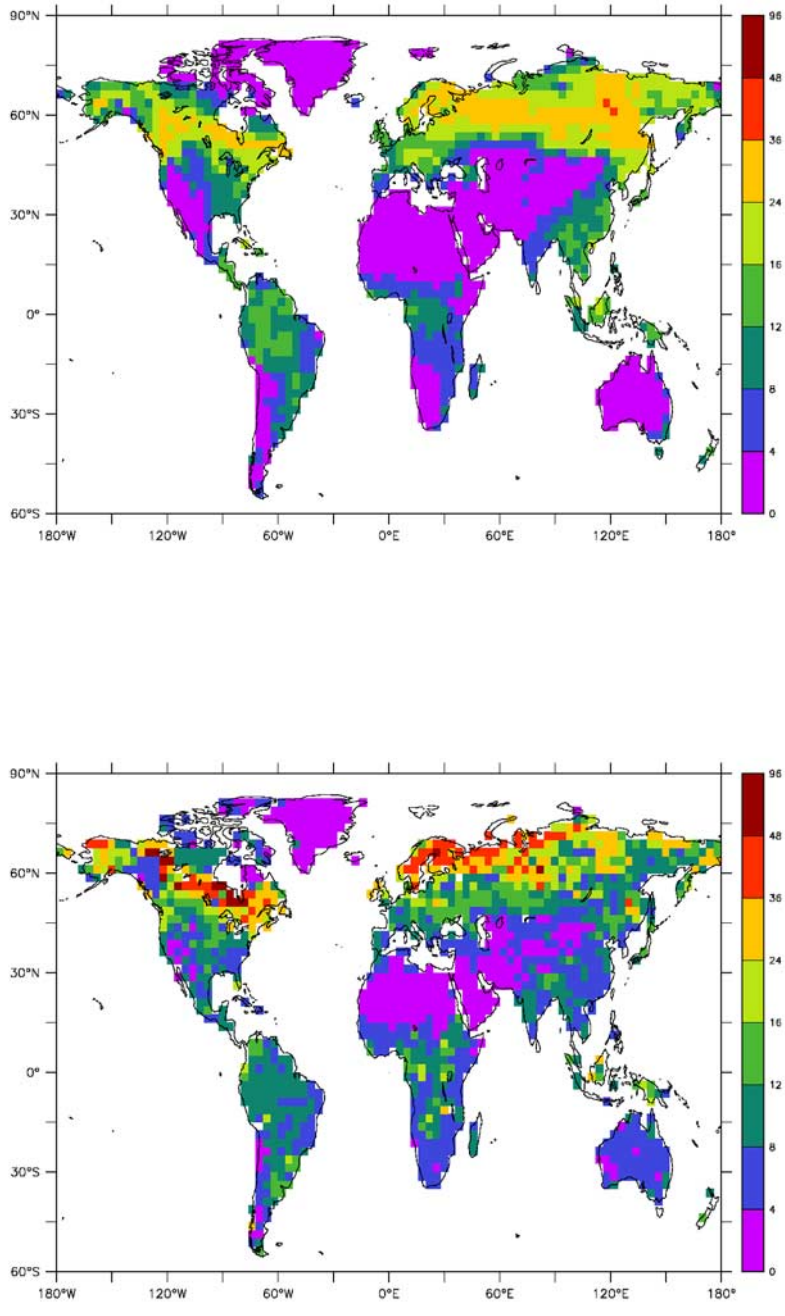

Figure 15. Organic soil carbon in kg m^{-2}: (top) simulated and (bottom) observed (N. H. Batjes, Global data set of derived soil properties, 0.5-degree grid (ISRIC-WISE), 2000, available online at http://www.daac.ornl.gov). The observed soil organic carbon (between 0 and 1 m depth) was interpolated to the model grid.